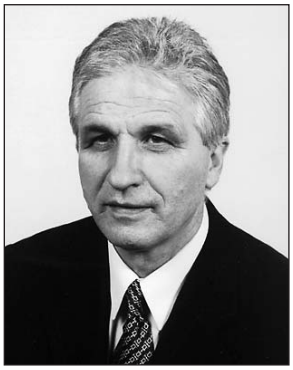

Dear reader,

you are holding in your hands the issue of our scientific letters Communications that is dedicated to transportation construction. This field is very important with regard to education and scientific activities at the Faculty of Civil Engineering, University of Žilina, and also topical in terms of realization of significant motorway and railway constructions in the Slovak Republic nowadays.

Transportation construction specialists these days face the problem of accelerated finalization of the motorway network, modernization of railway junctions in terms of new railway demands. The planned length of motorways and expressways in Slovakia is 830 km. 400 km of new roads still have to be built, including tenths of new road tunnels, bridges and geotechnical buildings. In railways also a number of buildings, bridges, tunnels and safety systems must be reconstructed. The value of these constructions is much greater as they are part of pan-European transportation corridors crossing Slovakia.

The editorial board of our Communications scientific letters believes that by publishing the presented articles, they can help to expand activities and importance of transportation construction industry in Slovakia.

Jan Čorej

https://doi.org/10.26552/com.C.2004.3.5-9

Marián Drusa – Nguyen Giang *

STRESS AND COMPRESSIBILITY CALCULATION IN SUBSOIL OF HIGH EMBANKMENTS AND EFFECTIVENESS OF SPEEDING UP SUBSOIL CONSOLIDATION

When designing a project of speeding-up consolidation of subsoil of high embankments, there are some influences that cannot be missed. Especially in geotechnical engineering, we have to work with influences and uncertainties that have origin in geological space and surveying possibilities. On a practical example we present a possible way of subsoil stress and compressibility calculation and influence of different input data on necessary time of 90% consolidation of subsoil of one leg of a high embankment that has impact also on design distance and amount of sand piles or geodrains.

1. Introduction

A current need of constructing highways is very urgent in Slovakia. As the direction and altitude leading severity are very variable, we have very often to face problems related to the building of the highway embankment on soft soils.

Besides the questions related to the stability of embankment body and subsoil, there has to be solved also questions of embankment settlement (subsoil compressibility) magnitude and settlement speed. In the case of subsoil with a very low oedometric modulus and permeability (e.g. high plasticity clay CH), compressibility of subsoil has a large magnitude (e.g. about 400 mm and more) and time of reaching 100% consolidation (to finish compressibility) is very long (e.g. about 180 years). We can not lay out the pavement on the embankment crown without some remedial operations because, on one hand – the pavement will be damaged by an excessive subsoil deformation. On the other hand, it is impossible to wait so long (until the settlement has been finished) and to lay out the pavement then. In such cases, the designer may require speeding up embankment subsoil consolidation, e.g. reach 90% consolidation within the period of 1 year, i.e.– after 1 year the pavement can be laid out without any risk of being damaged. One solution is speeding up the embankment subsoil consolidation so it is not necessary to wait so long. There are many methods for speeding up the consolidation- sand drains, prefabricated drains = geodrains, trenching lime, cement or rock columns (– improve subsoil deformations properties, too). As the sand drains and the prefabricated drains are used in the conditions of the Slovak Republic, we deal with these methods it this paper mainly from the point of view of their effectiveness.

2. Embankment Stability and Settlement

The method of stabilization of soft soils with vertical drains is applied on compressible, highly saturated soils, like clay and organic soil or peat. These soils are characterized by a soft structure and a big pore capacity, normally filled with water (porewater). In the case of a heavy load as when an embankment has been placed on top of clay or peat soils, settlements could occur due to the compressibility of the soil. These settlements could bring about serious construction problems.

The load caused by the surcharge is initially carried by porewater. However, when soil is not very permeable, water pressure will gradually decrease, as the porewater is able to flow away only very slowly. Increased water pressure may cause instability of the subsoil, which, on the other hand, may create slip planes. The instability might bring decreased rate of fill placement. A vertical drainage system enables a quicker construction of the embankment without any risk of landslides. In order to increase the settlement process and the reduction of water pressure, it is necessary to decrease the flow path of the porewater. This can be achieved by installing evenly spaced vertical drains. The presence of this drainage system enables the pressurized water to flow horizontally towards the nearest drain, and freely escape. Apart from the ongoing consolidation, a vertical drainage system can be a good support in maintaining the stability of an embankment in the course and after its execution. Instability of the subsoil may be manifested in two ways:

- sliding of the slope, where a part of the dike slides downwards along a slip circle,
- squeezing of the soft soil below the embankment.

* **Marián Drusa, Nguyen Giang**
Department of Geotechnics, University of Žilina, Faculty of Civil Engineering, Komenského 52, 010 26 Žilina, Slovak Republic,
Phone: +421-41-7634818. Fax: +421-41-7233502. E-mail: drusa@fstav.utc.sk, giang@fstav.utc.sk

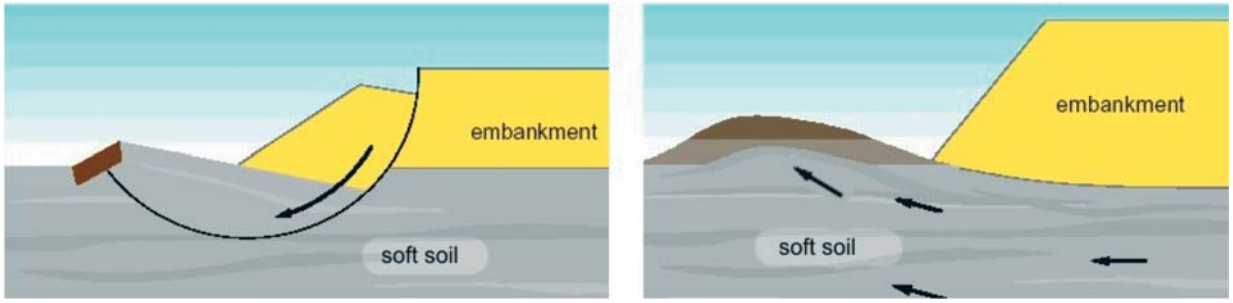

Fig. 1 Sliding and squeezing embankment

Calculation of settlement under the embankment requires calculation of stresses. For engineering practice there is possibility to use principle of superposition. This principle also allows us to split loading of trapezoidal shape to a simple rectangular and triangular strip and to apply known graphs for estimating stress in any point under loading. This way is simple, but, for calculations of the stresses in more points it is useless as it is impossible to computerize it. The second way is, to use some formulas that are not complicated, but input data, such as side angles towards the observed point varied frequently in dependence on its position. It is therefore recommended to apply the calculation method with finite element method.

For a practical example of calculations we chose one design leg of the highway embankment D1 Hričovské Podhradie – Lietavská Lúčka. The design parameters of embankment – height 7.8 m, width at top 28 m, slope 1:2, and total length 540 m. Subsoil consists of high and very high plasticity clay (CH, CV) of soft and firm to stiff consistency and has the following deformation properties:

- vertical coefficient of consolidation: $c_v = 0.015$ mm^2.s^{-1} extremely from 0.001 to 0.007 mm^2.s^{-1}
- horizontal coefficient of consolidation $c_h = 0.030$ mm^2.s^{-1}
- oedometric modulus $E_{oed} = 2.7$ MPa.

Under soft soils is an underlying stratum of impermeable claystones.

Stresses and settlements were computed by Nexis software using the program module Soilin. The Nexis is typical engineering software, which combines the FEM code for stress analysis with classic theory of strain of one dimensional compressibility. A main advantage of the Soilin module is interaction with subsoil through Winkler-Pasternak's model, characterized by the constants C_1 and C_2. By theory of virtual work we can write the condition for equilibrium in a vertical direction:

$$C_1 w + C_2 \Delta w - q = 0; \qquad (1)$$

where: C_1 [MN.m^{-3}] and C_2 [MN.m^{-1}] are constants of subsoil model and are defined by the formulas:

$$C_1 = \int_0^h E_{oed} \left(\frac{\partial \psi}{\partial z} \right) dz; \; C_2 = \int_0^h G \, \psi^2 \, dz; \qquad (2)$$

where: E_{oed} is oedometric modulus and G shear modulus, and ψ is function of vertical deformation of subsoil.

In our case we used a model of geoplate = reinforced layer of gravel by geogrids of the thickness of 600 mm, which carried out dead-weight of embankments being interacted with subsoil. The geoplate was defined by the unit weight 2000 kg.m^{-3}, Young's modulus $E = 150$ MPa, and Poisson's ratio 0.2. In order to obtain correct results of interaction it is very important to have defined geological profile to an adequate depth, and to have right starting values of the subsoil constants. The parameters of soils used in the computational model are presented in Tab. 2, for estimation of settlement layers were divided into thinner layers. The final result is shown in Fig. 2 with settlement uz from −54.2 to −428.4 mm.

Table 2

Geological layer	Depth [m]	No. of layers	E_{def} [Pa]	Poisson's ratio	Gama [N.m^3]	coeff m
1	9.4	10	1500000.0	0.42	20000.0	0.01
2	20.0	7	10000000.0	0.25	22000.0	0.30
3	30.0	5	35000000.0	0.15	23000.0	0.35

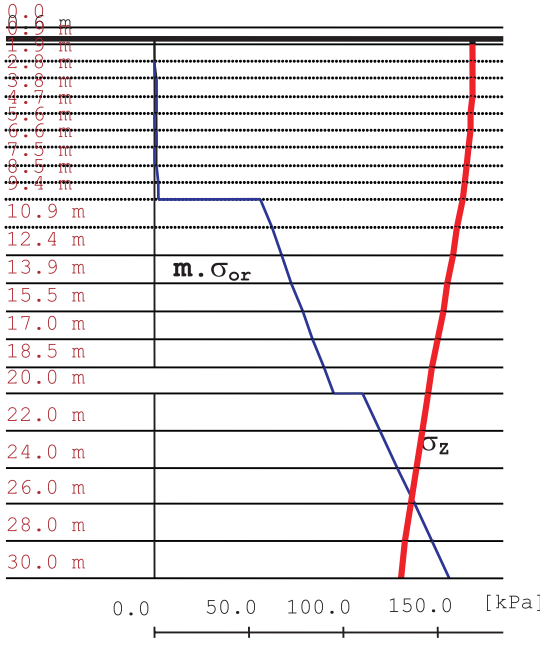

Fig. 3 Stress and structural resistance under center of embankment

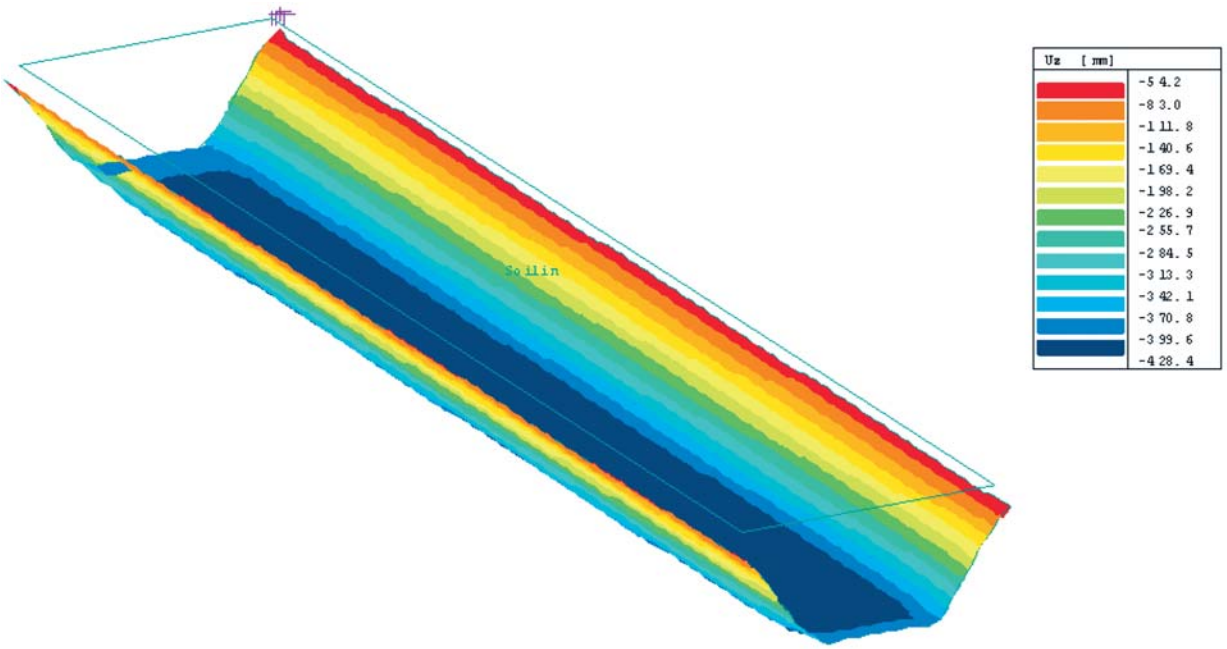

Fig. 2 Result of settlement calculation

An active zone under the embankment is deep and stress has influence on compressibility up to the depth of 25 m, Fig. 3.

3. The Principle of Speeding up Embankment Subsoil Consolidation

From history we know methods of speeding up the consolidation. The prefabricated vertical drains were used for the first time in Sweden in 1937. The drains were manufactured in cardboard, so-called cardboard wick. Approx. 10 years earlier, sanddrains were developed in California in order to expedite consolidation. Especially in the Netherlands, sanddrains have been applied in a large scale since 1950. The first synthetic drain was introduced in 1972 for a building pit at the Hemweg power station in Amsterdam. Its development was then accelerated. Synthetic drains are superior to sanddrains because of their flexibility and better filtration, and they became a formidable competitor.

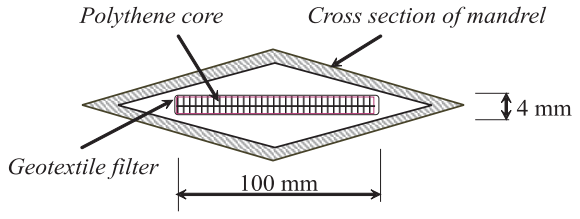

Fig. 4 Schematic cross section of prefabricated band-shaped drain with mandrel

The slow rate of consolidation in saturated clays of low permeability may be accelerated by means of vertical drains (Fig. 4). Consolidation then depends mainly on horizontal radial drainage, resulting in faster dissipation of excess porewater pressure. The vertical drainage becomes less important, then.

The traditional method of installing vertical drains is by driving boreholes through the clayey layer and backfilling with a suitably grade sand. Typical diameters are from 200 to 400 mm and drains are installed into depths over 30 m. The sand should be capable of allowing the efficient drainage of water without permitting fine soil particles to be washed in. Prefabricated drains are also used and are generally cheaper than backfilled drains. One such type consists of a filter stocking, generally of woven polypropylene, filled with sand of typical diameter of 65 mm. Compressed air is used to ensure that the stocking is completely filled with sand. This type of drain is very flexible and is usually unaffected by any lateral ground movements. Another type of prefabricated drain is the band drain, consisting of a flat plastic core with drainage channels, surrounded by a thin layer of filter fabric: the fabric must have sufficient strength to prevent it from being squeezed into the channels. The main function of the fabric is to prevent the passage of fine soil particles which may clog the channels in the core. Typical dimensions of the band drain are 100mm by 4mm and the equivalent diameter is generally assumed to be the perimeter divided by π.

Prefabricated drains are installed either by insertion into prebored holes or by placing them inside a mandrel or casing which is then driven or vibrated into the ground (Craig, 1995). The consolidation process in axial-symmetrical state can be calculated by the methods presented by Barron (1948) and Hansbo (1972, 1979). In these methods, linear stress-strain relationships and constant soil parameters are assumed in the deformation process, as well as constant vertical surface displacements throughout the drained

area (Jamiolkowski et al 1983). The effect of secondary compression is also neglected. With these assumptions, the equation of consolidation becomes:

$$\frac{\partial u}{\partial t} = c_h \cdot \left(\frac{\partial^2 u}{\partial r^2} + \frac{1}{r} \cdot \frac{\partial u}{\partial r} \right) + c_v \frac{\partial^2 u}{\partial z^2} \qquad (3)$$

where: c_v, c_h – coefficient of vertical and horizontal consolidation (m^2/year),
u – is excess pore pressure (kPa), t – is time of consolidation (years),
z – is vertical space coordinate (m), and r is radial space coordinate (m).

The degree of consolidation is defined as degree of dissipation of the excess pore pressure; it can be expressed as (Carillo. 1942):

$$U = U_h + U_V - U_h \cdot U_V \qquad (4)$$

In some literature the formula (4) is written as:

$$(1 - U) = (1 - U_h) \cdot (1 - U_V) \qquad (5)$$

The degree of vertical consolidation U_v is calculated according to Terzaghi's theory and the degree of horizontal consolidation U_h is calculated from Barron (1948):

$$U_h = 1 - \exp(-8T_h/\mu) \qquad (6)$$

where T_h is time factor:

$$T_h = c_h \cdot t/D^2 \qquad (7)$$

$$\mu = \frac{n^2}{n^2 - 1} \cdot \left(\ln n - \frac{3}{4} + \frac{1}{n^2} - \frac{1}{4 \cdot n^2} \right) \qquad (8)$$

$$n = \frac{D}{d} \qquad (9)$$

where D is diameter of dewatered soil cylinder (m) and d is drain diameter (m).

For calculation of the degree of total consolidation U, degree of vertical consolidation U_v is required, then the degree of horizontal consolidation U_h will be calculated (equation (6) or (7)). For the chosen drain diameter d the dewatered soil cylinder D can be calculated (see equations (6) up to (9)). The final spacing of drains in a square pattern can be obtained:

$$S = D/1.13\,. \qquad (10)$$

Spacing of drains in a triangular pattern is:

$$S = D/1.05 \qquad (11)$$

4. The Calculation of Effectiveness of Drains

For the selected leg of highway embankment D1 Hričovské Podhradie – Lietavská Lúčka the time needed for reaching 90% consolidation of subsoil was calculated, then necessary distance of sand drains diameter of 400 mm and prefabricated drains (dimension 100 mm by 4 mm) in a square pattern. At last costs of speeding up subsoil consolidations were evaluated. The results are introduced in the following tables 4, 5, and 6.

Time (in years) to reach 90% consolidation of subsoil of highway embankment depending on its thickness — Tab. 4

Values of c_v mm^2/s (m^2/year)	10 m	7.5 m	5.0 m	2.5 m
0.001 (0.03153)	2695.3	1516.4	673.8	168.5
0.015 (0.47304)	**179.7**	101.1	44.9	11.2
0.026 (0.81990)	103.7	58.3	25.9	6.5

Necessary distance of sand pile and prefabricated drains in square pattern to reach 90% consolidation of subsoil after 1 year depending on its thickness — Tab. 5

Thickness	10 m	7.5 m	5.0 m	2.5 m
Sand piles	1.727	1.733	1.747	1.806
Prefabricated drains	1.110	1.114	1.125	1.171

5. Conclusions

- A different way of calculation of stresses in subsoil under high embankments was presented by a FEM computational model.
- The difference in coefficient of consolidation values makes differences in time needed to reach 90 % consolidation that changes in a large range (even hundred years and more) depending on soil properties (mainly coefficient of consolidation values) and soil thickness and drain path as well.
- In this case the use of prefabricated drains is more economical (46.6 % of costs of sand drains).

Costs (in SKK) of speeding up the subsoil consolidations of highway embankment (thickness 10 m, 90% consolidation after 1 year) — Tab. 6

Type of drains	Distance	Pieces	Unit cost	Total cost	Costs difference
Sand piles	1.72	11 340	7000	79 380 000	42 336 000
Prefabricated drains	1.11	27 440	1 350	37 044 000	

References

[1] KOLÁŘ V., NĚMEC I.: *Contact Stress and Settlement in the Structure – Soil Interface.* Study ČSAV 16.91, ACADEMIA Praha, 1991.
[2] HARTLÉN J., WOLSKI W.: *Embankments on organic soils.* Elsevier. Amsterdam, 1996.
[3] CRAIG R. F.: *Soil Mechanics.* Fifth edition. Publisher Chapman & Hall, 1991.
[4] LANCELLOTA R.: *Geotechnical Engineering,* Balkema Rotterdam 1995.
[5] KLABLENA P., MIČA L.: *Driven compacted-in-place sand-gravel piers.* 7th International Conference with Exhibition on Piling and Deep Foundations, Vienna, p. 5.23.1–4, 1998.
[6] MIČA, L.: *Stabilization of the subsoil with using stiff integral geogrids*, In 4th International Conference on Ground Improvement Techniques, Kuala Lumpur, Malaysia, CI-PREMIER PTE LTD, 2002, p. 545 – 549.

https://doi.org/10.26552/com.C.2004.3.10-16

komunikácie
COMMUNICATIONS

Milan Moravčík *

VERTICAL TRACK STIFFNESS EFFECT ON DYNAMIC BEHAVIOUR OF TRACK STRUCTURE

The dynamic modelling of railway track response and of the interaction of vehicle and track at low and mid frequencies that are significant for the track deterioration, is presented. The response of the track subjected to a moving vehicle is simulated for a stationary randomly distributed ballast stiffness with a standard uniform distribution and a normal distribution. The response of the track components is solved by the Finite Element Method. Monte Carlo simulation was applied to estimate the dynamic track response. The dynamic amplification resulting from the simulated passage of the locomotive of the type E 499 (85 t) is presented.

1. Introduction

The dynamic response of a railway track subjected to moving vehicles in service conditions generally has a random character. Major sources of dynamic effects on the vertical response of track – isolated and periodic irregularities on the rail surface, repetitive effect of the sleeper spacing, random variations of longitudinal profile of the track, etc., are frequently investigated. The less attention is paid to the influence of the vertical track stiffness on the response of track components and on the evaluation of forces transmitted by the track components.

The model presented in this paper, developed at the Department of Mechanics [6], was addressed to the study of dynamic behaviour of track structure, especially the evaluation of the dynamic coefficient for the track components. The dynamic behaviour and the response of track components (rails, sleepers, the ballast) due to variability in the vertical stiffness of rail supports are presented in this paper. Time domain technique has been used to study these dynamic effects. The approach can be helpful in clarifying the influence of vehicle speed on the dynamic response of the track components.

Using the computer program Interaction [6] the Monte Carlo Simulations were applied. With the prescribed set of input values for system parameters, the simulation process yielded a specific measure of response.

2. Outline of solution techniques

The theoretical model of the rail as a beam on continuous elastic foundation loaded by a vertical concentrated force P moving along at a constant speed c introduced by Timoshenko provides a basis for the track design procedure and the stress analysis of the railway track components. The equation of motion of the rail for this case is [1, 5], see Fig. 1:

$$EI\frac{\partial^4 w(x',t)}{\partial x'^4} + \mu_x\frac{\partial^2 w(x',t)}{\partial x'^2} + 2\mu_x\omega_b\frac{\partial w(x',t)}{\partial t} + \\ + \kappa_z \cdot w(x',t) = P \cdot \delta(x') \qquad (1)$$

where: $w(x', t)$ is the vertical motion (dynamic deflection) of the rail in the stationary co-ordinates (x', t)

$C_b = 2\mu_x\,\omega_b$ is a damping coefficient of structure,
ω_b $[s^{-1}]$ is a angular damping frequency,
κ_z $[Nm^{-1}]$ is the stiffness per length of rail support,
EI is a flexural rigidity of rail,
μ_x is the mass of rail per unit length,
c is the speed of moving force P.

The equation of motion of the rail in the moving co-ordinates (x, t) has the form, [5]:

$$EI\frac{\partial^4 w(x,t)}{\partial x^4} + \mu_x\left[\frac{\partial^2 w(x,t)}{\partial t^2} - 2c\frac{\partial^2 w(x,t)}{\partial x\partial t} + c^2\frac{\partial^2 w(x,t)}{\partial x^2}\right] + \\ + 2\mu_x\omega_b\left[\frac{\partial w(x,t)}{\partial t} - c\frac{\partial w(x,t)}{\partial x}\right] + \kappa_z \cdot w(x,t) = \\ = P \cdot \delta(x - ct) \qquad (2)$$

where: $w(x,t)$ is the vertical displacement function (dynamic deflection) of the rail in the moving co-ordinates (x, t).

A number of other theoretical models [2, 5] have been developed for the track structure behaviour under vertical loads which include either separate components of the track structure (rails, fasteners, sleepers and subgrade) or total characteristics of the track structure, see Fig. 2.

The differential equation (2) of the problem can be solved either in the frequency or in the time domain, [2]. But for the sto-

* **Milan Moravčík**
Department of Mechanics, Faculty of Civil Engineering, University of Žilina, Komenského 52, 010 01 Žilina, Slovak Rep.,
E-mail: mimo@fstav.utc.sk

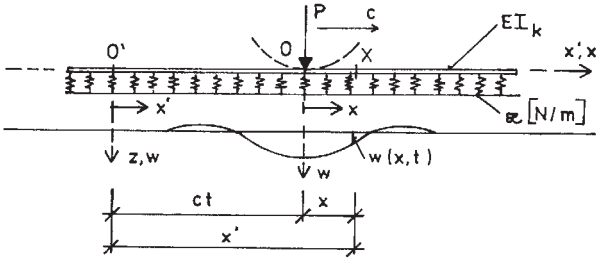

Fig. 1 Rail as a beam on continuously elastic foundation

chastic modeling of the track stiffness $\kappa = \{\kappa(x)\}$ solving of Eq. 2 brings about serious troubles. At present, the Finite Element Approach (FEA) is adopted for solution of these effects. Fig. 2 shows the used physical modeling of the track components in vertical direction corresponding to the FEA application. The mechanical properties of the track components are modeled by a set of springs and dampers in one or two layers. The characteristics of springs and dampers can be determined by the laboratory load tests of these components or by the field measurements in typical track conditions.

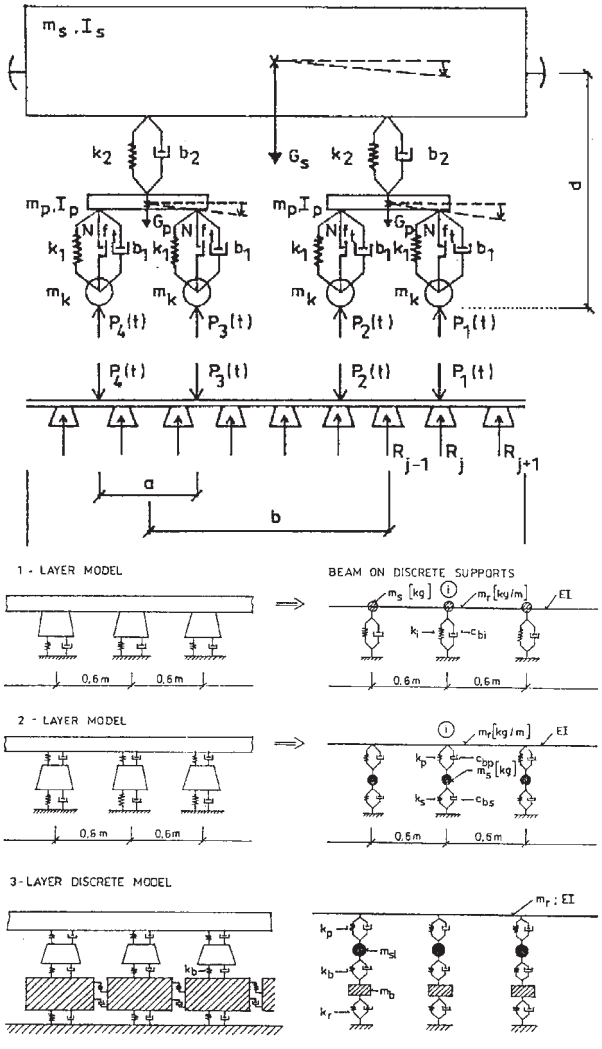

Fig. 2 Theoretical models of track structure in vertical direction

3. Approach

The track behaviour under dynamic loading conditions is reproduced by an interactive dynamic model with three model components:

- the dynamic model of vehicle,
- the linear track model,
- the stiffness of discrete rail supports.

A plain mathematical model is adopted aiming at the vertical vehicle-track interaction problem for low and medium frequency ranges, say for the frequency bandwidth of 0 – 200 Hz. The Finite Element Method is used for modeling of the track and the Composite Element Method is used for the modeling of a vehicle. The vehicle-track/interaction model is schematically shown in Fig. 3. This model allows to describe the dynamic behaviour of the two subsystems – the vehicle and the track.

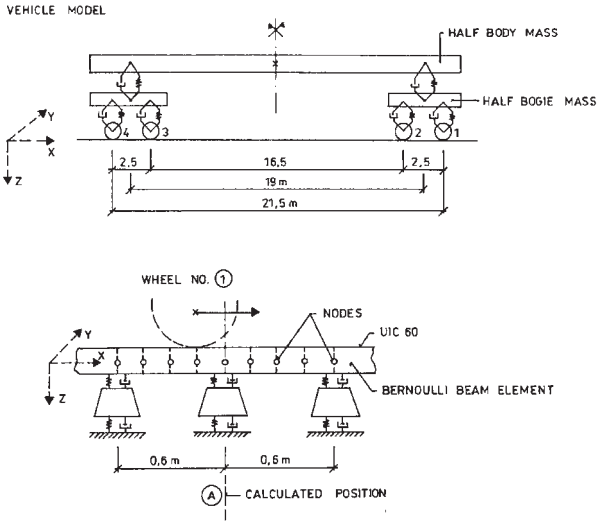

Fig. 3 Scheme of the vehicle-track/interaction model

The rail with its elastic properties is modelled as an Euler-Bernoulli beam using the finite element approach. The nodes of the finite elements lie above each sleeper and have two degrees of freedom – vertical translation and pitch rotation. The four elements belong to one sleeper bay. The cubic polynomial functions are used to describe the element displacement. The sleepers are considered as rigid bodies. The stiffness and damping of railpads, the ballast and the subgrade are simulated for each sleeper. The resulting equations of motion of the track structure are:

$$[M]\{\ddot{U}\} + [C]\{\dot{U}\} + [K]\{U\} = \{P\} \qquad (3)$$

where [*M*], [*C*] and [*K*] are the mass, damping and stiffness matrices of the track structure respectively, and {*P*} is the nodal load vector. {*U*} is the nodal vertical displacement vector.

The vehicle is modelled by the Composite Element Method as a system described by three quantities: its mass or inherent properties, its internal force elements (springs and dampers) and the generalised coordinates. The equation corresponding of motion is given by

$$[m]\{\ddot{u}\} + [c]\{\dot{u}\} + [k]\{u\} = \{F\} \qquad (4)$$

where: [*m*], [*c*] and [*k*] are the mass, damping and stiffness matrices of the vehicle system respectively, and {*F*} is the nodal load vector. {*u*} is the nodal vertical displacement vector.

Numerical algorithms consisting of finite-element procedures to model the track structure and time -step integration to calculate the response have been used, [3]. The solution algorithm for the time-domain technique is illustrated in Fig. 4.

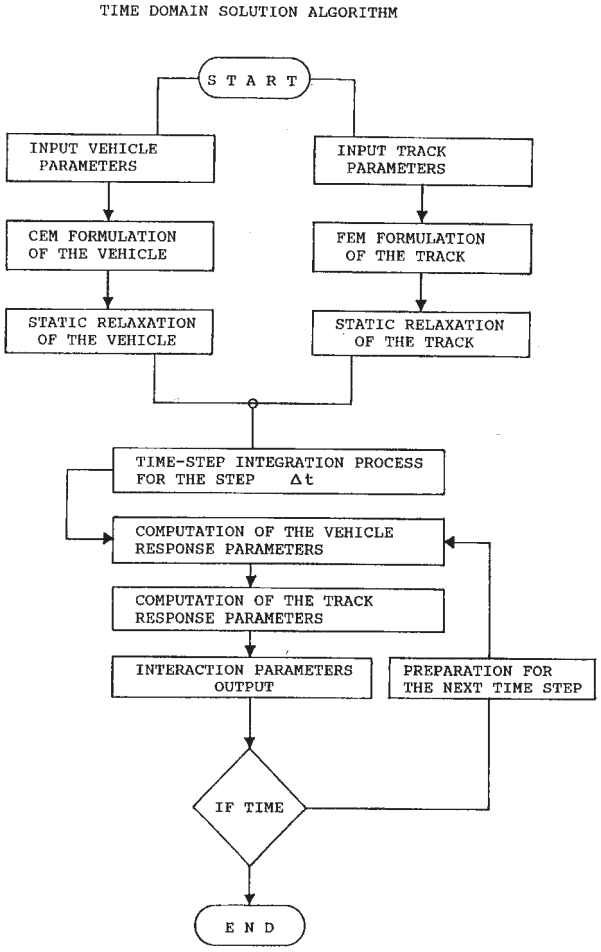

Fig. 4 Time domain solution algorithm

3.1 Variable vertical track stiffness modeling

In order to examine the effect of variable track stiffness conditions, the five characteristic vertical ballast stiffness ${}^{(i)}k_b$, $i=1 \div 5$, of the track were taken to model low, medium, and high track stiffness conditions. The mean values of the vertical ballast stiffness and the vertical pad stiffness k_f are shown in Tab. 1.

The stiffness levels (i) in Tab. 1 are considered the basic mean values for the simulation of discrete random variables ${}^{(i)}k_{b,j}$ of the vertical track stiffness k_b for the study of influence of the track stiffness on the response. In this study only the variability of vertical track stiffness is considered to be a random input quantity and the next input parameters are considered the deterministic ones.

Mean values of the modelled vertical stiffness of track Tab. 1

Track type (i)	Level of Support Stiffness	Vertical Ballast Stiffness ${}^{(i)}\overline{k_b}$ [N/m]	Vertical Pad Stiffness $\overline{k_f}$ [N/m]	
A	low	40.10^6	1	150.10^6
			2	60.10^6
B	medium	80.10^6	1	150.10^6
			2	60.10^6
C	medium	120.10^6	1	150.10^6
			2	60.10^6
D	high	220.10^6	1	150.10^6
			2	60.10^6
E	very high	480.10^6	1	150.10^6
			2	60.10^6

Two models for the random discrete rail stiffness supports were considered:

1/ *The stationary randomly distributed stiffness of the discrete rail supports* due to the random ballast stiffness $k_{b,j}$ with:
- the standard uniform distribution,
- the normal distribution.

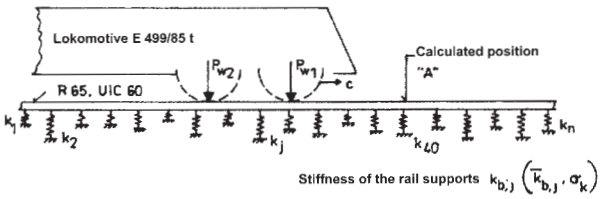

Fig. 5 Stationary randomly distributed vertical stiffness of the rail supports

The relative vertical ballast stiffness $\kappa_{b,,j}$ can be applied on each stiffness level (i).

$$k_{b,j} = \frac{{}^{(i)}k_{b,j}}{{}^{(i)}\overline{k_b}} \qquad (5)$$

where: ${}^{(i)}\bar{k}_b$ is the mean value of the ballast stiffness on the level (i).

The relative ballast stiffness $k_{b,j}$ has been generated for the simulation studies and Monte -Carlo analyses, $k_{b,j} = k_{b,j,gen}$, and the calculation has been carried out for:

a) the uniform distribution $k_{b,j}$

The relative ballast stiffness ${}^{(i)}k_{b,j}$ was considered from the interval:
- Case 1: $0{,}75 < {}^{(i)}k_{b,j,gen} < 1{,}25$, with the mean $\bar{k}_{gen} = 1{,}0$ and the standard deviation $\sigma_{\kappa,gen} = 0{,}145$.
- Case 2: $0{,}5 < {}^{(i)}k_{b,j,gen} < 1{,}5$, with the mean $\bar{k}_{gen} = 1{,}0$ and the standard deviation $\sigma_{\kappa,gen} = 0{,}288$.

b) For the normal distribution $k_{b,j}$

The relative ballast stiffness ${}^{(i)}k_{b,j}$ were considered with parameters:

Case 1: $\bar{k}_{gen} = 1{,}0$; $\sigma_{\kappa,gen} = 0{,}316$, $\sigma^2_{\kappa,gen} = 0{,}1$,

and coefficient of variation $V_\kappa = \dfrac{\sigma_{\kappa,gen}}{\bar{k}_{gen}} = 0{,}316$.

Case 2: $\bar{k}_{gen} = 1{,}0$; $\sigma_{\kappa,gen} = 0{,}447$, $\sigma^2_{\kappa,gen} = 0{,}2$,

and coefficient of variation $V_\kappa = \dfrac{\sigma_{\kappa,gen}}{\bar{k}_{gen}} = 0{,}447$.

The corresponding real ballast stiffness ${}^{(i)}k_{b,j}$ is:

$$ {}^{(i)}k_{b,j} = {}^{(i)}\kappa_{b,j,gen} \cdot {}^{(i)}\bar{k}_b \,. \qquad (6) $$

4. Results of numerical simulation

Simulation results include the chosen amplitudes of the dynamic track response $Y_{dyn} = (w,P,M..)$: the rail deflection w in the position above the sleeper "A", the sleeper - ballast force P_{s-b} under the sleeper "A", and the rail bending moment M, etc.

The simulation was made for the locomotive Skoda E 499 (85 t) operating speeds of 20 and 50 m/s. The results of dynamic response Y_{dyn} are compared with the static response Y_{st} for the modelled track stiffness type. In this paper are presented only some results for the track of the type B, see Table. 1. 2 000 simulation runs were performed for both static and tested speeds of 20 m/s and 50 m/s.

- *Track stiffness B1 - the static response*

Characteristics of response for the static rail deflection w, the sleeper ballast force P_{s-b}, for the uniform distribution of vertical support stiffness $k_{b,j}$ and for the Gaussian distribution of vertical support stiffness $k_{b,j}$ are presented in histograms in Fig. 6.

- *Track stiffness B1 - the dynamic response*

Characteristics of response for the dynamic rail deflection w and the sleeper ballast force P_{s-b}, for the Uniform distribution of vertical support stiffness $k_{b,j}$, and for the Gaussian distribution $k_{b,j}$, are presented on histograms in Fig. 7 and Fig. 8.

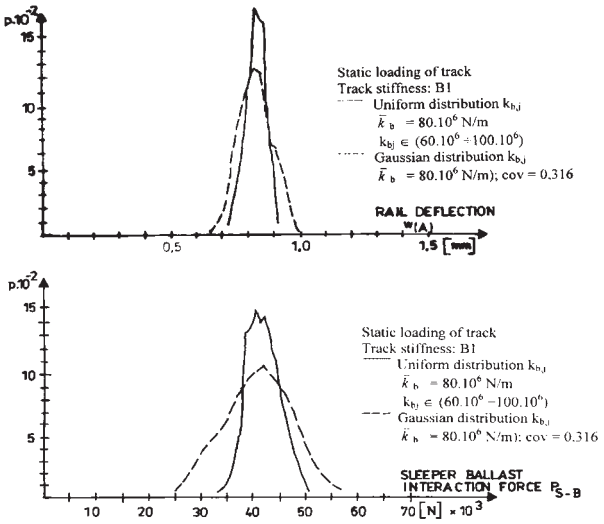

Fig. 6 Histograms of rail deflections w and the sleeper ballast force P_{b-s}, for the Uniform and the Gaussian distribution of the vertical súpport stiffness k_{bj}, - the static case (the locomotive speed c = 0)

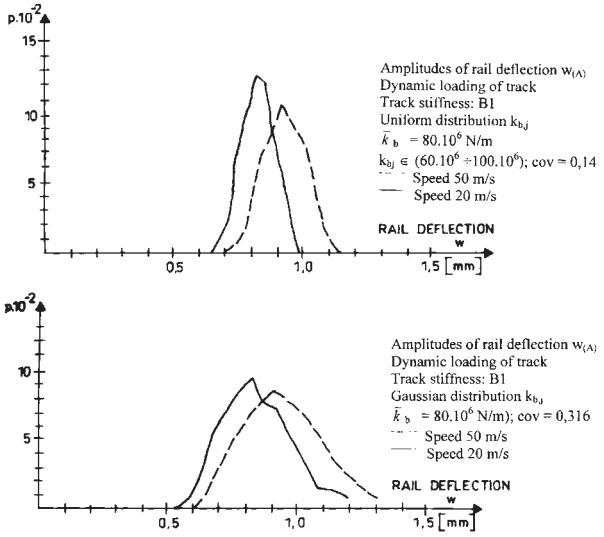

Fig. 7 Histograms of dynamic amplitudes of the rail deflection w for the Uniform and the Gaussian distribution vertical support stiffness k_{bj}, for the locomotive speed 20 m/s and 50 m/s

Track stiffness B1 - Comparison results of the static and dynamic response for the uniform and Gaussian distribution of the vertical supports stiffness k_{bj}, see Fig. 9 ÷ Fig.10.

5. Dynamic coefficient

A moving vehicle on a track with stochastic rigidity of the substructure in the vertical direction generates deflections and stresses

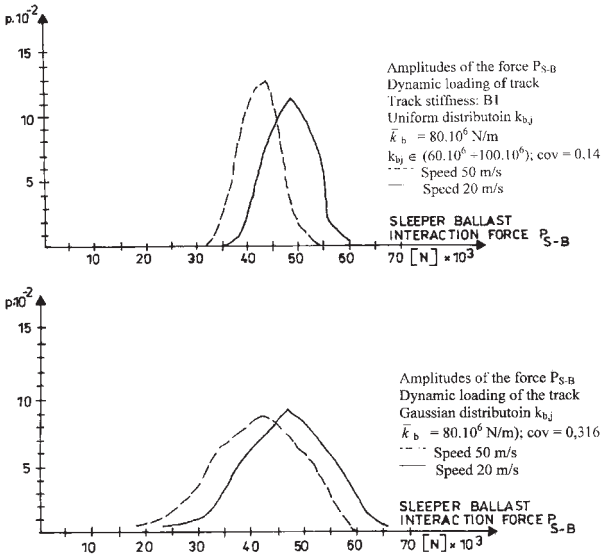

Fig. 8 Histograms of dynamic amplitudes of the sleeper-ballast force P_{s-b} for the uniform and Gaussian distribution vertical support stiffness k_{bj}, for the locomotive speed 20 m/s and 50 m/s

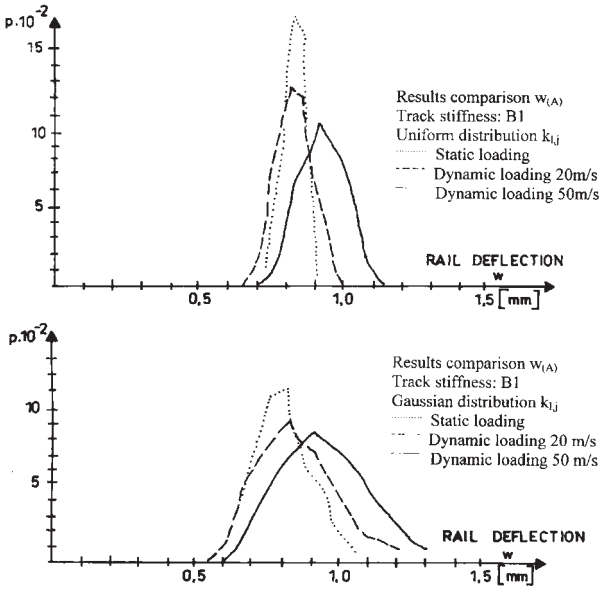

Fig. 9 Histograms of the rail deflection w - comparison the static and dynamic response for the Uniform distribution and Gaussian distribution of the stiffness $k_{b,j}$

in the track structure that are generally greater than those caused by the same vehicle load applied statically or moving on the track with constant rigidity of the substructure. The dynamic amplification δ resulting from the passage of the vehicle over the track section with the simulated stiffness of supports can be defined as the ratio of the maximum dynamic amplitude of a quantity $Y_{dyn(rand)}$ (rail deflection w, bending moment M, etc.) to the static amplitude of a quantity $Y_{st(cons)}$, for the tested type of the track (i) with constant stiffness of supports $k_{b,j}$.

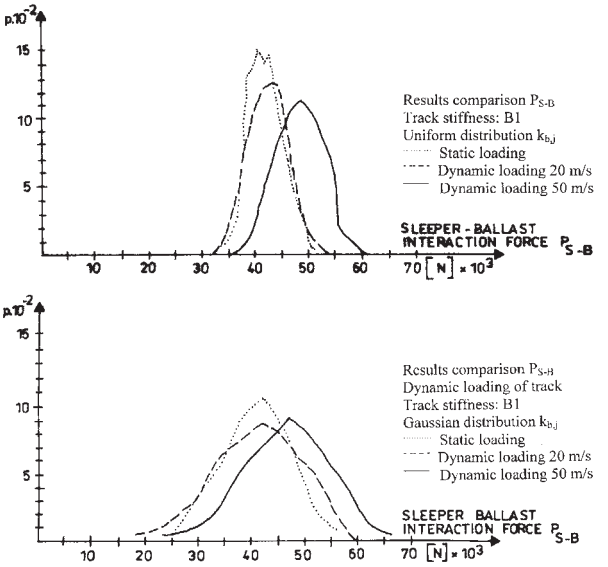

Fig. 10 Histograms of the sleeper-ballast force amplitude P_{s-b} comparison the static and dynamic response for the Uniform distribution and Gaussian distribution of the stiffness $k_{b,j}$

$$\delta = \frac{Y_{dyn(rand)}}{Y_{st(cons)}} \tag{7}$$

The passage of each wheelset induces a peak of the observed quantity Y_{dyn} and the results may be treated statistically as shown in histograms in previous figures. Thus, the histograms may be exploited for the statistically expected values of the dynamic coefficient for the rail deflection, bending moments, etc. The dynamic coefficients δ of the chosen quantities for the track B1, for constant stiffness of supports, are presented in Tab. 2.

Dynamic coefficient δ for the constant stiffness of support, $k_{b,j}$ = const. Tab. 2

Track B1	Response			Dynamic coefficient $\delta = Y_{dyn}/Y_{st}$	
	Y_{st}	Y_{dyn}			
		20 m/s	50 m/s	20 m/s	50 m/s
Rail Deflection $Y = v$ [mm]	0.796	0.821	0.908	1.03	1.14
Sleeper-ballast Force $Y = P$ [kN]	41.5	42.9	47.7	1.03	1.15

Using the mean values of the response quantities $\bar{Y}$ and the standard deviation σ_Y, the dynamic coefficient δ may be determined, see Tables 3 ÷ 6.

The dynamic coefficient δ for the constant stiffness of supports, see Tab. 3, is small for the low vehicle speed and increases with the vehicle speed. The effect of stochastic rail support stiff-

Dynamic coefficient δ for the Uniform distribution of support stiffness $k_{b,j}$, case 1 Tab. 3

Track B1	$k_{b,j} \in < 60.10^6 - 100.10^6$ N/m >					
	$\delta = \overline{Y}_{dyn}/Y_{st}$		$\delta = (\overline{Y}_{dyn} + \sigma_y)/Y_{st}$		$\delta = (\overline{Y}_{dyn} + 2\sigma_y)/Y_{st}$	
	20 m/s	50 m/s	20 m/s	50 m/s	20 m/s	50 m/s
Rail Deflection $Y = w$	1.03	1.15	1.18	1.33	1.33	1.51
Sleeper-ballast Force $Y = P_{s-b}$	1.01	1.14	1.17	1.5	1.32	1.50

Dynamic coefficient δ for the Uniform distribution of support stiffness $k_{b,j}$, case 2 Tab. 4

Track B1	$k_{b,j} \in < 60.10^6 - 120.10^6$ N/m >					
	$\delta = \overline{Y}_{dyn}/Y_{st}$		$\delta = (\overline{Y}_{dyn} + \sigma_y)/Y_{st}$		$\delta = (\overline{Y}_{dyn} + 2\sigma_y)/Y_{st}$	
	20 m/s	50 m/s	20 m/s	50 m/s	20 m/s	50 m/s
Rail Deflection $Y = w$	1.06	1.20	1.25	1.43	1.44	1.67
Sleeper-ballast Force $Y = P_{b-s}$	1.00	1.14	1.19	1.38	1.39	1.62

Dynamic coefficient δ for the Gaussian distribution of the support stiffness $k_{b,j}$, case 1 Tab. 5

Track B1	$\overline{k}_b = 80.10^6$ N/m; $V_k = 0.316$					
	$\delta = \overline{Y}_{dyn}/Y_{st}$		$\delta = (\overline{Y}_{dyn} + \sigma_y)/Y_{st}$		$\delta = (\overline{Y}_{dyn} + 2\sigma_y)/Y_{st}$	
	20 m/s	50 m/s	20 m/s	50 m/s	20 m/s	50 m/s
Rail Deflection $Y = w$	1.08	1.21	1.30	1.47	1.51	1.73
Sleeper-ballast Force $Y = P_{s-b}$	1.00	1.14	1.23	1.41	1.47	1.69

Dynamic coefficient δ for the Gaussian distribution of the support stiffness $k_{b,j}$, case 2 Tab. 6

Track B1	$\overline{k}_b = 80.10^6$ N/m; $V_k = 0.316$					
	$\delta = \overline{Y}_{dyn}/Y_{st}$		$\delta = (\overline{Y}_{dyn} + \sigma_y)/Y_{st}$		$\delta = (\overline{Y}_{dyn} + 2\sigma_y)/Y_{st}$	
	20 m/s	50 m/s	20 m/s	50 m/s	20 m/s	50 m/s
Rail Deflection $Y = w$	1.14	1.31	1.44	1.67	1.74	2.04
Sleeper-ballast Force $Y = P_{s-b}$	1.00	1.14	1.29	1.52	1.58	1.90

ness can not be ignored, in particular for the higher vehicle speed, see Tab.3 ÷ 6. The results obtained confirm that the large values standard deviations of support stiffness can be one of the important factors causing an intensive dynamic response of the track components.

6. Conclusions

The response of a railway track that includes uncertainties in the vertical track supports stiffness subjected to a moving railway vehicle (the locomotive of the type E 499 / 85 t) is solved by the finite element method and time-step integration. The computer program developed can incorporate most rail-track parameters and irregularities of the track structure and is suitable for low and mid frequency analyses of the problem. In this study only the variability of vertical track stiffness is considered to be a random input quantity and the rest input parameters are considered deterministic ones, i.e. the simulation passages of the locomotive E 499 (85 t) were made on the track without irregularities.

Monte Carlo simulation was applied for these cases to estimate the dynamic track response to variations of the subgrade stiffness that was simulated as a stationary randomly distributed ballast stiffness with a standard uniform distribution and a normal distribution. The herein presented simulation results of the dynamic interaction are concerned in the low and mid frequencies, say 0 – 200 Hz, and they are applied to the track with the stiffness type (B1).

The dynamic amplification resulting from the simulated passage of a vehicle over the simulated track section can be calculated as the ratio of the maximum dynamic response Y_{dyn} (deflection w, bending moment M, etc.) to the static response Y_{st} on a given track stiffness level.

Some obtained results can be summarised as follows:
- The dynamic response results due to the tracks with the constant stiffness of supports (deterministic cases) show a low dynamic amplification $\delta = 1{,}05 - 1{,}2$ for the track response $Y = (w, P, M$, etc.) in relation to the vehicle speed c.

- The dynamic response due to the stationary randomly distributed stiffness of supports $k_{b,j}$ with the standard uniform and normal distribution follows the results of the static analysis and shows how the vehicle speed influences the track response. In these cases the effect of stochastic rail support stiffness can not be ignored, in particular for higher vehicle speeds. While the mean value of the response amplitudes and $\overline{Y}$ the corresponding dynamic coefficients δ attain no high values for these cases, the individual response amplitudes Y can attain values that can not be ignored. Thus, the expected values of the dynamic coefficient δ may be expected form the histograms of the amplitudes of a quantity $Y_{dyn(rand)}$.
- The standard deviations of support stiffness σ_k is an important factor affecting the dynamic response on a given level of support stiffness. For example, the maximum dynamic amplitudes of a quantity $Y_{dyn(rand)}$ for the track of the type (A) and (E) can differ nearly by 100%. Generally we can state that the dynamic track response with a low support stiffness is more sensitive than the track with a higher stiffness.

References

[1] FRÝBA, L.: *Vibration of solids and structures under moving load.* Academia Praha, 1973.
[2] KNOTHE, K., GRASSIE, S. L.: *Modelling of railway track and vehicle/track interaction at high frequencies.* Vehicle System Dynamic, 22 (1993).
[3] MORAVČÍK, M.: *Experience in Railway Track Testing for Validation of Theoretical Dynamic Analysis,* Communications – Scientific Letters of the University of Zilina, EDIS ŽU 1/99.
[4] MORAVČÍK, M.: *Vertical track stiffness in service conditions (in Slovak).* Technical report for the Slovak Railways. University of Žilina, 1996, 148 p.
[5] MORAVČÍK, M., MORAVČÍK, M.: *Track mechanics I* (300 p), II 320 p), III 220 p), EDIS Žilina, 2002.
[6] SIČÁR, M.: *Vehicle-track interaction concentrated to the track response (in Slovak).* PhD Thesis, University of Žilina, 1996, 180 p.

https://doi.org/10.26552/com.C.2004.3.17-21

Peter Koteš – Josef Vičan *

MUTLI-ELEMENT SYSTEM RELIABILITY USING MARKOV CHAIN MODEL

Up to now our researches have focused on determining the existing bridge element reliability level. However, the real structures occurring in practice are not just one-element structures, but they are a set of multiple elements with various signification of single element in structure. On this account, current research activities were focused on determining multi-element structure reliability level. In the presented paper, the steel grid system with m-elements subjected to bending was considered. The Markov chain models were used to calculate structure reliability. The results are compared with analytic solution of system reliability. Analogously, the degradation of material properties and its influence on reliability of overall multi-element grid system was considered.

1. Introduction

In the frame of research activities of the Department of Structures and Bridges, the increased attention was concentrated on determining the reliability level for evaluation of existing bridge structures. The reliability level, which respects the positive influence of new information achieved by regular inspection of existing bridges, was determined using a probabilistic theory. The positive result of inspection is a condition for survival of a structure in the remaining lifetime. It means that any component of the structure has not exceeded any limit states until the inspection time. The reliability level depends on time of inspection and on a planned remaining lifetime of bridges [1], [2]. The values of a modified reliability level, which are expressed by a failure probability P_{ft} resp. reliability index β_t, were used to specify partial safety factors for actions and material properties in the partial safety factors method.

Whereas the reliability level was deduced for one-element structure, nowadays, further possibility of reliability level specification considering multi-element system is observed. The model of multi-element structures more correctly describes the real structures. In current approaches, the series or parallel systems or their mutual combinations are elaborated. Moreover, it is assumed that elements of a system fail independently of each other. The details can be found in [3]. However, the real bridge structure is not either one of these theoretical models in most cases, therefore, the well-turned formulation of a multi-element system reliability is found.

In the theoretical approach, the steel grid system with *m*-elements subjected to bending was considered. The reliability of the grid system is defined by Markov chains model, which describes the multi-element system preferably compared to analytic solution.

The basic idea of theoretical approach and the results of parametric study are presented in the paper. The influence of material degradation on the change of a multi-element system reliability level in time in comparison with one-element system is also taken into account.

2. The reliability of a multi-element structure

In the approach, the grid bridge structure consisting of *m*-elements is considered. Each of the elements has the resistance R_j (for $j = 1 \ldots m$). It is assumed that the single resistances R_j of the elements are independent normally distributed random variables $N(m_j, s_j)$, (for $j = 1 \ldots m$). Moreover, the normally distributed random variables $N(\mu,\sigma)$ loads effects S_i have effected on the bridge structure. The load effects S_i occur in succession but randomly in time and their occurrence is considered as a random variable having Poisson distribution with parameter $\lambda(t)$, $\lambda(t) > 0$ for $t \in (0,T)$. The load is distributed to all system elements and the load effects $E_{ij} = a_{ij} \cdot S_i$ are induced. The following marginal conditions are valid for the factor a_{ij}

$$-1{,}0 \le a_{ij} \le 1{,}0, \text{ and for a grid system } \sum_{j=1}^{m} a_{ij} = 1{,}0$$

shall be fulfilled. (1)

The load effects E_{ij} are normally distributed random variables with the mean value $\mu_j = a_{ij} \cdot \mu$ and the standard deviation $\sigma_j = a_{ij} \cdot \sigma$.

The failure probability P_{fj} of *j* element of the *m*-elements system subjected to a Poisson live load process with intensity λ can be expressed according to [4] by a formula

$$P_{fj} = \int_{-\infty}^{\infty} \phi\left(\frac{a_{ij} \cdot x - m_j}{s_j}\right) \cdot f_{max}(x)dx \,. \quad (2)$$

The failure probability P_{fjk}, when the m-elements system fails due to the failure of element j together with element *k*, can be expressed by the relation

* **Peter Koteš, Josef Vičan**
Department of Structures and Bridges, Faculty of Civil Engineering, University of Žilina, Komenského 52, 010 26 Žilina
Tel. +421-41-41868, Fax. +421-41-41868, E-mail kotes@ fstav.utc.sk, vican@fstav.utc.sk

$$P_{f,ijk} = \int_{-\infty}^{\infty} \phi\left(\frac{a_{ij} \cdot x - m_j}{s_j}\right) \cdot \phi\left(\frac{a_{ik} \cdot x - m_k}{s_k}\right) \cdot f_{max}(x)dx \,. (3)$$

In the case of a failure of any system element, the failure probability P_f of the system is expressed by a formula

$$P_f = 1\left[\left(\int_{-\infty}^{\infty} \prod_{j=1}^{m} \left(1 - \phi\left(\frac{a_{ij} \cdot x - m_j}{s_j}\right)\right) \cdot \right.\right.$$

$$\left.\left. \cdot f_{max}(x)dx\right) + e^{-L(t)}\right], \quad (4)$$

where $f_{max}(x) = F_{max}(x) \cdot \frac{L(T)}{\sigma} \cdot \varphi\left(\frac{x - \mu}{\sigma}\right)$, (5)

and $F_{max}(x) = \sum_{n=0}^{\infty}\left[\phi\left(\frac{x - \mu}{\sigma}\right)\right]^n \cdot \frac{L(T)}{\sigma} \cdot e^{-\left(L(T)\left[1 - \phi\left(\frac{x-\mu}{\sigma}\right)\right]\right)}$ (6)

The details of the above-described mathematical model can be found in [4] or [5]. Then, the reliability indices of any elements and whole system can be determined as follows

$$\beta_j = -\phi^{-1}(P_{fj}), \text{ respect. } \beta = -\phi^{-1}(P_f). \quad (7)$$

The probability of no system failure due to any loads is also included in the relation (4).

3. Dependent failure of elements

In the standard approaches for multi-element systems it is assumed that the elements of a system fail independently of each other. It means that the failure of the one element does not influence the failure of another element. This incorrect assumption was demonstrated in paper [6]. Therefore, the approach using dependent failure of elements, which better describes the multi-element grid system, was found.

It was considered in the mathematical model that the failure of the system comes into being when the elements *j* and *k* fail, but in this case the elements of system fail dependently of each other. It means that the failure of one element influences the failure of another element. The five-element grid system was considered in the parametric study. This system represents the plate girder bridge subjected to bending.

The random variables resistances R_j of the elements were considered as normally distributed $N(m_j, s_j)$ with parameters m_j = = 159.66 MPa and s_j = 12.993 MPa, for j = 1, 2, 3, 4, 5.

The random variables load effects S_i were also considered as normally distributed with parameters μ = 125.50 MPa and σ = = 30.00 MPa. The load effects S_i are divided to individual elements of the system by proportions p_i(%). The values of the proportions p_i represent transversal load distribution, for which determination the model of rigid transversal beam was used. The lifetime of the system T = 80 years and the constant parameter $\lambda(\tau)$ = 0.0125 of the failure rate were considered. It means that the most loaded element of the system was designed for a reliability level given by the reliability index β_j = 3.80.

The problem with dependent failure of elements was solved by means of changing proportions p_i of load effects on elements. The same load effects S_i shall be carried by $m-1$ elements system after failure of one element without any changes of remaining elements resistances R_j and any changes of load positions.

In the case of five-element system, the proportions p_i are equal to (see Fig. 1 a) p_1 = 60 %, p_2 = 40 %, p_3 = 20 %, p_4 = 0 % and p_5 = −20 %.

Then, it was considered that the most loaded element (p_1 = = 60 % - outer beam) had failed. New proportions pi were determined from the new four-element system (see Fig. 1 b) p_2 = 100 %, p_3 = 50 %, p_4 = 0 % and p_5 = −50 %.

After failure of the next most loaded element (now, it is p_2 = = 100 % - outer beam of the four-element system), new proportions pi were considered for the new three-element system (see Fig. 1 c) p_3 = 183.333 %, p_4 = 33.333 % and p_5 = −116.667 %.

The results of the parametric study are presented in Tab. 1

The failure probability P_f and the reliability index β of the five-element system after failure first, second and third element. Tab. 1

Failure of element	Failure probability P_f	Reliability index β
1	7.20269 E-05	3.801
1 and 2	1.33782 E-01	1.109
1, 2 and 3	5.90448 E-01	-0.228

In the case of independent failure of elements, proportions p_i of the load effects on elements are not changed, so the second most loaded element takes just 40 % (p_2 = 40%) from the loads (see Fig. 1 a) . Then using the formula (3), the failure probability of the system is influenced by the failure probability of the second most load element and it is equal to $P_f = 1.10^{-12}$ [6]. Such probability of failure is unrealistic for real structures.

From the results given in Tab. 1 using the dependent failure of elements, it can be seen that the reliability level is influenced by the most loaded element (the most faithless element) of the five-element system. After its failure, the reliability level of the system given by the reliability index β strongly decreases (β = 3.80 → β = 1.11 - difference is about 71 %). So big loss of the reliability level and the failure of the most loaded element are inadmissible for real grid structures. Moreover, the failure of the next element decreases the reliability level to β = −0.23 corresponding to the failure probability of P_f = 0.59.

However, the disadvantage of the analytic solution is the fact that the failure of two or more elements given by the formula (3) is able to come into being only together. But this failure in reality

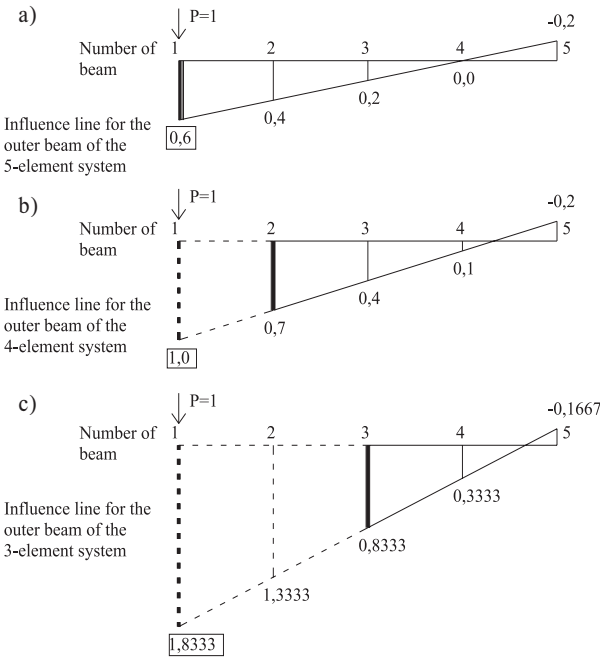

Fig. 1 Dependent failure of five-element system – successive changing load distribution after failure of the elements

is able to come into being by steps – the first element fails and then the second element is able to fail, not just together. Therefore, a more correct approach to define the reliability level or the failure probability of m-element system was found.

4. Approach using homogeneous Markov chains model

The multi-element system is observed at time steps (periods) $k = 1, 2, 3 \ldots$. The system is assumed to have $(r+1)$ possible states numbered $j = 0, 1, 2 \ldots r$. The system is in state i at time k with probability $p_k(i)$. Many systems have transitions that can be approximately described by a stochastic process with the Markov property. If the probability $p_k(i)$ depends just on the state in time $k-1$ (not on states in time $k-2$, $k-3$, ...) for every state i, the system is called Markov chains. Given that a system is in state i at time k, the future states $(i+v)$ do not depend on the previous states $(u < i)$. In other words, when its present state is known, the probability of any particular future behaviour of the process is not altered by additional knowledge about its past behaviour. Moreover, $P(i,j) = p(i,j)$ is the transition probability that the system is in state j at time t if the system was in state i at time $(t-1)$. It is homogeneous Markov chain model, if the probability $P(i,j)$ does not depend on time t. The matrix of array $P(i,j)$, for $i,j = 0, 1, \ldots r$, is called the matrix of homogeneous system.

Next, $P_m(i,j)$, for $i,j = 0, 1, \ldots r$, is the probability that the Markov chain is in time $t+m$ in state j if it was in time t in state i (do not depend on time t). So, $P_m(i,j)$ is called as the transition matrix after m-steps and following relation is valid

$$P_m(i,j) = \sum_{k=1}^{r} P_{m-1}(i,j) \cdot P(k,j) = \sum_{k=1}^{r} P(i,j) \cdot P_{m-1}(k,j),$$

for $i,j = 0, 1, \ldots r$. (8)

Owing to a successive institution it can be seen that

$P_m(i,j) = P^m(i,j)$, it means m-exponent of transition matrix $P(i,j)$. (9)

Firstly, m-element system without degradation was considered in the approach. One year was given as a time step. The states of the system were determined by a number of possible failed elements with respect of their location and their significance in the structures. It means $m+1$ states for m-element system. The transition probabilities between individual states can be solved analytically using the formulae (2), (3) and (4). So, the development of the probabilities of single states in time as a chosen member of the transition matrix $P_m(i,j)$ after m-steps is observed.

In the parametric study, the same parameters as in the analytic solution were used.

The values of probabilities for lifetime T are achieved by multiplying the transition matrices. The results of the parametric study are shown in Fig. 2 and in Fig. 3. The reliability index development of the most loaded element in time t is shown in Fig. 2 in comparison with analytic solution and time development of the same single element reliability. The reliability index development of the second most loaded element of the five-element system in time t is shown in Fig. 3 in comparison with an analytic solution.

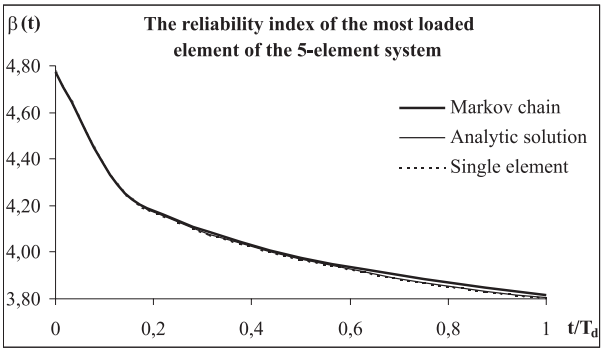

Fig. 2 The change of the most loaded element reliability index of the five-element system in time

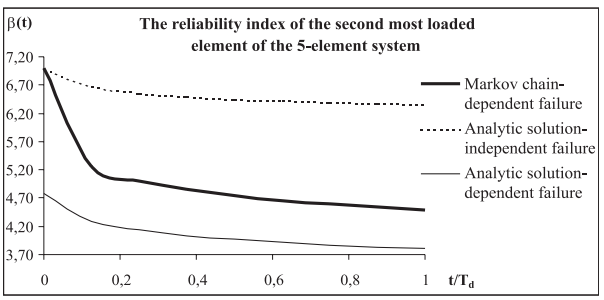

Fig. 3 The change of second element reliability index of the five-element system in time

From the achieved results it can be seen that the Markov chains model describes the real system reliability more appropriately due to considering the dependent failure of elements (and the failure of elements) in stages (Fig. 3). Moreover, it can be seen that the reliability level of the system is significantly influenced by reliability of the most loaded element (the most faithless element) so that the element could be investigated without considering the system (Fig. 2).

5. Approach using inhomogeneous Markov chains model

If the probability $P(i,j)$ depends on time t, the process is called inhomogeneous Markov chain model and the denotation $P(i,j) = P_t(i,j)$ can be established. The inhomogenity of the transition between stages can be caused by degradation of material. The resistance $R_j(t)$ changes in time using material degradation, so, the transition probability given by the formulae (2), (3) and (4) is also change in time. On this account, the transition matrix $P(i,j)$ is not constant in time between stages, but these transition matrices between single stages have to be solved in particular time. Now, the transition matrix after m-steps $P_m(i,j)$ is achieved by multiplying the matrices $P_t(i,j)$.

The steel grid five-element system was considered in the parametric study. The corrosion of the I-steel beams flanges was considered as degradation of the material and the resistance $R_j(t)$. The corrosion is a time dependent factor that influences not only resistance $R_j(t)$, but also influences the flexural stiffness and the redistribution of the moments over the system. The corrosion model of Albrecht and Naeemi [7], which was successfully applied in works [8], [9], given by the formula

$$d_{corr} = A_0 \cdot t^{A_1}. \tag{10}$$

was used.

The dependence (10) was estimated by mathematical approximation of values, which were achieved by measurement of flange thickness decrease in case of the real steel bridge I – beams. The constants A_0, A_1 take into account the location of the beams in the grid system and the following values were recommended

1. $A_0 = 0.13218$, $A_1 = 0.595478$ for the outer girder of the grid,
2. $A_0 = 0.12151$, $A_1 = 0.568652$ for the second outer girder of the grid,
3. $A_0 = 0.03015$, $A_1 = 0.690171$ for the internal girder of the grid.

The geometric and material parameters are considered as random variables quantities and the denotation of the geometric parameters are shown in Fig. 4. The values of random variables are shown in Tab. 2.

Time dependent resistance $R_j(t)$ of the elements subjected to bending is given by the following formulae

$R_j(t) = f_y \cdot W(t)_{pl,y}$, for cross-section of the class 1 and 2, (11)
$R_j(t) = f_y \cdot W(t)_{el,y}$, for cross-section of the class 3, (12)

Values of random variables Table 2

Variable	I 800		Distribution function
	m	s	
f_y [MPa]	281.00	27.80	Empirical
b_f [mm]	250.00	2.00	Normal.
t_f [mm]	25.525	0.925	Normal
d [mm]	750.00	2.00	Normal
t_w [mm]	10.210	0.37	Normal

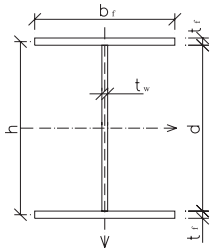

Fig. 4 Geometrical parameters of the observed cross-section

where f_y is the random variable yield strength,
$W(t)_{pl,y}$ is random variable time dependent plastic section modulus,
$W(t)_{el,y}$ is random variable time dependent elastic section modulus.

Time dependent plastic section modulus for cross-section of class 1 or 2 taking into account the corrosion of the flanges is described by the formula

$$W(t)_{pl,y} = 0{,}25 \cdot t_w \cdot (d + A_0 \cdot t^{A_1})^2 + \\ + b_f \cdot h \cdot (t_f - A_0 \cdot t^{A_1}), \tag{13}$$

and similarly, time dependent elastic section modulus for cross-section of class 3 taking into account the corrosion of the flanges is describ-ed by the following formula

$$W(t)_{el,y} = \left[\frac{t_w \cdot (d + A_0 \cdot t^{A_1})^2}{6} + b_f \cdot h^2 \cdot (t_f - A_0 \cdot t^{A_1}) \right] / \\ / \, [\mathrm{d} + 2 \cdot (t_f - A_0 \cdot t^{A_1})], \tag{14}$$

The numerical application of the above-mentioned process of time dependent resistance calculation considering steel T-beam flanges corrosion was carried out using simulation by Monte Carlo method. For other usage the results of simulation were approximated by mathematical relations

$m_R(t) = m_R(t_0) \cdot e^{p_1 \cdot t^{p_2}}$, for the mean value of resistance (15)
$s_R(t) = s_R(t_0) \cdot e^{p_3 \cdot t^{p_4}}$, for the standard deviation of resistance (16)

where $m_R(t_0)$, $s_R(t_0)$ are the mean value and the standard deviation of resistance in time $t=0$,
p_1, p_2, p_3, p_4 are constants achieved by mathematical approximation.

Values of constants p_1, p_2, p_3, p_4 for I-beam Table 3

I-beam	Parameters					
	$m_R(t_0)$	p_1	p_2	$s_R(t_0)$	p_3	p_4
I 800 – 1(A0,A1)	1792.906	−0.00347	0.63309	186.036	−0.00205	0.72949
I 800 – 2(A0,A1)	1792.906	−0.00314	0.60814	186.036	−0.00169	0.72502
I 800 – 3(A0,A1)	1792.906	−0.00055	0.80400	186.036	−0.00003	1.49558

The values of constants p_1, p_2, p_3, p_4 and $m_R(t_0)$, $s_R(t_0)$ for I-beams taking into account the location of beam in grid system given by constants A_0, A_1 are shown in Tab. 3.

Time dependent resistance given by (11) or (12) described by the mean value and the standard deviation enters into relations (2), (3) and (4). Now, it is able to solve the transition probabili-

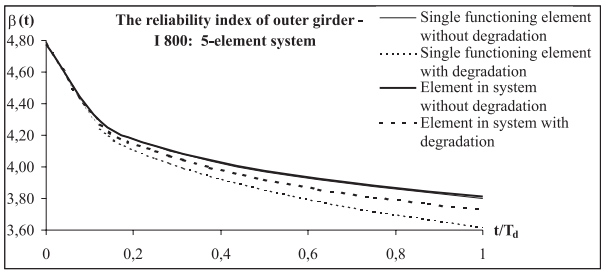

Fig. 5 The change of reliability index of the element in time

ties $P_t(i,j)$ depending on time steps due to degradation of resistance. The transition matrix after m-steps $P_m(i,j)$ is achieved by multiplying the different matrices $P_t(i,j)$.

The comparison of the results achieved by considering the same element (outer girder of the grid) single functioning and in the five-element system and considering corrosion or without corrosion is shown in Fig. 5.

6. Conclusions

From the results it can be seen that the reliability level of the system is significantly influenced by the most loaded element (generally, it is the outer girder of the grid system). Therefore, the element can be investigated without considering the system if corrosion is neglected. It means that we can focus just on one most loaded element in the system and investigate it without considering the whole system (see Fig. 2). On this account, the ultimate limit state of the overall system is defined by a failure of the most loaded element However, if the corrosion of steel I-beam flanges is considered, the new lower reliability indices are achieved (Fig. 5). By comparison of the result, when the element under corrosion is considered and investigated in the system, the element has a higher reliability level ($\beta = 3.73$) at the end of lifetime T against the same element considered as just single functioning ($\beta = 3.62$). The difference is about 9.6 %. This difference was achieved by changing flexural stiffness and the redistribution of the actions over the system.

In the case of an element with degradation, it is more correct to investigate the element in the system due to a possible higher reliability level of the element and the overall system. The conclusion is very important from the viewpoint of a reliability-based evaluation of existing structures where the effects of degradation are much more significant.

Acknowledgements

The research work presented in this paper has been supported by the Slovak Grant Agency, Grant No. 1/0344/03.

References

[1] KOTEŠ, P., VIČAN, J.: *Reliability of Concrete Structure Members under Corrosion Attack.* Proceedings of a 19-th International conØference 'Durability Design and Fracture Mechanics of Concrete Structures', Minsk, 2003, 38–46.
[2] VIČAN, J., KOTEŠ, P.: *To Evaluation of existing Railway Bridges.* Inžinierske stavby, roč. 50, 2002, č.4, str. 19–22.
[3] HØYLAND, A., RAUSAND, M.: *System reliability theory – Models and statistical methods.* John Wiley and sons., 1994.
[4] KOTEŠ, P., SLAVÍK, J., VIČAN, J.: *Reliability of multi-element bridge system.* Proceedings of VII. Scientific Conference with International Participation, Košice 2002, p. 121–124.
[5] VIČAN, J., SLAVÍK, J.: *Reliability level differentiation for existing bridge member.* Proceedings of International Symposium "Theoretical and Technological Problems of Steel Structures", Bratislava 1999, p. 151–156.
[6] KOTEŠ, P., SLAVÍK, J., VIČAN, J.: *Multi-element bridge systems reliability.* Proceedings of International Conference "Reliability and diagnostics of transport structures and means", Pardubice 2002, p. 173–179.
[7] ALBRECHT, P. – NAEEMI, A. H.: *Performance of Weathering Steel in Bridges.* National Cooperative Highway Research Program, Report 272, 1984.
[8] ESTES, A. C. – FRANGOPOL, D. M.: *System Reliability for Condition Evaluation of Bridges.* IABSE Workshop "Evaluation of Existing Steel and Composite Bridges", Lausanne 1987, p. 47–56.
[9] FRANGOPOL, D. M. – ESTES, A. C.: *Lifetime Bridge Maintenance Strategies Based on System Reliability.* Structural Engineering International 3, 1997, p. 193–198.

https://doi.org/10.26552/com.C.2004.3.22-27

kamUNikácie
COMMUNICATIONS

Patrik Kotula – Štefan Zemko *

SHEAR CAPACITY OF RC BEAMS STRENGTHENED WITH EXTERNALLY BONDED FRP COMPOSITE SHEETS

The strengthening of concrete structures using fibre reinforced polymer (FRP) materials has become a growing area in the construction industry over the last few years. Valuable research work is going on all over the world.

This work is focused on theoretical, numerical and experimental analysis of the RC beam strengthened with a carbon fibre reinforced polymer (CFRP) sheet of the MBT-MBrace CF 640 type in a shear span of the RC beam.

The aim of this paper is to present a simple design approach of calculation of a CFRP sheet contribution to the shear capacity of the RC beams and to compare results with values obtained from numerical analysis based on the finite element method (FEM) with ATENA-2D program being employed and with experimental results.

The experiment confirms availability of CFRP sheets for shear strengthening of RC beams.

1. Introduction

Fibre-based composite materials (CM), often noted as fibre reinforced plastic (FRP), and their implementation in building industry are gaining on their popularity.

Low weight, flexibility, corrosion, magnetic and chemical resistance of the FRP materials are so much convincing that they are frequently used as an additional external reinforcement (e.g. lamella, sheet) or for strengthening of the RC beams, columns, slabs, walls, tunnels and soils, and in prestressed concrete. On the other hand, their cost is higher than the cost of common building materials.

Theoretical part is focused on mechanics of the uni-directional composite, on derivation of equations for further calculation of uni-directional composite properties in the fibre direction as well as in the transverse direction to fibres. The calculated values were used as material properties of CM to the numerical model. The ATENA-2D program based on FEM analyses, was used for numerical non-linear analysis.

Since the original work covers extended experiments, this paper presents only comparisons made on numerical and calculated values of the RC beams of one series. Additionally, a practical RC beam design approach with externally bonded carbon sheet will be introduced.

2 Experimental program

During experimental part, two different A and B series of three RC beams were prepared and tested (i.e., 3 beams of A series and 3 beams of B series) with 100 × 300 × 2700 mm.

The A series has an internal shear reinforcement (stirrups). RC beams of the first A series were loaded to 70% of shear resistance of the RC beam. Then, the corrupted beams were repaired (closing shear cracks) and strengthened by added external shear reinforcement.

The B series (Fig. 1) had no internal shear reinforcement since the traditional shear reinforcement was replaced by external bonding of the MBT-MBrace CF 640 (old designation S&P C Sheet 640) type. The main longitudinal reinforcement is of 2 ϕ 16 BST 500s. Four 700 mm carbon sheets of 150 mm width at the 250 mm axial distance were bonded in the shear area of the RC beams. The A4/B4 two-component epoxy resin was used for the bonding of carbon strips on concrete surface.

The epoxy resin has the following properties: compressive strength $f_{m,c}$ = 85 MPa; tensile strength $f_{m,t}$ = 35 MPa; modulus of elasticity E_{mk} = 9 000 MPa; Poisson's ratio ν = 0.37; ultimate elongation ϵ_{mu} = 0.0037.

Properties of the MBT-MBrace CF 640 sheet are following: modulus of elasticity $E_{f,k}$ = 640 GPa; Poisson's ratio ν = 0.2; tensile strength f_{fy} = 2 650 MPa; ultimate elongation ϵ_{fu} = 0.004; theoretical thickness t_f = 0.190 mm.

For design, the maximum strain of carbon fibers shall not exceed 0.2 ~ 0.3 %. Partial safety factor γ_{sf} was considered γ_{sf} = = 1.2 for wet lay-up installation technique [1].

For concrete strength verification, 12 cubes with dimensions 150 × 150 × 150 mm were made. Compressive strength after 28 days was determined on 3 cubes. On 9 remaining cubes after following 213 days compression strength was determined.

* [1]Patrik Kotula, [2]Štefan Zemko
[1]Department of Building Constructions and Bridges, Faculty of Civil Engineering, University of Žilina, Komenského 52, 010 26 Žilina, Slovakia.
E-mail: kotula@fstav.utc.sk
[2]Osloboditeľov 20, 010 01 Žilina

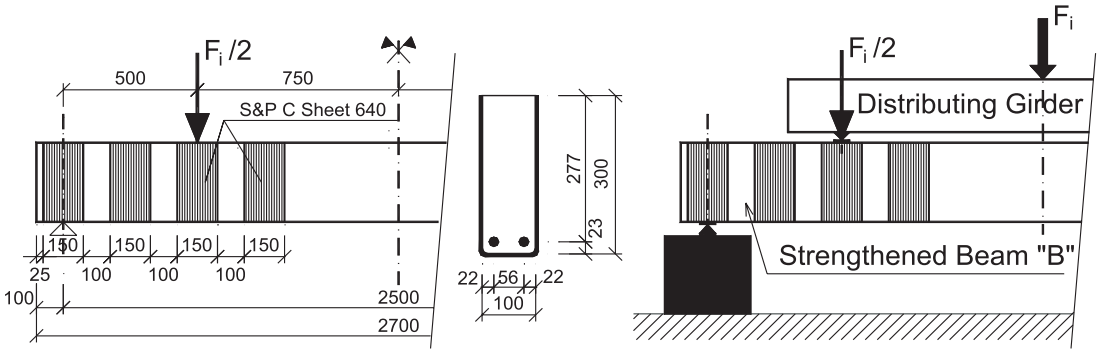

Fig. 1 RC beams - B Series

According to the compressive test, properties of the concrete are: f_{ck} = 46.652 MPa; f_{cd} = 46.652/1.5 = 24.881 MPa; E_{cm} = = 33 870.79 MPa; $f_{ctk,0.05}$ = 2.345 MPa.

3. Theoretical analysis

Uni-directional composite laminate or sheet consists of two components: carbon fibres and epoxy resin create an anisotropic material with different stress-strain law in the fiber direction and in the transverse direction to fibers (Fig. 2).

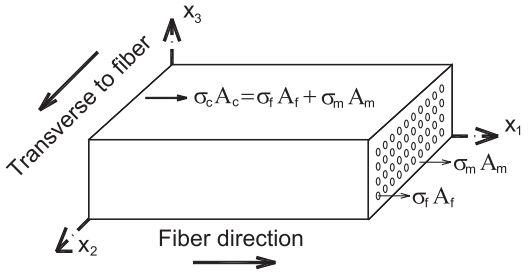

Fig. 2 Uni-directional composite laminate or sheet - stress in the fibre direction

Typical properties of the composite laminate or sheet:
- tensile strength in x_1,
- compressive strength in x_1,
- tensile strength in x_2,
- compressive strength in x_2,
- shear strength in x_{12}.

Unitary volume of composite laminate or sheet V_c is given by the sum of fibre volume V_f and matrix volume V_m, Eq. (1):

$$V_c = V_f + V_m = 1 \tag{1}$$

Uni-direcftional composite laminate has two possible arrangements of fibers: square array of fibers or hexagonal array of fibers (Fig. 3).

The assumption that axial x_1 strain is the same for laminate, carbon fiber and matrix is used for determination of longitudinal

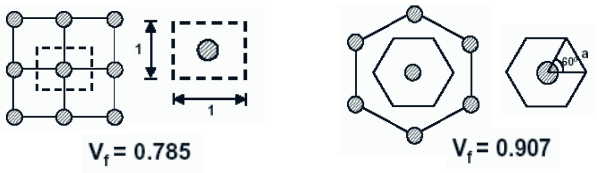

Fig. 3 Square and hexagonal array of fibres in a cross section of the composite laminate or sheet

modulus of elasticity E_1 of CM and Poisson's ratio ν_{12} and then the rule of mixtures:

$$E_1 = E_c = E_f V_f + E_m(1 - V_f) \tag{2}$$

$$\nu_{12} = \nu_f V_f + \nu_m(1 - V_f) \tag{3}$$

Providing that the transverse strain in laminate is the same as in matrix and fibres, so-called the rule of reciprocity can be used for determination of E_2:

$$\frac{1}{E_2} = \frac{V_f}{E_f} + \frac{(1 - V_f)}{E_m} \tag{4}$$

The assumption that shear stress is the same for laminate, carbon fiber and matrix is used for determination of G_{12}:

$$\frac{1}{G_{12}} = \frac{V_f}{G_f} + \frac{(1 - V_f)}{G_m} \tag{5}$$

Simple assumptions that arrangement of fibers in composite is ideal are is for derivation of formulas (4) and (5). Since the real composite laminate or sheet has not ideal arrangement of fibers, it is more appropriate to use a more precise one for determination of transverse properties of uni-directional CM according to [2]:

$$E_2 = E_m \frac{1 + \xi_1 \eta_1 V_f}{1 - \eta_1 V_f};\ \eta_1 = \frac{E_f - E_m}{E_f + \xi_1 E_m};$$

$$\xi_1 = 2 \text{ - for fiber of circular section} \tag{6), (7}$$

$$G_{12} = \frac{G_m 1 + \xi_2 \eta_2 V_f}{1 - \eta_2 V_f};\ \eta_2 = \frac{G_f - G_m}{G_f + \xi_2 G_m};\ \xi_2 = 2 \tag{8), (9}$$

Ultimate tensile strength $F_{1,f}$ in the x_1 direction is determined from the ultimate elongations of fibers and used epoxy matrix, as shown in fig. 4.

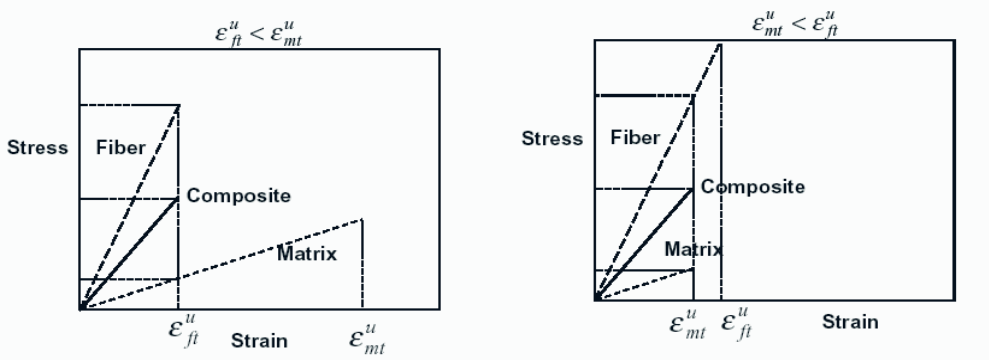

Fig. 4 Stress-strain diagram of CM for determining ultimate tensile strength $F_{1,t}$ depending on ϵ_{ft}^u and ϵ_{mt}^u.

$$F_{1,t} = E_f \epsilon_{ft}^u V_f + E_m \epsilon_{ft}^u (1 - V_f) \text{ if } \epsilon_{ft}^u < \epsilon_{mt}^u \quad (10)$$

$$F_{1,t} = E_f \epsilon_{mt}^u V_f + E_m \epsilon_{mt}^u (1 - V_f) \text{ if } \epsilon_{ft}^u > \epsilon_{mt}^u \quad (11)$$

Material properties of uni-directional composite sheets consisting of two components (MBT-MBrace CF 640 and epoxy resin A4/B4), obtained from Eq. (2), (3), (6)–(9) and (11), are presented in table 1.

Properties of uni-directional composite sheets Table 1

Fiber array in cross section	E_1 [MPa]	E_2 [MPa]	ν_{12}	$F_{1,t}$ [MPa]
Square ($Vf = 0.785$)	504 335	91229.93	0.236	1916.473
Hexagonal ($Vf = 0.907$)	581 317	189393.98	0.216	2029.005

4 Design shear equation

The nominal shear strength $V_{R,Rd}$ is expressed as the sum of three contributions given by the concrete ($V_{c,Rd}$), the shear steel reinforcement ($V_{s,Rd}$) and the FRP reinforcement ($V_{KM,Rd}$):

$$V_{R,Rd} = V_{c,Rd} + V_{s,Rd} + V_{KM,Rd} \quad (12)$$

The first two terms of Eq. (12) according to Eurocode 2 [3] may be rewritten:

$$V_{c,Rd} = V_{Rd1} = [\beta \tau_{Rd} k(1{,}2 + 40\rho_1) - \\ - 0{,}15(N_{sd}/A_C)] b_w d \quad (13)$$

$$V_{s,Rd} = V_{wd} = \rho_{sw} f_{ywd} b_w (0{,}9d) \quad (14)$$

The design approach based on fracture of the FRP sheet is quite similar to the approach used to compute the contribution of steel shear reinforcement. Triantafillou [4] has presented an equation expressing FRP sheet contribution based on the stress concentrations in the sheet:

$$V_f = \rho_f E_f \epsilon_{fe} b_w 0.9d(1 + \cot \beta)\sin \beta. \quad (15)$$

In our case, Eq. (15) may be rewritten:

$$V_{KM,Rd} = \rho_f E_{1,ef} \epsilon_{KM,ef} b_w 0.9d(1 + \cot \beta)\sin \beta. \quad (16)$$

where: $\rho_f = (2t_f w_f)/(s_f b_w)$ - is FRP shear reinforcement ratio,

β is the angle between the principal fiber orientation and longitudinal axis of the beam,

t_f is the thickness of the FRP sheet on one side of the beam,

w_f is width of the FRP strip,

b_w is width of the beam cross section,

s_f is spacing of the FRP strips,

$\epsilon_{KM,ef}$ is effective strain considered value 0.002 [1]

γ_{sf} is partial safety factor considered $\gamma_{sf} = 1.2$ of according to [1] for wet lay-up installation technique,

$E_{1,ef}$ je $E_1/1.2 = 420279$ MPa.

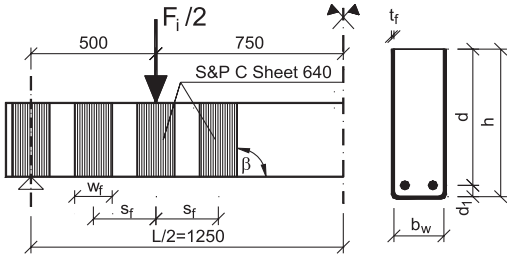

Fig. 5 Calculation of $V_{KM,Rd}$

5 Numerical analysis

Numerical analysis for non-linear FEM calculations of the RC corrupted constructions has been solved by means of the program ATENA-2D. For this analysis, making a half beam model with a sustained symmetry is sufficient (Fig. 6).

A material model of concrete "Concrete-Sbeta Material" derived from CEB-FIP MC 90 and other sources [5] was assigned to the 2D macro-elements of thickness 0.1 m. The main longitudinal reinforcement (2 ϕ 16 BST 500s) was modelled as uni-directional reinforcement element.

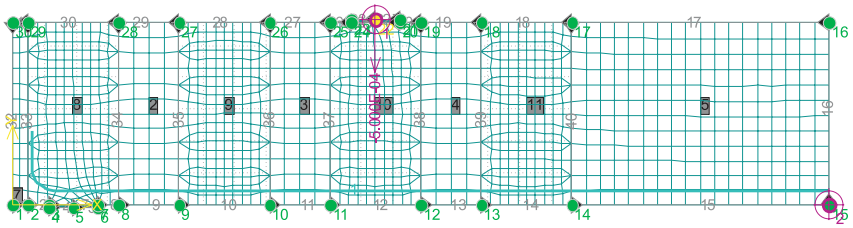

Fig. 6 Numerical model of the beam B series - ATENA-2D

In a good agreement with experiment, the model of composite sheet consists of two layers of smeared reinforcement in concrete arranged in defined strips (more densified net is depicted in Fig. 6). The first layer covers transverse properties of CM and the second layer the CM longitudinal properties of CM.

The CM material constants are presented in table 1. The volumes share of $V_f = 0.785$ (square arrangement) was used in this case. Stress-strain diagrams of concrete and CM, used in numerical analysis are shown in Fig. 8.

Non-linear calculation was run until the CM fibre rupture, i.e. until reaching the $F/2 = 64.25$ kN value (Fig. 9). The maximum shear crack on achievement of the fibre strain limit state was $w_{max} = 0.3198$ mm, which is higher than the limit crack width ($w_{lim} = 0.3$ mm) according to EC2.

6 Result comparison

From the non-linear FEM analysis it is clear that the most important for the ultimate shear capacity of the strengthened RC beam is the second ultimate state – the ultimate crack width. In table 2 there is a review of FEM calculated shear capacity values of strengthened and un-strengthened RC beams before achievement of the critical width of the shear crack $w_{lim} = 0.3$ mm.

Contribution of the CM sheets from the equation (16) is higher when compared to the experiment. It follows that there is a strong need to correct the equation (16) in order to take into account the CM strain and the CM transverse load in a laminated part of the cross section. This will be a focus of further study.

Of course, there are more different ways of the CFRP sheet calculation based on mechanics of failure by the CM delamina-

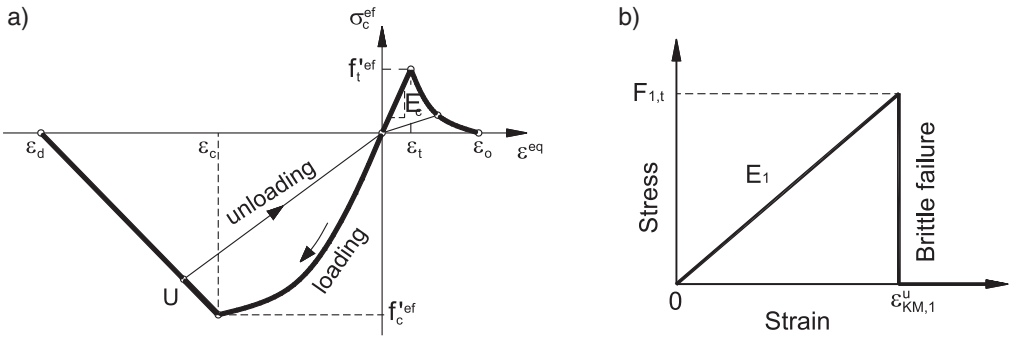

Fig. 8 Stress-strain diagrams used in ATENA-2D analysis: a) concrete, b) composite sheet in fibres direction

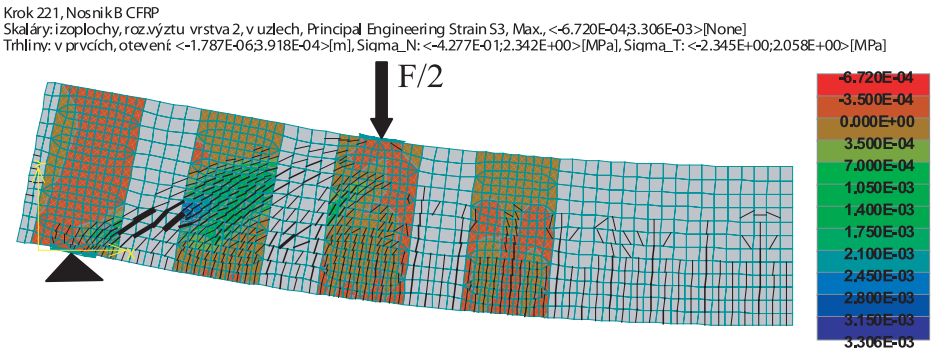

Fig. 9 Principal stress in composite sheets and development of shear and bending cracks obtained by the ATENA -2D

The review of the results from the test and numerical calculation Tab. 2

	V_{Rd1} (13) [kN]	V_{wd} (14) [kN]	$V_{KM,Ed}$ (16) [kN]	$V_{R,Rd}$ (12) [kN]	$V_{AT,1}$ no CFRP [kN]	$V_{AT,2}$ no CFRP w = 0.184 mm [kN]	$V_{AT,3}$ with CFRP [kN]	$V_{AT,4}$ with CFRP w = 0.298 mm [kN]	$V_{AT,5}$ with CFRP $\epsilon = 3.29.10^{-3}$ m [kN]	V_{exp} [kN]
B1	38.614	–	47.770	86.384	59.250	42.000	64.420	54.320	64.250	45.00
B2										61.75
B3										80.75

Relationships between measured and calculated contributions of the used CFRP sheet Tab. 3

	$V_{exp}/V_{R,Rd}$	$V_{exp}/V_{AT,1}$	$V_{exp}/V_{AT,2}$	$V_{f,exp}/V_{AT,3}$	$V_{f,exp}/V_{AT,4}$	$V_{f,exp}/V_{AT,5}$
B1	0.52	0.76	1.07	0.70	0.83	0.70
B2	0.71	1.04	1.47	0.96	1.14	0.96
B3	0.93	1.36	1.92	1.25	1.49	1.26

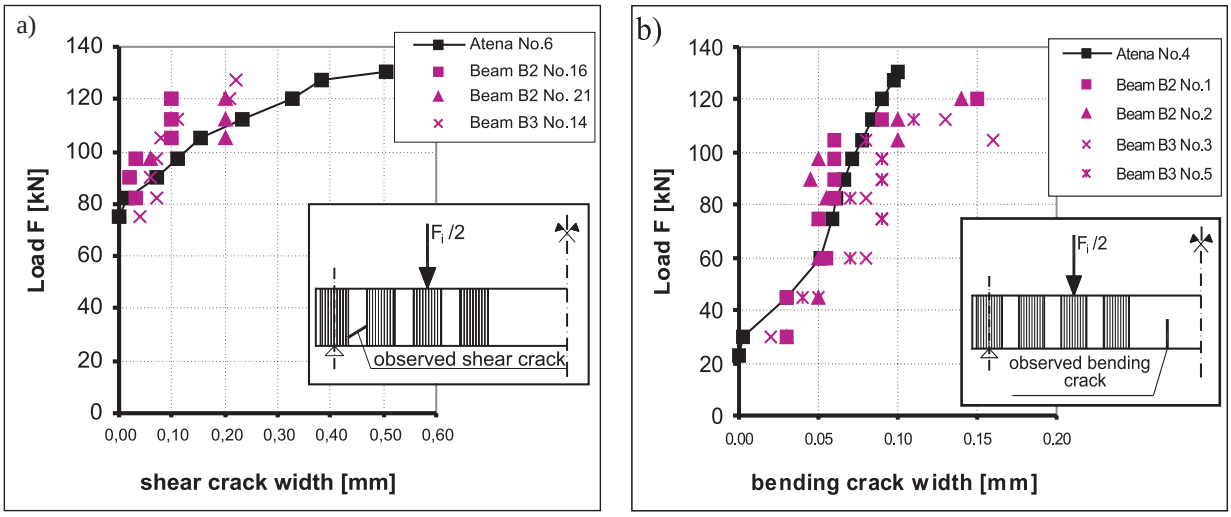

Fig. 10 Comparison of computed and measured widths of shear and bending cracks

tion from the concrete surface or by a combined effect of the CM delamination and rupture. These calculations give different $V_{KM,Rd}$ values from the values presented in this paper. A detailed comparison is offered in [6].

Fig. 10a shows a development of shear crack width No. 6 obtained by the ATENA-2D program and measured values from the B2 and B3 beams. No similar crack occurred in the B1 beam. Fig. 10b shows development of the bending crack width No. 4 obtained by the ATENA-2D and measured values from the B2 and B3 beams. Since the B1 beam was used only for testing purposes, its crack widths are not considered.

7 Conclusions

Conclusively, the externally bonded carbon sheet of the MBT-MBrace CF 640 type is suitable as additional reinforcement for shear strengthening of RC beams.

The RC beams used in the experiment were damaged by shear, i.e. by delamination of CM sheet from the concrete surface and consequent development of a critical shear crack. Only in one case of the B3 beam damage of the carbon sheet was a result of rupture.

Differences in obtained ultimate shear loads of the beams of the same series were caused by the quality of sheet bonding.

The most important shear load criterion of the introduced 2D FEM model is excess of the limit width of the critical shear crack that appeared before the composite material rupture.

The experiments clearly show that adhesion between composite material and concrete surface has a significant effect on shear capacity of the strengthened RC beam.

In future we will focus on improvement of calculating the CM contribution to shear capacity of RC beams taking into account

an effect of adhesion between composite material and concrete surface.

Acknowledgements

The research work presented in this paper has been supported by the Slovak Grant Agency, Grant VEGA SR No. 2/3035/23.

References

[1] Design guide FRP: *Fiber reinforcement polymer for S&P Products,* June 2000, 70 p.
[2] HALPIN, J. C. – TSAI, S. W.: *Effect of Environmental Factors on Composite Materials,* AFML-TR, 1962
[3] STN P ENV 1992-1-1: *Design of concrete structures*, Part 1: General rules and rules for buildings, Bratislava, May 1999
[4] TRIANTAFILLOU, T. C.: *Shear Strengthening of Concrete Members Using Composites, Non-Metallic (FRP) Reinforcement for Concrete Structures, Proceedings of the Third Symposium*, Vol. 1, Japan, Oct 1997, p. 523–530.
[5] ATENA *Program Documentation*, PART 1, ATENA Theory Manual, CERVENKA CONSULTING, 2000
[6] KOTULA, P.: *Shear Capacity of RC Beams strengthened with CFRP sheets* (in Slovak), Proceedings of conference Staticko-konštrukčné a stavebno-fyzikálne problémy stavebných konštrukcií, Tatranská Lomnica, Vysoké Tatry, November 2003, p. 187–192, ISBN 80-232-0221-9.

https://doi.org/10.26552/com.C.2004.3.28-30

komunikácie
COMMUNICATIONS

Ján Čelko – Matúš Kováč *

EVALUATION OF PAVEMENT FRICTION ACCORDING TO EUROPEAN STANDARDS

Pavement friction was measured in Slovakia by SKIDDOMETER BV 11. An evaluation of skid resistance by Mu index value for use in the Slovak Pavement Management System (PMS) is based on one parameter of friction, only. The tendency to adapt the Slovak PMS to European standards involves creation of criteria for the skid resistance evaluation by International Friction Index IFI. The Slovak SKIDDOMETER BV11 did not participate in the PIARC harmonisation experiment for pavement friction measurement. Therefore the new approach for IFI calculation was required. The PIARC experiment and concerned equipment were analysed in detail. The British Portable Tester TRL was chosen as subsidiary equipment depending on Canadian experiences. The new methodology for IFI calculation by the Slovak SKIDDOMETER was suggested depending on comparison measurements and experiences analyses. On the base of new methodology criteria for pavement skid resistance evaluation were created.

1. Introduction

Pavement skid resistance is an important factor of pavement serviceability and traffic safety. The factor indicates wet pavement friction and describes an interaction between a tire and road surface by a friction coefficient. The friction coefficient is frequently determined according to one type of the road surface texture - microtexture or macrotexture, only. Obtained value can be misleading whereas the friction parameters depend on both characteristics. Thus, the same value of the friction measurement obtained from two pavements can indicate very different friction properties.

In 1992, the World Road Association PIARC carried out extensive test with pavement friction and texture measurement devices. The proposal of criteria for evaluation of the pavement skid resistance by International Friction Index (IFI) was a result of the test [1]. IFI describes the skid resistance properties like a result of the simultaneous measurements of the friction and macrotexture. The IFI contains two parameters: a speed constant derived from the macrotexture measurement indicating the speed dependence of the friction, and a friction number that is a harmonized level of friction for a slip speed 60 km/h.

2 International Friction Index IFI

The determination of the IFI consists of two basic steps:
1. Evaluation of the macrotexture (TX).
2. Evaluation of the friction.

2.1 The macrotexture evaluation

Several methods for pavement surface macrotexture determination are used at present. The determination of the surface texture depth by the sand patch test is the most widely used method. The Mean Texture Depth (MTD) is a resulting value.

The PIARC experiment confirmed Mean Profile Depth (*MPD*) as the best parameter for describing of the macrotexture subject to statistical evaluation. Very subjective sand patch test used for determination of *MPD* is the source of inaccuracy so the laser method is contemplated in future The surface macrotexture is described by the coefficient S_p (speed constant) determined by equation (1) [8].

$$S_p = a + b * TX. \quad (1)$$

In equation a, b are regression coefficients determined for each type of macrotexture measurement, *TX* is parameter characterised the macrotexture (*MPD*, *MTD*, *ETD*).

The best results in the IFI calculation are achieved using the Mean Profile Depth method. The sand patch test also provides good results despite of the subject effect. The essential formulas are described in (2) and (3).

$$S_p = 89.7 * MPD + 14.2 \quad (2)$$

$$S_p = 113.6 * MTD + 11.6 \quad (3)$$

In equations *MPD* and *MTD* are expressed in mm and S_p in km/h.

* **Ján Čelko, Matúš Kováč**
University of Žilina, Faculty of Civil Engineering, Department of Highway Engineering, E-mail: jan.celko@fstav.utc.sk, matutko@fstav.utc.sk

By combination of (2) and (3) formulas we can determine the relation between *MTD* and *MPD* (4):

$$MTD = 0.79 * MPD + 0.23 . \quad (4)$$

Using (4) the Estimated Texture Depth (*ETD*) is determined and the value S_p is calculated by equation (5).

$$S_p = 93.0 * ETD + 17.63 \quad (5)$$

2.2 Friction evaluation

The friction coefficient is a basic value determined by all measuring equipment. For general use and comparison with different equipment the recalculation to the conventional slip speed (*S*) 60 km/h is needed. The slip speed value is dependent on equipment type and measuring speed (*V*).

a) In case of a locked wheel $S = V$.
b) In case of a slipped wheel $S = V * slip$. Relation $S = 0.17 * V$ is valid for 17% slip.
c) In case of a wheel with a slip angle $S = V * \sin(Q)$, where *Q* is the slip angle.

The friction coefficient *FRS* obtained from measuring equipment with current slip speed *S* is recalculated to the unified speed 60 km/h by (6):

$$FR60 = FRS * \exp\lfloor (S - 60)/S_p \rfloor . \quad (6)$$

In the equation FR60 is adapted friction coefficient for 60 km/h equivalent of the slip speed; FRS is the friction coefficient for current slip speed S; and Sp is a speed constant according to (1).

The value FR60 is used for IFI determination by relations (7) and (8).

$$F60 = IFI = A + B * FR60 + C * TX \quad (7)$$

$$F60 = IFI = A + B * FRS + \\ + \exp[(S - 60)/(a + b * TX)] + C * TX \quad (8)$$

where *A*, *B*, *C* are calibration constants for each equipment [8]; and *C* is zero for the smooth tyre.

2.3 The methodology for IFI calculation by SKIDDOMETER BV11

The Slovak Road Administration uses SKIDDOMETER BV11 [2] for friction measurement. Unfortunately, the equipment did not participate in the International PIARC Experiment to Compare and Harmonize Texture and Skid Resistance Measurements [1]. Therefore, the two steps were required. An implementation of the coefficients related to SKIDDOMETER BV11, and realization of the comparison measurements for IFI estimating. The three equipment were chosen as a reference – Canadian SKIDDOMETER BV11, side force device *SCRIM* and analysis of friction measurements by British Portable Pendulum Tester (*BPT*). The results from PIARC experiment [1], Cenek [3] and Canadian [4] experiences were used.

The measured values from devices *BPT*, *SCRIM* and SKIDDOMETER BV11 were compared and recalculated to the IFI value by well-known formulas first. The comparison of results from devices *SCRIM* and SKIDDOMETER BV11 showed that the values obtained from devices are very similar, in spite of different principles. Following this, the results from SKIDDOMETER were used for IFI calculation by SCRIM [1], [3].

The long-time observed road sections in Slovakia were used for evaluation of the relations between *IFI* values. Computation was realized on the base of friction index by SKIDDOMETER BV11 (expressed by Mu value), macrotexture measurement by sand patch test and by *BPT* friction. Measured results were obtained from 31 random selected measurement sections.

Following the analysis the methodology for *IFI* calculation by SKIDDOMETER BV11 was created. The next values are necessary for calculation:

- Friction index from SKIDDOMETER BV11, expressed by the parameter *Mu*.
- Measuring speed of the device.
- Slip speed of the device.
- Macrotexture determined by the volumetric method hp (sand patch test), determined as the Mean Texture Depth (*MTD*).

On the basis of the described input data the friction index is calculated by equation (9), adapted for Slovak conditions.

$$IFI = 0.065' + 0.92 * Mu * exp^{\lfloor (0.17*v-60)/S_v \rfloor} - \\ - 0.075 * h_p , \quad (9)$$

where: $S_p = 113.6 * h_p - 11.6 \quad (10)$

Mu is a friction index from SKIDDOMETER BV11, v is measuring speed of the device in km/h, h_p is the macrotexture determined by sand patch test in Mean Texture Depth (*MTD*).

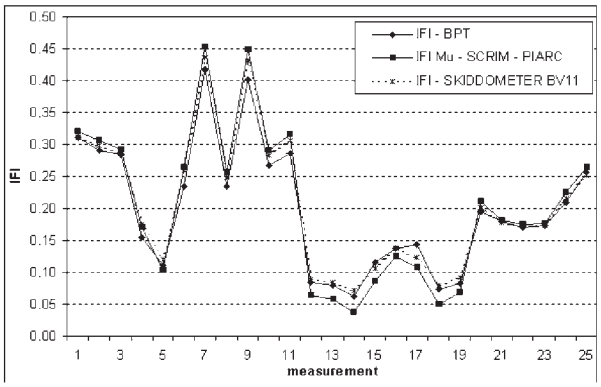

Fig. 1 Comparison of the proposal methodology of IFI calculation

The recommended equations were tested for a routine use by experimental measurements in the long-time monitoring experimental sections of the Slovak Road Administration. The obtained results are presented in the next figures. The comparison of the designed methodology with present practices valid for chosen reference devices are presented in Fig. 1. The results confirm the correctness of the created methodology for *IFI* calculation by using SKIDDOMETER BV11.

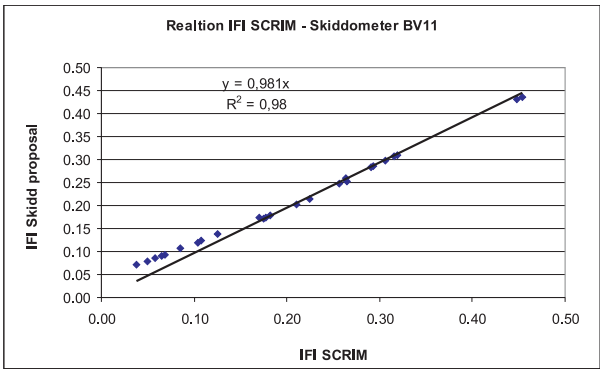

Fig. 2 Comparison of the SCRIM and SKIDDOMETER design method values

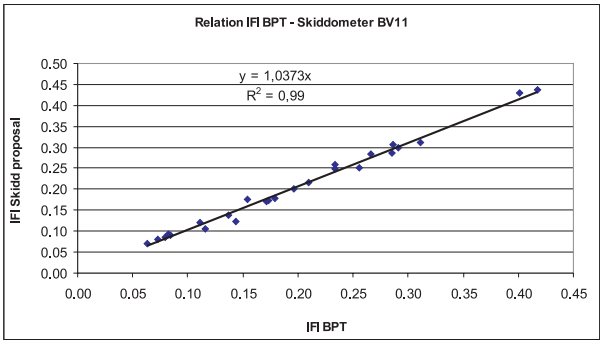

Fig. 3 Comparison of the BPT and SKIDDOMETER design method values

Fig. 2 and Fig. 3 show relations between the calculated *IFI* values by a designed formula for measurements of *Mu* factor by SKIDDOMETER BV 11 and reference devices *BPT* and SCRIM under the same edge conditions.

3 Criteria for the pavement friction evaluation by IFI

The *Mu* value only is used in the Slovak Pavement Management System for evaluation of the pavement friction characteristics at present. The proposal of new criteria by *IFI* value was created on the base of the presented analysis. The criteria are shown in Table 1.

Friction quality evaluation — Table 1

Evaluation	Type of road Design speed $v_n >= 80$ km/h		Type of road Design speed $v_n < 80$ km/h	
	by Mu	by IFI	by Mu	by IFI
Insufficient quality	$Mu < 0.53$	$IFI < 0.14$	$Mu < 0.53$	$IFI < 0.16$
Applicable quality	$0.53 < Mu \leq 0.79$	$0.14 < IFI \leq 0.31$	$0.53 < Mu \leq 0.68$	$0.16 < IFI \leq 0.33$
Good quality	$Mu > 0.79$	$IFI > 0.31$	$Mu > 0.68$	$IFI > 0.33$

4 Conclusion

The presented results are based on the measuring samples and afforded values from past experiments. The multiple comparison measurements are inevitable for verification or modification of them. Following this, the classification of the pavement friction by *IFI* will be used in the Slovak PMS.

References

[1] International PIARC Experiment to Compare and Harmonize Texture and Skid Resistance Measurements, PIARC Report 01.04.T, The World Road Association, Paris, 1995.
[2] CELKO, J., MORAVCIKOVA, R., KOVAC, M.: *Measurement and evaluation of the asphalt pavements friction by SKIDDOMETER BV 11* (in Slovak), Technical regulation of Slovak Road Administration, 05/2000.
[3] CENEK, P. D., JAMIESON, N. J., MCLARIN, M. W., BROWN, E. C.: *Use of the international friction index (IFI) to predict actual vehicle braking performance*, www.transit.govt.nz/.
[4] Joint Winter Runway Friction Measurement Program (JWRFMP), Transportation Development Centre Canada, 1999, http://www.tc.gc.ca/tdc/publication/.
[5] CELKO, J. at al: *The surface characteristics of the pavements,* Science monographs. EDIS ZU, Zilina 2000, ISBN 80-7100-774-9.
[6] "Calculating International Friction Index of Pavement Surface", ASTM Standard Practice E-1960, Vol. 04.03, American Society for Testing and Materials, West Conshohocken, Pa., 1999.
[7] CELKO, J., KOVAC, M., TABAK, M.: *Evaluation of the pavement skid resistance by EU standards,* Final report, Slovak Road Administration Bratislava, 11/2003.

https://doi.org/10.26552/com.C.2004.3.31-36

Ján Čorej – Martin Korenko – Eva Remišová *

CLIMATIC CHARACTERISTICS AND THE TEMPERATURE REGIME OF ASPHALT PAVEMENTS

Traffic density and climate are important external factors influencing pavement mechanics. Climatic conditions influence the service life of materials, damage to roads etc. In many countries the climatic characteristics are implemented into calculation systems for pavement construction. The importance of the implementation of climate characteristics into the calculation systems is increasing in the context of global climatic processes and changes, especially the changes in air temperature. The aim of the following paper is to highlight the changes of climatic characteristics used in highway engineering and their effect on the change of pavement thermal flow.

1. Introduction

Besides traffic density, climate is the second important external factor influencing pavement mechanics. There are several climatic characteristics, which must be taken into consideration, regarding pavement behaviour:

- air temperature
- minimum and maximum air temperature
- frost index
- sun radiation
- rainfall
- atmospheric moisture etc.

Air temperature changes during daily and yearly cycles develop the changes of strength and deformation characteristics of particular pavement layers as well as the changes in bearing capacity of the pavement subgrade. Air conditions also influence the service life of materials, damage to roads etc.

Therefore in many countries climatic characteristics are implemented into the calculation systems of pavement construction. The importance of the implementation of climate characteristics into the calculation systems is increasing in the context of global climatic processes and changes, especially the changes in air temperature. The aim of the following paper is to highlight the changes of climatic characteristics used in highway engineering and their effect on the change of pavement thermal flow.

The measurement of air temperatures in five characteristic localities of Slovakia between 1980 – 2001 were used to study the problem of climatic conditions. The temperature data was received from the Hydrometeorological Institute in Bratislava, and from experiments on air, road and pavement temperatures carried out by the authors [1, 2, 3, 4]. The presented problem is solved in the research projects num. 1/8194/01 and the project "The research of influence of climatic and traffic conditions on pavement mechanics", supported by the grant agency VEGA and by the Ministry of Education SR Bratislava [1].

2. Results of air temperature measurements in Slovakia

One climatic characteristic which must be measured in order to determine the thermal flow of the pavement is air temperature. Knowledge of air temperature and its characteristics is used in the design and evaluation of the pavements in practise. The analysis of thermal conditions in Slovakia with its characteristics was made on the basis of air temperature measurements made over 21 years from 1. 1. 1980 to 31. 12. 2001 in the following five characteristic localities in Slovakia:

1. Bratislava, south-western locality of Slovakia,
2. Žilina, north-western Slovakia
3. Hurbanovo, southern Slovakia
4. Poprad, northern and mountainous region of Slovakia,
5. Košice, eastern Slovakia east.

From the results obtained, the following climatic characteristics can be given:

- the yearly flow of average daily air temperatures (T_s),
- the medium yearly air temperatures (T_m),
- the characteristics of the winter period as the frost index (I_m), number of days where ice is present, frosty periods, minimum air temperatures (T_{min}).

2.1 Daily and yearly characteristics of air temperatures

a) Average daily air temperature (T_s)

The air temperature changes cyclically achieving minimum and maximum values. The daily temperature flow is expressed by average daily air temperature T_s, that is defined in the next formula

* **Ján Čorej, Martin Korenko, Eva Remišová**
University of Žilina, Faculty of Civil Endineering, Department of Road Engineering, Komenského 52, 010 26 Žilina, E-mail: corej@fstav.utc.sk

$$T_s = \frac{T_7 + T_{14} + 2 \cdot T_{21}}{4} \qquad (1)$$

where indexes 7, 14 and 21 are the times of air temperature measurement T in °C. This temperature is measured 2 m above ground level.

b) Average yearly air temperature T_m

The average yearly air temperature is another important characteristic of air conditions. It is the temperature defined as the ratio of the average daily air temperature summary during one year to the number of days in a year:

$$Tm = \frac{\sum_{i=1}^{365} T_s}{365} \qquad (2)$$

The evaluation example of the yearly flow of the average daily air temperatures between 1980 and 2001 in Žilina is shown in figure 1.

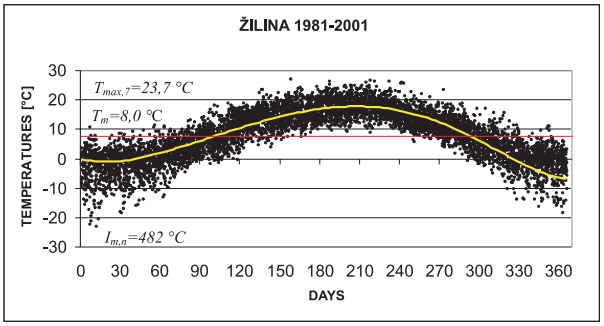

Fig. 1 Yearly flow of average daily air temperatures

The air temperatures at particular measuring stations in Slovakia were evaluated using the same method. The example of average yearly air temperature flows over 21 years in two characteristic regions of Slovakia – Žilina in the north of Slovakia and Bratislava in the south is presented in figure 2.

One of the aims of this paper is to show the range of changes in thermal characteristics as a consequence of global changes. The differences in average yearly temperatures in particular years as well as an increase in average air temperatures are evident. The regression analysis of the trend of temperature changes over 21 years is shown in figure 3. The time behaviour of air temperatures has an increasing character.

A review of the average yearly air temperatures T_m which are statistically evaluated over the period of 21 years in five defined stations is presented in table 1. Data of average yearly temperatures in SR used according to the Map of the average yearly air temperatures [5] is shown. The average yearly temperature increases by about 1 °C.

The next characteristics of a period of one year are the maximum and the minimum average daily air temperatures T_{max}

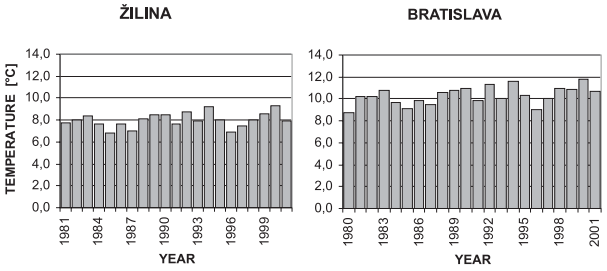

Fig. 2 Average yearly air temperatures in Žilina and in Bratislava during the period of 1980 – 2001

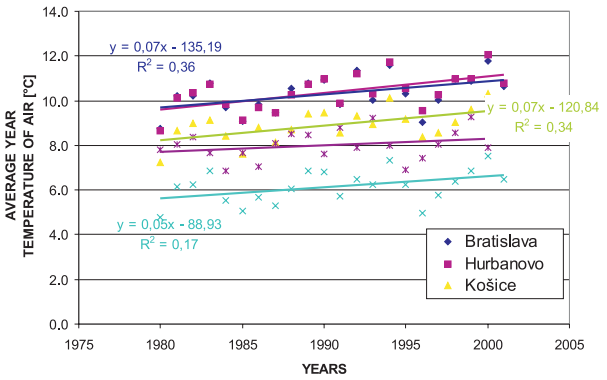

Fig. 3 Trends of the average yearly air temperatures

and T_{min}. The statistics of T_{max} and T_{min} during 21 years are presented in table 1.

The yearly characteristics of air temperatures — Table 1

Region	Elevation above sea level	Thermal characteristics [in °C]		
		T_m	T_{max}	T_{min}
Poprad	695	6 (5)	22	−16
Žilina	365	8 (7)	24	−15
Košice	230	9 (8)	25	−12
Bratislava	131	10 (9)	27	−10
Hurbanovo	115	10 (9)	28	−11

2.2 Characteristics of a summer period

One of the important problems of asphalt pavements is their resistance to rutting during traffic in summer. The intensity of the Sun's radiation and air temperatures influence the input parameters of asphalt surfaces, such as resilient modulus, strength characteristics etc. The basic characteristics of the summer period that influence the mechanical behaviour of pavement layers are:

- the maximum summer air temperature,
- the thermal index.

a) Average maximum 7-day air temperature

The air temperature is a variable factor that depends on a balance of thermal energy on the pavement surface. The maximum air temperatures are used to determine the border air temperatures (tab. 1). The temperatures, which have long-term effects, are important for the stabilization of the thermal field. One of the possibilities is an empirical determination of the maximum air temperatures during seven consecutive days with maximum air temperatures $T_{max,7}$. The average maximum 7-day air temperature in a year is determined as the ratio of the summary of temperatures over seven consecutive days to the number of days – 7 days.

The standard value of maximum 7-day air temperature $T_{air,max}$ (in °C) according to the program SHRP (Strategic Highway research program) [6] is statistically the value of the average yearly values from a long term monitoring (20 years):

$$T_{air,\,max} = \overline{T}_{max,7} + 2\sigma \qquad (3)$$

where $\overline{T}_{max,7}$ is the average 7-day air temperature during the monitoring period, in °C,
σ is standard deviation.

The example of a search for a 7-day period in a year with maximum temperatures and flow of maximum air temperatures in the Bratislava region during the 21-year period is presented in figure 4.

b) Thermal index

The *thermal index* I_t is the characteristic which represents summer thermal conditions, especially asphalt pavement defects characteristic to the summer period. It is defined as the summary of the average daily air temperatures that are higher than 20 °C in the summer period. For illustration results from the Bratislava and Žilina stations are shown in figure 5. It is evident that there is a significant difference between these two regions. The values in Bratislava are greater than the values in Žilina.

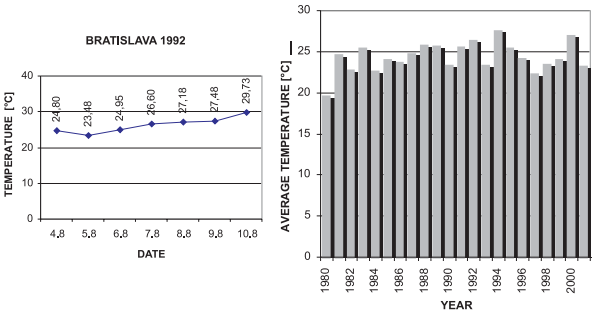

Fig. 4 Flow of the average 7-days' maximum temperatures

The summer period is characterised also by the number of summer days n_L (those with temperatures above 20 °C) and the average summer temperature $T_{p,L} = (I_t/n_L)$. The summer period characteristics are in table 2.

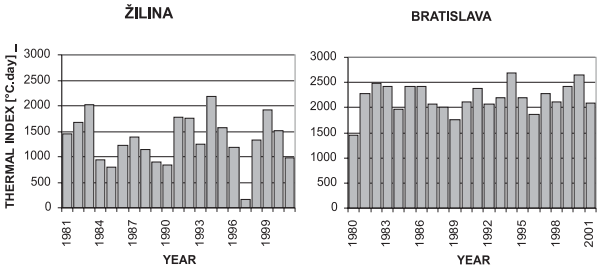

Fig. 5 Flow of the thermal index, 1980–2001

Monitoring characteristics of the summer period Table 2

Region	Elevation above sea level	Thermal characteristics [in °C]			
		n_L	$T_{p,L}$	I_t	$T_{air,max}$
Poprad	695	47	16,0	767	22
Žilina	365	76	17,5	1332	24
Košice	230	102	18,7	1941	26
Bratislava	131	112	19,6	2195	28
Hurbanovo	115	123	19,5	2384	27

2.3 Characteristics of a winter period

The most important characteristic of a winter period from a highway engineering point of view *is frost index* I_m (in °C) It is the characteristic which expresses the intensity and the duration of a frost period. According to [5] the frost index is defined as the maximum negative value of a summary of the average daily air temperatures T_s in a winter period:

$$I_m = \sum_{t_z}^{t_k} T_s \qquad (4)$$

where t_z is the beginning of a winter period,
t_k is the end of a winter period.

The flow of the frost indexes during the years 1980 – 2001 in the Bratislava region and Žilina region is shown in figure 6.

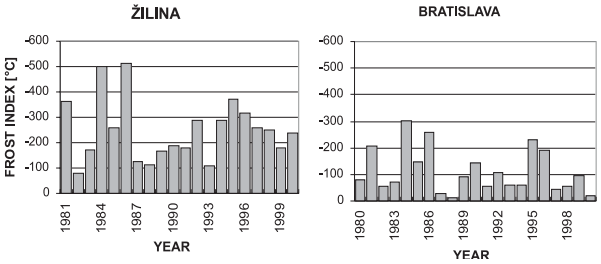

Fig. 6 The Frost index values for a period of twenty years

The frost index values are changed from a minimum value of 20 °C in Hurbanovo in winter 2000/01 up to a value of 742 °C in Poprad in winter 1986/87. For practical purposes the design value

of the frost indexes *Im,n* determined statistically from a long-term monitoring is used. The statistics of the frost indexes during the 21-year period and the values according to the Map of designed frost indexes STN 73 6114 [5] are in table 3.

The main characteristics of winter period Table 3

Region	Elevation above sea level	Thermal characteristics [in °C]	
		Im,n	*Im,n* [STN 73 6114]
Poprad	695	733	700
Žilina	365	482	475
Košice	230	473	450
Bratislava	131	272	300
Hurbanovo	115	272	300

The design values of frost indexes decrease; the winter periods are warmer.

3. Thermal flow of the pavement

The research into the effect of thermal conditions on pavement thermal flow was realised by using "Experimental stand of pavement mechanic" built in the authors' place of work. The stand consists of two testing pavements with a system of scanning and registration of temperatures [7]. The constructions of pavements with the position of thermometers are shown in figure 7. The testing pavements are different in type and in the thickness of their base layers.

In the research into the thermal flow of pavements results were used which had been measured and registered continually since 2002. The characteristic air temperature flow, as well as the temperature flow at the surface and bottom of the asphalt layers, is presented in figure 8.

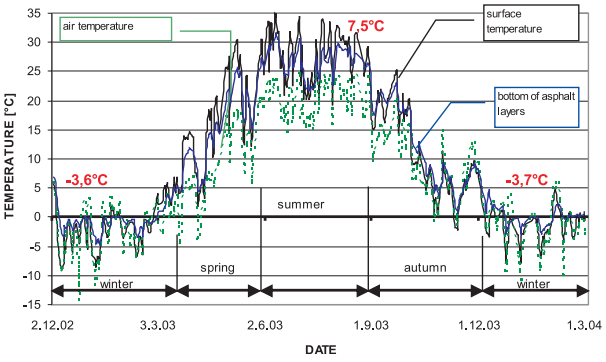

Fig. 8 Air temperature flow and pavement temperature flow for the period of 2003 - 2004

3.1 Research into the relationship between the air temperature and the pavement surface temperature

One of the important characteristics of pavement thermal flow is the temperature of the pavement surface. The pavement surface is the most loaded part. The theoretical deduction of the mathematical relation of pavement surface temperature goes out the thermal balance at surface [5]. According to SHRP it is possible to determine the maximum temperature of the asphalt pavement surface $T_{max,p}$ in the summer period at a depth of 20 mm and the minimum temperature of the asphalt pavement surface T^{min} in the winter period

$$T_{max,p} = (T_{air,max} - 0{,}00618.LAT^2 + 0{,}2289.LAT + 42{,}2) \cdot 0{,}9545 - 17{,}78 \quad (5)$$

$$T_{min,p} = T_{air,min} \quad (6)$$

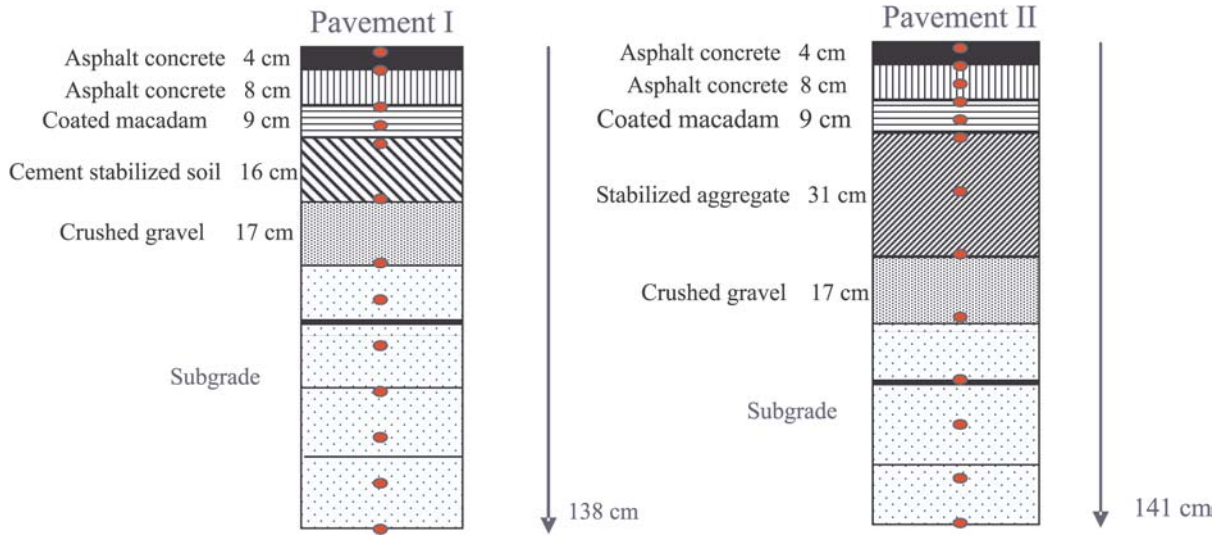

Fig. 7 Pavements' construction of the experimental stand

where $T_{max,p}$ is the maximum design temperature of the asphalt pavement surface to a depth of 20 mm with 98% reliability in [°C]
$T_{min,p}$ is the minimum design temperature of the asphalt surface, in [°C]
$T_{air,max}$ is the maximum design air temperature, according to (3), in [°C]
$T_{air,min}$ is the minimum design air temperature, in [°C]
LAT is the geographic latitude of the monitoring locality.

The design temperatures of asphalt pavements in five localities of Slovakia are as follows:

- in Žilina 41,9 °C
- in Poprad 40,0 °C
- in Košice 44,1 °C
- in Hurbanovo 45,3 °C
- in Bratislava 46,1 °C.

The utilisation of these equations in Slovak conditions was studied at the experimental stand in Žilina. The relation between the air temperature and the pavement surface temperature (temperatures measured during the summer period of 2003) is presented in figure 9.

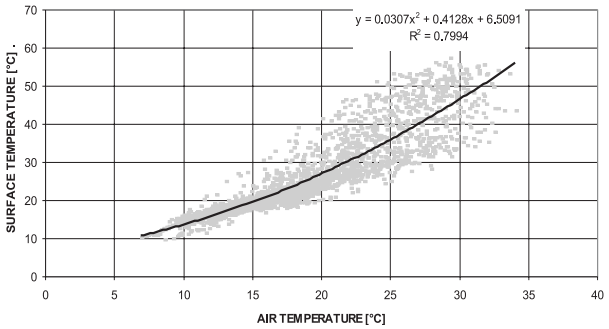

Fig. 9 Relation between the pavement temperature and the air temperature; in the period of 22.5. - 5.9. 2003

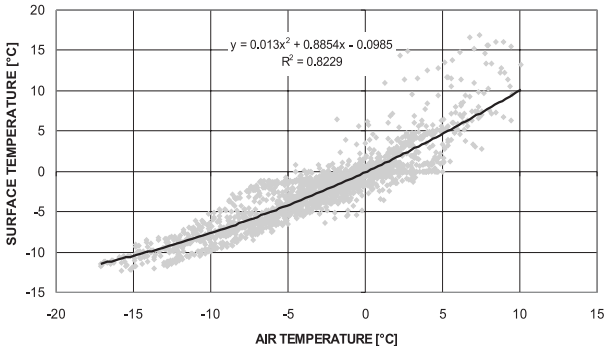

Fig. 10 Relation between the pavement temperature and air temperature; during the period of 2. 12. 2002 - 4. 3. 2003

The pavement surface temperature is about 36 °C, according to figure 9, at an air temperature of 25 °C in Žilina. However, the result does not correspond with the temperature 41,9 °C determined according to SHRP. The relation between the air temperature and the pavement surface temperature in the winter period of 2002/2003 is presented in figure 10. The measurement of this relation in the winter period shows a narrower spread of results.

The following research characteristic is the yearly range of temperatures in particular layers in respect of the thermal loading. Figure 11 shows the temperature distribution in a one year cycle, 2003/04, the thermal range of "a hot summer day" (green line), "a cold summer day" (blue line) and "the coldest winter day" (red line). It is quite evident that the wearing course is thermally the most loaded layer (approximately 65 °C in summer), the temperature on the subgrade changes within a range of 25 °C and about 16 °C at a depth of 140 cm.

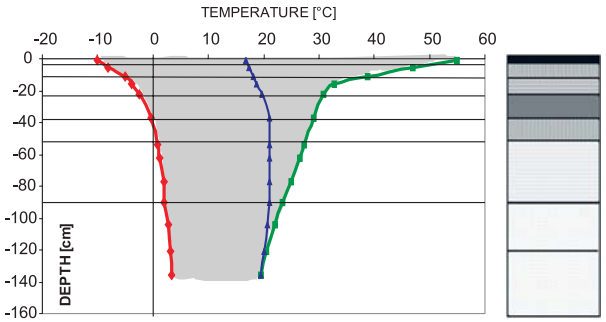

Fig. 11 One year temperatures range in pavement I

Another important characteristic is the temperature of the asphalt layers in terms of evaluating pavement behaviour (fig. 12).

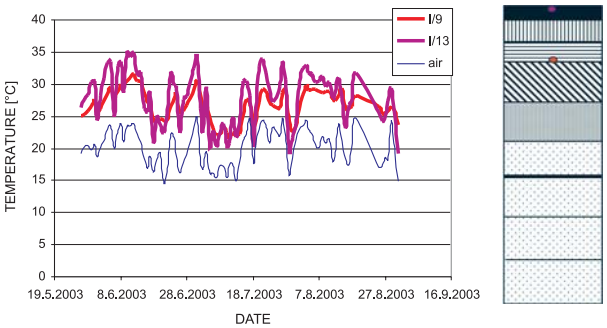

Fig. 12 Temperatures on the pavement surface and in the bottom level of asphalt layers

4. Conclusions

The presented paper analyses two important problems with respect to pavement design methods:

1. the trend of changes in climatic characteristics used in highway engineering following global climatic changes and then
2. the results of these changes on pavement thermal flow.

Although the monitoring period of 21 years is not sufficient to present a complete summary, it is quite possible to put forward some conclusions that could be applied in practice. One of them is the requirement for continued monitoring of, and research into, the problem. The thermal effects influence markedly the thermal flow and thereby the pavement degradation. The following important facts were observed at five monitoring stations in Slovakia during the period of 21 years:

- the increase of the average yearly temperature T_m by about 1 °C,
- the increase of 7-day air temperatures and the thermal indexes,
- and slow regress of the intensity of the winter period.

The measured results of the influence of climatic effects on pavement thermal flow showed a clear relationship between the air temperature and the pavement surface temperature. These results allow detailed analyses of the temperature of particular pavement layers and research their effect on the mechanics of different layers. An important result is also the knowledge that the method of the pavement thermal flow measurement at the experimental stand proved to be useful and it also helps the investigation of important thermal characteristics of road pavements.

References

[1] ČOREJ, J. AND COL.: *The research of influence of climatic and traffic conditions on pavement mechanics,* Grant projects VEGA, 2004.
[2] ČOREJ, J., REMIŠOVÁ, E.: *Analysis of climatic conditions from the road pavement mechanics point of view.* Science, Education and Society. 11. International Scientific Conference, section 1, Žilina, 17. - 19. 9. 2003, ISBN 80-8070-116-4.
[3] ČOREJ, J., KORENKO, M., ŠEDIVÝ, T.: *The characteristics of summer period and pavement thermal flow*, Proceedings from VIII, Conference Diaľnica, 6.-7.11.2003, Bratislava 2003.
[4] BANDŽÁKOVÁ, M.: *The monitoring and evaluation of climatic characteristics and pavement thermal flow,* diploma work, April 2003.
[5] STN 73 6114: Highway pavements, Basic setting, 1997.
[6] BLAB, R.: *Analytische Methoden zur Modellierung der Verformungseigenschaften flexibler Fahrbahnaufbauten,* 11 Mitteilungen, ISTU Wien 2001.
[7] ČOREJ, J., ČELKO, J., TROJANOVÁ, M.: *Water and thermal flow of baulk subgrade*, ES VŠDS Žilina 1994, ISBN 80-7100-174-0.

https://doi.org/10.26552/com.C.2004.3.37-43

komunikácie
COMMUNICATIONS

Libor Ižvolt – Martin Mečár *

EXPERIMENTAL VERIFICATION OF RAILWAY SUBSTRUCTURE WITH APPLICATION OF REINFORCED GEOCOMPOSITE

In the paper the authors present results of experimental measurements realized in a testing stand which was built for evaluation of reinforced effect of geocomposite MACRIT GTV/50-50 B applied into a railway substructure. Methodology of experimental measurements, observed physical characteristics of used grounds and results of static loading tests for various granularity and thickness of subbase material (150 mm –600 mm) are described. The main result of the experimental evaluation of two-tested subbase materials is a proposal of nomograms for dimensioning the railway substructure with application of topical geosynthetic material.

1. Introduction

Modernization of the main basic railway of the Slovak Railways (ŽSR) that belong to the Trans-European corridors and expected higher loadings for axle and railway speeds require essentially higher demands not only for an excellent condition of railway superstructure, but for railway substructure, too. It is common knowledge that the long-time reliable spreading of the train set loading, which affects throughout the rail, railway bed and subbase to the subgrade surface without permanent cracks of the particular construction levels of the sleeper subgrade is a basic assumption of safe and trafficable railway. In the case of insufficient loading capacity of the subgrade surface special deformation problems rise in the railway construction, especially in the railway substructure, which influence the quality and traffic reliability of the railway.

Increase in loading capacity of the railway substructure is possible through various methods, as for example the changing of subgrade surface of small loading capacity with stabilization of surface soils or with the strengthening of sleeper subgrade construction. In the present time geosynthetic reinforced elements, named as reinforced construction layers, application into the railway substructure, have ever more utilizations in the process of increasing the railway substructure loading capacity.

According to the amended annexe No. 2 of Regulation S4 of ŽSR, geosynthetic reinforcement can be applied into the railway substructure body as are, for example: geogrids, geocomposites, geocells, or reinforced geotextiles. The main shortcoming of an objective and effective use of particular geosynthetic materials into the railway substructure is absence of relevant methodology of dimensioning, or nomograms to propose and evaluate the reinforced construction layers of substructure. According to [2], the calculated thickness of a construction layer can be decreased during the application of geosynthetic reinforcement, by about 25% (if the construction layer consists of material with rounded grains) or by about 30% (if the used material is crushed), or, according to [3], the calculated thickness of a construction layer can be reduced by about 0.10 m during geosynthetic reinforced element application.

On the author's personal experience, which was gathered during diagnostics of many constructions with geosynthetic materials in construction layers of the railway substructure, the above dispositions are only estimative and are not valid for various combinations of geosynthetic elements and materials of construction substructure. For that reason, an outdoor and internal testing stand was built in the Department of Railway Engineering and Track Management (DRETM), to test various reinforced construction layers from the point of view of their loading capacity and climate resistance, and consequently, to define subbase dimensions to the required value of equivalent deformation module in the level of railway surface.

Further more, in the paper the methodology and up to time results of experimental testing of railway substructure with using geosynthetic reinforced element MACRIT GTV/50-50 B will be presented with various characteristics of construction layer material (subbase layer of different granularity curve) and with respect to constant loading capacity of subgrade surface.

2. Testing Stand and Methodology of Experimental Measurement

The experimental measurement of reinforced effect of geosynthetic material MACRIT GTV/50-50 B was realized on the great internal testing stand of DRETM.

The testing stand (Fig. 2.1) has the following dimensions in length × width × height: 3400 mm × 1950 mm × 1200 mm. Because of preservation of cross – and lengthwise stand stability, its bottom and walls are reinforced with transversal and vertical angle steel ribcages (reinforcements). In its upper level there is

* **Libor Ižvolt, Martin Mečár**
University of Žilina, Faculty of Civil Engineering, Department of Railway Engineering and Track Management, Komenského 52, 010 26 Žilina. Slovak Republic, Tel: +421-41-7634818, E-mail: libori@fstav.utc.sk, mecar@fstav.utc.sk

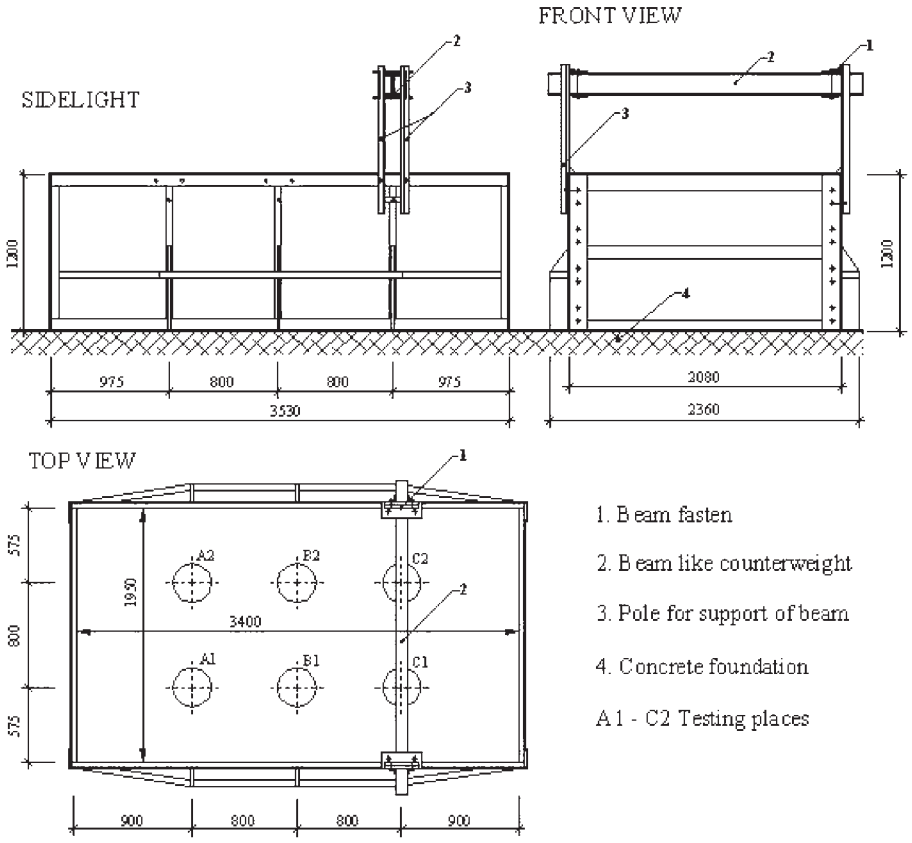

Fig. 2.1 Testing stand of DRETM

a steel beam which can be fixed in three positions in length of the stand and which acts as counterweight during static loading tests.

The testing stand is fulfilled with soil, up to the height of 600 mm, which is characterized as sandy clay (the results from soil laboratory tests are described in chapter 4) according to the granularity analysis. The average value of static deformation module E_0 for experimental measurements was about 7 MPa before building the particularly layers and about 9,5 MPa after taking off the whole material of subbase construction.

Before the subbase building maximal and minimal volume weight for broken sand was found out (to determine the compaction criterion, formulated via relative lying down I_D according to the Slovak Technical Standard STN 72 1018) and necessary heightening before the compaction so that the required thickness of subbase would be kept. Decreases after compaction were found out with a special experiment done in the bin of 305 mm in diameter for the subbase thickness after compaction 100 and 150 mm.

Further building of the tested construction continueed as follows:

- Bedding, tightening and fixation of geosynthetic material MACRIT GTV/50-50 B on the subgrade surface in the edge of stand with steel pike.
- Bringing subbase material into the calculated height to have layers of thickness of 150, 300, 450 or 600 mm (measured with levelling) after compaction with vibrating-plate-compactor ViDo 25/40 to the required compaction criterion.
- Gradual working in each particular layer:
  - 6 static loading tests.
  - 15 dynamic tests before and 15 after static plate loading tests (in places around A_1, A_2, B_1, B_2, C_1, C_2, position).
  - 3 tests of volume weight with the hole method in the positions where static loading tests were done.
  - Determination of humidity and swept away elements of subbase material.

No compacted sheet of material with thickness of about 150 mm was left near the stand walls, to eliminate the influence of rigid stand walls. After realization of all the above measurements, the subbase material was taken off and control tests of loading capacity of subgrade surface were done.

3. Methodology of Finding the Deformation Characteristics Out

Deformation characteristics of evaluated construction layers of railway substructure and subgrade surface were found out with a static loading test and with a dynamic loading test for control,

with convention with amended annexes No. 20 of regulation [4]. The compaction quality of built-in materials was found out according to the regulation [4].

The process of the static loading test consists of the following activities:

- The surface of tested layer is compound with dry fine-grained siliceous sand to fill in surface unevenness.
- A solid circle board with diameter of $d = 300$ mm is embedded up to the treated surface.
- To a spherical hinge of loading board is embedded hydraulic system consisting of ahydraulic lifter *ENERPAC model RC-59* with maximal imply force of 50 kN, a manually controlled hydraulic pump – *ENERPAC model P-142*, with the maximal imply liquid pressure 70 MPa, a manometer *BGF-168SR* with a range of 0–50 kN with the least scale division of 0.1 MPa and a hydraulic compressive hose with the length of 2.5 m.
- The hydraulic lifter stretches on a steel beam, which was fixed in three points lengthwise the testing stand.

The loading capacity of particular layers of the tested railway substructure and subgrade surface was measured with static loading tests, done in *2 loading cycles* with equipment in fig. 3.1. The main loading levels 0, 25, 50, 75 and 100 kPa and unloading levels 75, 50, 25 and 0 kPa were chosen to find the loading capacity of the subgrade surface in both cycles. In case of testing subbase material the following loading levelswere chosen: 0, 50, 100, 150, 200 kPa and unloading was done in levels: 150, 100, 50 and 0 kPa.

For each loading level, the value of deformation was read after a compaction consolidation via 3 digital sensors MITUTOYO, placed regularly into a triangle in the edge of the solid circle board. From such readings the following was determined:

- Static transform module E_0,
- Static deformation module E_{def1} and E_{def2}

The static transform module E_o is characterized according to the [1] with the equation:

$$Eo = \frac{1.5 \cdot p \cdot r}{y} \quad [\text{MPa}] \qquad (3.1)$$

where p is the specific pressure to the loading board (0.1 MPa, or 0.2 MPa),
r is the radius of loading board in meters (0.15 m),
y is the whole average pressure of loading board in meters, in the second loading cycle,
1.5 is the constant considering the surrounding patterns and actions, which are necessary during loading with circle board.

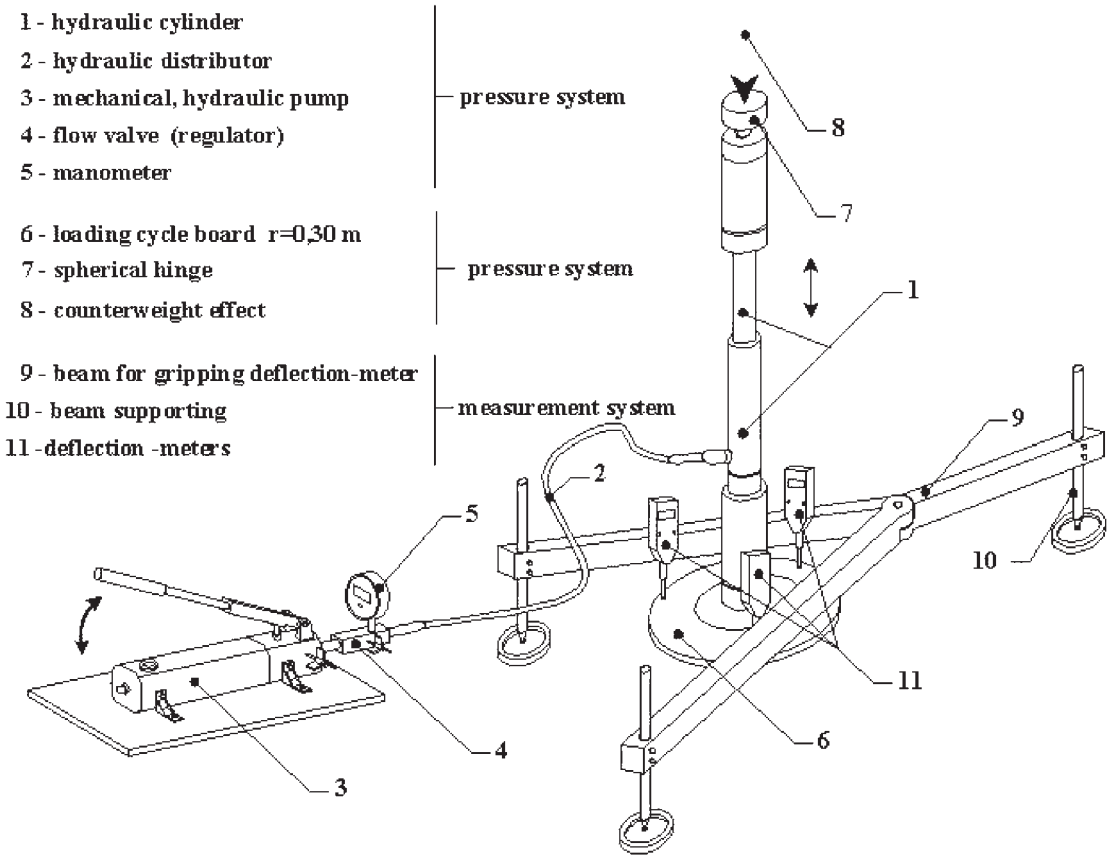

Fig. 3.1 Equipment for finding out the static transform module

Figure 3.2 shows the principle of determining the transform module with using two loading cycles.

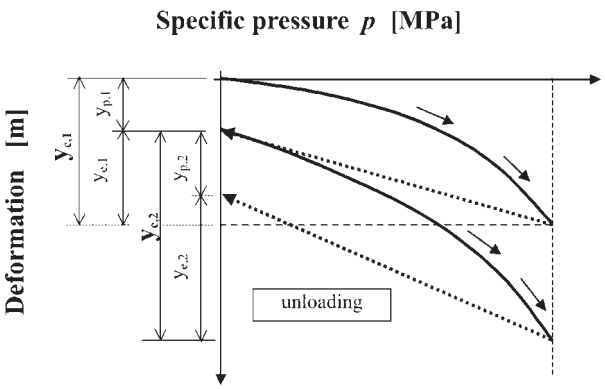

Fig. 3.2 Principle of the deformation modulus calculation

The deformation module E_{01} was determined from the first loading test and E_{02} from the second one. Compaction was considered to be adequate when the proportion of both of deformation modules for subbase reached the value $E_{02}/E_{01} \leq 2.2$ and for subgrade surface $E_{02}/E_{01} \leq 2.5$. The range of compaction work was chosen so that the reached values were similar to those in situ (according to the experience they are by 10 – 20 % higher than the minimal required values).

4. Characteristics of Built-in Materials in Testing Stand

Physical characteristics of composite soil and subbase material were necessary to identify for evaluation of reinforcing effect of geosynthetic MACRIT GTV/50-50 B. Physical characteristics of materials used for the tested construction of railway substructure that was placed on a large testing internal stand were evaluated in the laboratory of DRETM separately for subgrade surface material and for subbase material.

4.1 Description of Reinforced Geosynthetic MACRIT GTV/50-50 B

Geosynthetic material MACRIT GTV/50-50 B (Fig. 4.1) is a polystyrene geocomposite, compound with non-woven geotextile (ensures separating and filtrating function) and reinforced geogrid ARTER. Geotextile protects geogrid before damage when the cover layers are built-in and compacted and so it brings higher assurance during geocomposite building-in. The reinforced effect of geogrid ARTER is reached thanks to directionality Oriented Structure (D.O.S) that causes that the reinforced fibres have been straighten already during production.

Technical parameters of geocomposite MACRIT GTV/50-50 B:

- Pulling force (longitudinal/transversal) 50/50.
- Elongation (longitudinal/transversal) [%] 12/12.
- Pulling force during 2% elongation [kN/m] 11/12.
- Pulling force during 3% elongation [kN/m] 15/16.
- Pulling force during 5% elongation [kN/m] 27/27.
- Basic weight [g/m^2] 500.
- Maximal width [m] 100.

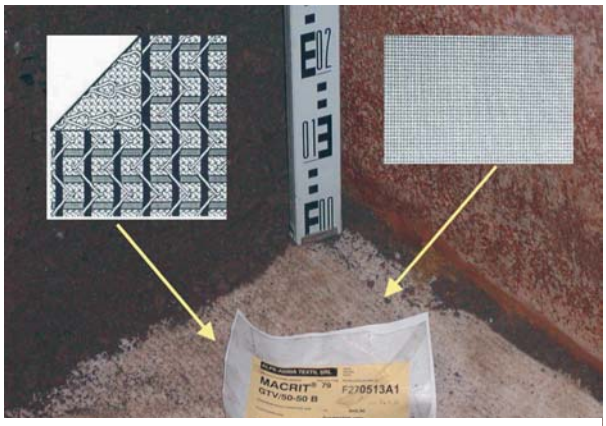

Fig. 4.1 View on the arrangement and structure of geocomposite MACRIT GTV/50-50 B

4.2 Subgrade Surface

Soil from the locality Žilina – Solinky was applied for the subgrade surface to reach the required bearing capacity of about 7 MPa. The soil samples from subgrade surface of the testing stand were brought from the localities where the static loading stands are.

For soil classification according to the USCD system we have to make a granularity analysis to find out the Atterberger limits: humidity in the yield limit w_L, humidity in the plastic limit w_P and plastic index I_P. Laboratory evaluation of samples granularity composition was done according to [5]. Atterberger limits were calculated according to [7] and [8] and humidity according to [6]. These tests were adjusted via the software SOILAB.

On the base of the above laboratory results, soil was classified in terms of [9] as sandy clay with symbol $F_4 = CS$. Further characteristics of subgrade surface soil:

- Humidity in the plastic limit w_P [%] 14.9.
- Humidity in the yield limit w_L [%] 41.9.
- Humidity w [%] 22.0.
- Volume weight of humid soil ρ [kg/m^3] 2081.0.
- Volume weight of dry soil ρ_d [kg/m^3] 1707.0.

4.3 Subbase

Broken stone of fraction 0–32 mm was used to build-in subbase of the tested railway substructure. In the first phase of the experimental measurements the subbase material conforms from the view of its granularity [9] and in the second phase we admixed to the previous material 30% of broken stone weight of fraction

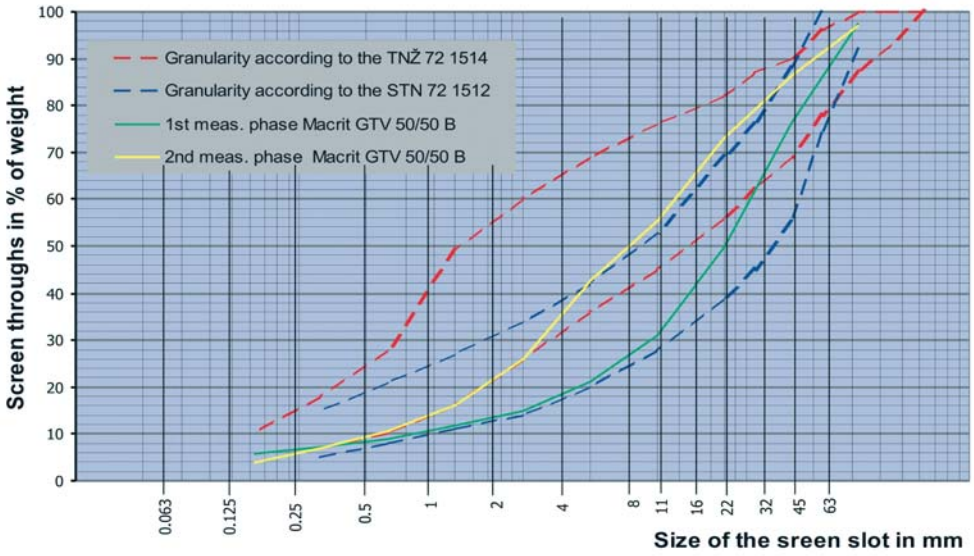

Fig. 4.2 Granularity curves of subbase material

0–4 mm. This mix material conformed the required demands concerning to the granularity curve in subbases according to [10].

The granularity curves of material applied into subbase of the tested railway substructures are presented in figure 4.2 with required granularity limits presented in [9] and [10].

On the base of granularity analysis soil was classified as gravel with good granularity with symbol $G1 = GW$.

Before the experimental measurements we measured granularity, minimal volume weight ρ_{dmin}, maximal volume weight ρ_{dmax}, number unequal-granularity C_u and number of curvature C_c in the subbase material. In the process of subbase building, we took from each particularly tested construction layer 3 samples to determine the volume weight of humid ground ρ, the volume weight of ground after dry out ρ_d, humidity w wash-away elements and relative settlement I_D.

The complex outline of reached results from the samples taken from particular layers of the tested subbase that were calculated according to the demands described in [10] is shown in tables 4.1 and 4.2.

5. Evaluation of Loading Tests and Proposal of Nomograms for Dimensioning of reinforced Subbase

In table 1, there are average values of static transform module during applying the reinforced geocomposite MACRIT GTV/50-50 B in particular layers of subbase (layers divided according to the

Outline of measured parameters of subbase material – 1st phase — Tab. 4.1

Characteristics of material / construction thickness	0.150 m	0.300 m	0.450 m	0.600 m
Minimum bulk density $\rho_{d,\,min}$ [kg.m^{-3}]	1635			
Maximal bulk density $\rho_{d,\,max}$ [kg.m^{-3}]	2156			
Bulk density of of soil ρ [kg.m^{-3}]	2087	2140	2181	2204
Dry bulk density of soil ρ_d [kg.m^{-3}]	2030	2083	2128	2130
Moisture w [%]	2.8	2.7	2.5	3.5
Wash-away elements	5.65	5.31	5.37	5.66
Relative density I_D	0.81	0.89	0.96	0.96
Coefficient of uniformity C_u	> 15			
Coefficient of curvature C_c	> 1			

Outline of measured parameters of subbase material – 2nd phase — Tab. 4.2

Characteristics of material / construction thickness	0.150 m	0.300 m	0.450 m	0.600 m
Minimum bulk density $\rho_{d,\,min}$ [kg.m^{-3}]	1504			
Maximal bulk density $\rho_{d,\,max}$ [kg.m^{-3}]	2047			
Bulk density of of soil ρ [kg.m^{-3}]	2023	2065	2017	1986
Dry bulk density of soil ρ_d [kg.m^{-3}]	1950	1996	1955	1922
Moisture w [%]	3.7	3.5	3.1	3.4
Wash-away elements	5.92	5.89	6.70	5.63
Relative density I_D	0.86	0.93	0.87	0.82
Coefficient of uniformity C_u	> 15			
Coefficient of curvature C_c	> 1			

broken stone of fraction 0–32 mm) of both tested constructions. The values of static transform module in particular construction layers of subbase are defined as an average value from 6 results of static loading tests that were done in the following places (see figure 2.1): A_1, A_2, B_1, B_2, C_1, C_2.

On the base of results of static loading tests which were done on the big internal testing stand of DRETM it is possible to determine progress of static transform module. Figure 5.1 represents the proposal of nomogram for dimensioning the railway substructure for the following construction:

- Subgrade surfaces about 7 MPa.
- Geocomposite MACRIT GTV/50-50 B.
- Subbase is broken stone of fraction 0–32 mm with two various granularity curves of graded thickness from 150 mm to 600 mm.

To compare reinforced and non reinforced railway substructure we used methodology shown in annex No. 21 regulation [1]

Average values of static deformation modulus during applying reinforced geocomposite MACRIT GTV/50-50 B in the particular subbase layers of fraction 0–32 mm. Tab. 5.1

Description of tested place	Static deformation modulus E_0 [MPa]	
	1st phase (Curve of subbase material grain-size complains to STN 73 1001)	2nd phase (Curve of subbase material grain-size complains to TNŽ 72 1514)
Subgrade surface	7	7
Subbase of thickness 0.150 m	14	17
Subbase of thickness 0.300 m	37	33
Subbase of thickness 0.450 m	62	55
Subbase of thickness 0.600 m	80	62

that represents the basic methodology for designers. Using this information we reached following values of bearing capacity expressed with the equivalent transform modules E_{e1} to E_{e4} on the particular construction layers of subbase and in the level of subbase surface without built-in geosynthetic element (tab. 5.2):

6. Contribution

Two phases of experimental measurements that were realized in the railway substructure with built in reinforced geocomposite MACRIT GTV/50-50 B bring results on the basis of which we can confirm not only the expected effect of used geosynthetic but also the influence of chosen subbase material on the resulted bearing capacity of the whole railway substructure.

Lower values of the equivalent transform module on the particular subbase surfaces in the second phase of experimental measurements (in about 12 till 30%) were predicted because of granularity as subbase material required in [10] a has higher proportion of fine fraction 0 – 2 mm (nearly 70%) in comparison with granularity defined in [9] (about 42%). This higher proportion of fine fraction causes lower permeability of the built in subbase, but we reach higher bearing capacity. However there is higher danger that a high proportion of fine fraction increases the ability of crushed

Equivalent deformation modulus E_i [MPa] determined according to the methodology of regulation [1], annex No. 21. Tab 5.2

Thickness of subbase h_i /static deformation modulus of subbase E_i [MPa]	h_1 = 0.150 m	h_2 = 0.300 m	h_3 = 0.450 m	h_4 = 0.600 m
Minimum E_1= 60 MPa	15	23	28	32
Maximum E_2 = 80 MPa	17	27	34	40

Fig. 5.1 Progress of static transform module for construction with geocomposite MACRIT GTV/50-50 B

material to keep the humidity and so that frost susceptibility will show primary and secondary frost effects.

When comparing both values of the equivalent static deformation module, which were determined according to the regulation S4, annex No. 21 and values reached in experimental verification of the railway substructure with geocomposite MACRIT GTV/50-50 B (see tab. 5.1 and 5.2) we can confirm its reinforced effect. The difference between the calculated value of non-reinforced and reinforced tested construction moves in the first phase of experimental measurements from about 160% to about 250% and in the second phase from about 140% to about 200%, under consideration of the transform module of subbase material $E_1 = 60$ MPa and its graded thickness from 150 mm to 600 mm. When considering the transform module of subbase material $E_1 = 80$ MPa, the difference in the first phase of experiment is from about 140% to 200% and in the second phase from about 120% to 160%.

When thickness of the subbase construction was smaller than 0.150 m, reinforced effect of geocomposite MACRIT GTV/50-50 B was not remarkable either in both phases of measurements. Other evaluated results allow assuming the availability of geocomposite MACRIT GTV/50-50 B, like geosynthetic material, for applying in such technology aimed to increase the bearing capacity of the railway substructure in the Slovak Railways. However, one question is open: behaviour of this material during long-time traffic loading.

The authors of the paper would like to *thank the grant commission VEGA for supporting the project No. 1/0341/03*, which allows the realization of experimental measurements and consequently obtaining the relevant results that are presented in this paper.

References

[1] Regulation of Slovak Railways (SR) S4: *Railway substructure*. NADAS Praha, 1988.
[2] Regulation of Czech Railways (CR) S4: *Railway substructure*. Annex No. 11, 1998.
[3] Richtlinie DB 836 *Erdbauwerke planen, bauen und instand halten*, modul 0503, 1999.
[4] STN 72 1006: *Control of Soils and Bulk Material Compaction.*
[5] *Technology of laboratory tests in soils and ground mechanics,* Czech Geological Office, Praha 1987,
[6] STN 72 1012: *Laboratory determination of soil natural moisture.*
[7] STN 72 1013: *Laboratory determination of plastic limits.*
[8] STN 72 1014: *Laboratory determination of liquidity limits.*
[9] STN 73 1512: *Solid gravel for building purposes. Technical demands.*
[10] TNŽ 72 1514: *Technical and ecological conditions to supply material into construction of track bed and subbase layers.*

https://doi.org/10.26552/com.C.2004.3.44-46

komunikácie
COMMUNICATIONS

Hana Krejčiříková – Martin Lidmila *

EXPERIMENTAL AND MATHEMATICAL ANALYSIS OF A MULTI-LAYER SYSTEM OF RAILWAY TRACK

Based on experimental measurement of a model of a multi-layer non-linear system with inserted geosynthetic layers of the permanent way structure, a new design method will be designed for dimensioning the sleeper subgrade structure using classical and geosynthetic materials or sub-ballast vibration-damping matting. The results of measurements on a track structure model in a 1:1 scale performed in a testing box will be verified by means of a numerical model. A two-dimensional solution will be subsequently verified by means of a spatial model. Numerical modelling will serve for transferring the values measured on the experimental model into a current railway track structure.

The Czech Republic has launched a process of gradual modernization of selected, so-called corridor tracks, to allow for train velocities of up to 160 km.h^{-1}. The railway track construction must be designed in such a way to ensure long-term stability of geometric rail parameters. A necessary precondition for this is a sufficient bearing capacity of the substructure even in climatically unfavourable seasons, ensuring thus the overall needed bearing capacity of the railway track construction. In unfavourable geotechnical conditions, the design practice applies structural layers below the ballast bed using various building materials. Numerous geosynthetic materials are also applied to reinforce individual structural layers. In order to reduce noise and vibrations, elastic sub-ballast matting is used, too. No exact design method for the dimensioning of the track bed bearing construction, however, has been developed to-date, either abroad or in our country. Exploitation of innovative materials in the structural layers of railway tracks is solely based on empirical knowledge obtained from applications implemented at individual sites.

Fig. 1 View of testing box with inserted partition

The project concept is based on a mathematical calculation of the bearing capacity of a multi-layer track bed construction of the railway track, and verification of the results of a theoretical solution by means of experimental measurements carried out on a model of a railway track section in a 1:1 scale in laboratory conditions. Experimental measurements will apply a testing box of the Central laboratories of the Faculty of Civil Engineering, CTU in Prague.

The project output will be an exact design method of the railway track bed bearing construction, which will not only allow designing track bed bearing constructions for various geotechnical conditions, but will also optimize these constructions with regards to cost-effectiveness. The project achievements will be applied in updating selected parts of the ČD S4 Regulation "Substructure", in the operational practice of the Czech Railways as well as in the design practice within the next stage of modernization of railway lines managed by the Czech Railways. Designing optimum railway track constructions with the required load-bearing capacity will be cost-effective, too.

The preconditions for reaching the project objectives are completion of experimental measurements using a track construction model in a 1:1 scale in the testing box (Fig. 1) for:

- a track bed of unbonded layers,
- a track bed of unbonded layers with reinforcing synthetic geotextiles,
- a track bed of unbonded layers with sub-ballast antivibration matting,

the design of numerical models of the railway track construction, verification of the results of experimental measurements by means of a numerical model, verification of the two-dimensional solution of the numerical model of the railway track construction with the help of a three-dimensional model, the development of a new design method of the load-bearing construction of the railway track under

* **Hana Krejčiříková, Martin Lidmila**
Department of Railway Structures, Faculty of Civil Engineering, Czech Technical University, Thákurova 7, 166 29 Prague 6, Czech Republic,
E-mail: krejcirikova@fsv.cvut.cz

various geotechnical conditions applying different track bed constructions.

The first grant project year (2003) was used for the completion of the following works:

Verification of the behaviour of the railway superstructure and substructure subjected to loading in the testing box was a basis for the design of measurement methodology.

Measurement methodology was designed and verified using a model of the railway superstructure and substructure construction. The following track bed construction was selected for verification:

- ballast bed 32–63 mm with a thickness of 35 cm,
- a layer of partially crushed gravel 0–32 mm with a thickness of 15 cm,
- rubber plates with a thickness of 54 mm simulating subgrade with a bearing capacity of 15 MPa.

The track bed was loaded with a half of a concrete sleeper B 91S with a piece of a rail UIC 60, which was exposed to a force of 50 kN. The loaded model was used for the measurement of the following parameters:

- sleeper subsidence,
- ballast bed subsidence,
- simulated subgrade subsidence (Fig. 2),
- moduli of deformability on the ballast bed surface, on the surface of the layer of partially crushed gravel and on the surface of rubber plates (Fig. 3),

Fig. 3 View of a measurement of modulus of deformability on the ballast bed surface in testing box

a)

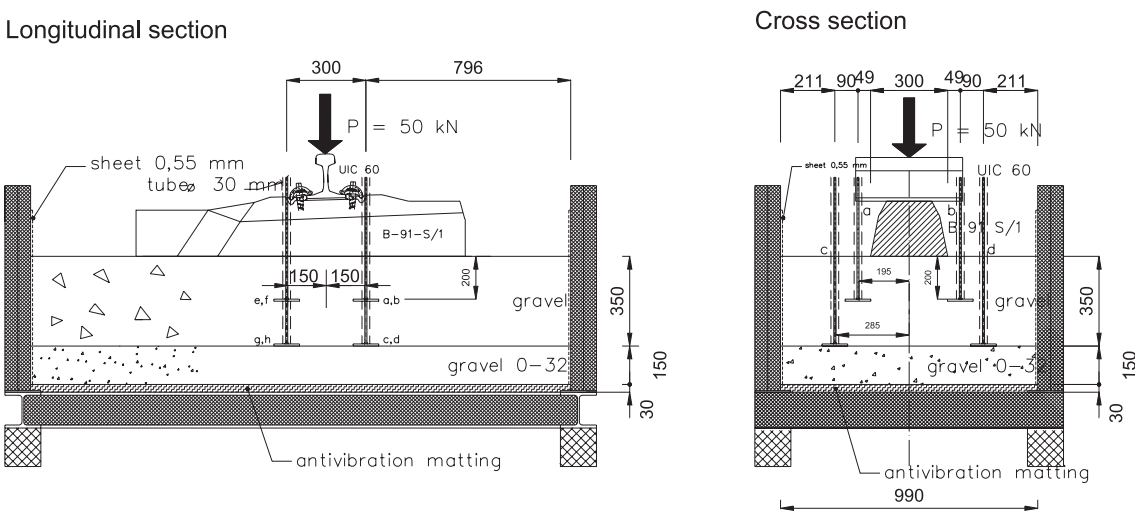

b)

Fig. 2 Measurement of sleeper subsidence under load of rail by hydraulic set ENERPAC with a force of 0 - 50 kN a) scheme b) view

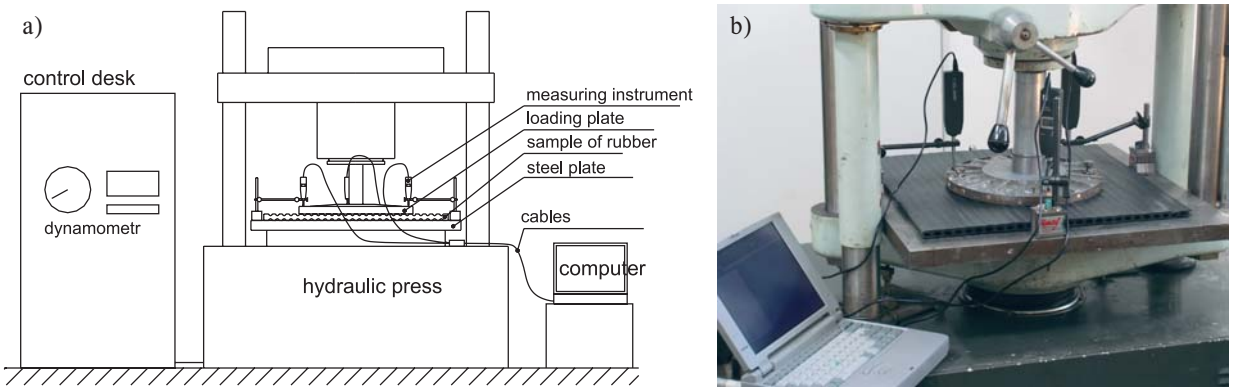

Fig. 4 Measurement of static modulus of deformability of sub-ballast matting VM 12-01, a) scheme of measurement unit fabric, b) view of measurement unit

- stress at the level of sleeper loading area, on the surface of the layer of partially crushed gravel and on the surface of rubber plates simulating the subgrade.

The measurements of moduli of deformability on sub-ballast antivibration matting of Phoenix VM 12-01 brand laid on a stiff base were made.

Experimental investigation of the effect of sub-ballast antivibration matting of Phoenix VM 12-01 brand on the overall bearing capacity of the track bed was performed (Fig. 4).

This investigation applied the following track bed model in the testing box:

- ballast bed 32–63 mm with a thickness of 35 cm,
- with and without a layer of partially crushed gravel with a thickness of 15 cm,
- sub-ballast antivibration matting of Phoenix VM 12-01 brand,
- stiff base (testing box bottom) or simulated subgrade consisting of a layer of partially crushed gravel with a thickness of 12 cm laid on a layer of rubber with a thickness of 30 mm, which was laid on a stiff base (testing box bottom).

A measurement of modulus was performed in three unoverlaping places situated by longitudinal axe of the testing box. Results of measurement are given on Fig. 5.

(Numeral values determined modulus of deformability on the construction in the level of labelled layer.)

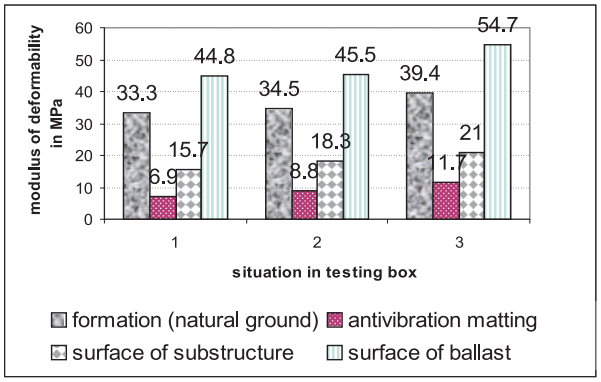

Fig. 5 Results of measurement of static modulus of deformability in testing box

The project results and their exploitation in the operational practice of the Czech Railways will contribute to a more objective design of the load-bearing construction of the railway track. At the same time, they will facilitate the design of a construction with optimum cost-effectiveness. The analysis of the railway track construction also represents a general solution of the distribution of force effects due to railway operation within the construction of a multi-layer track bed system. The project is aimed at developing an innovative design method for dimensioning the track bed construction using standard building materials as well as geosynthetics, or using sub-ballast antivibration matting.

References:

[1] KREJČIŘÍKOVÁ, H., TYC, P.: *Geomembranes for ČD Tracks*, conference „Geosynthetics in Transport Construction", 2003,
[1] KREJČIŘÍKOVÁ, H.: *Railway Track Stiffness as one of its Characteristics*, II. Miedzynarodowa konferencja Naukowo-Techniczna, Wroclaw, 2003, pp. 29–32,
[1] HORNÍČEK, LIDMILA, M.: T*he Effect of Antivibration Matting on the Tram Track Bearing Capacity*, the professional conference of doctoral students, volume 10 – Construction Management Economics, VUT Brno, Faculty of Civil Engineering, 2003, pp. 97–101.

https://doi.org/10.26552/com.C.2004.3.47-50

Dana Sitányiová – Soňa Masarovičová *

GIS APPLICATION FOR SOLUTION OF THE PROBLEMS OF PUBLIC TRANSPORTATION SYSTEM IN ZILINA

The paper deals with the public transportation system in Zilina. The research study initiated by the Transportation Company of Zilina has been performed with the aim to solve the problems concerning public transportation service in the urban area. The main goal of the research study was to evaluate how well the bus stops serve the public and to identify the segments of the traffic routes, which are risky for buses and trolleybuses operation. Geographic information system was applied to solve these problems by analysing the geospatial data referring to the transportation system. The paper includes the outputs from these analyses.

Defining the problem

This paper deals with the public transportation system in Zilina. It includes the outputs from the research study "Public Transportation System in the City of Zilina", that has been carried out in the Department of Geotechnics at the Faculty of Civil Engineering since 2002. The research staff of the department has performed the research study with the assistance of two students, who solved some partial problems in their diploma theses. The Transportation Company of Zilina initiated the research study with the aim to solve the problems of public transportation services in the urban area. Although in 1996 the company began with the overall electronisation of the city public transport system and Zilina is the only town in Slovakia, which completely monitors the operation of public transport using on-board computers, there are still several problems that cannot be solved without the assistance of efficient tools providing analyses of geospatial data. One of those tools, geographic information systems (GIS), is becoming more and more familiar to the planners, analysts and researchers as the best way to assess traffic safety, sustainability, and convenience. The main goal of the research study has been to use the tools of GIS for the effective solution of the following problems:

1. To evaluate how well the bus stops serve the public.
2. To identify the segments of the traffic routes, which are risky for buses and trolleybuses operating.

The first problem concerns determination of service coverage of the bus stops, the second one is related to identification of those traffic routes segments that have unsuitable slope of the pavement for operating the public transportation vehicles.

Methodology

In the urban area of Zilina, the public transportation service is provided by the fixed-route bus and trolley bus system. From the perspective of a bus operator, a basic unit of analysis is a bus-trip. Although varying in format, each bus company maintains a complete list of bus trips for each of several regular schedules (e.g., weekday, weekend days, holiday, etc.). On December 31, 2002 the transportation company employed 400 persons and managed 58 buses and 43 trolley buses. It operated 8 trolley bus and 13 bus lines for a total length of 13.867 km on workdays. Vehicles are equipped with automatic validation machines for paper tickets and travel chip cards and on-board computers, which store information on vehicle operation. Information is stored in a database and periodically evaluated and analysed with special software. Although this information provides a very useful basis for operational analyses, it is not directly connected with geospatial data.

Network Structure

A complexity associated with GIS data is the variability of transportation data entities [2]. Transportation entities can have physical description and logical relationships with other transportation entities. They exist both in the real world and virtual world – in the database. Since the Department of Geotechnics disposes of the software GIS ArcView 3.1 (without ArcView Network Analyst extension), we decided to use non directed node-arc representation for a planar network model representing the transportation system, however, emerging transportation network models treat multiple modes in a more-sophisticated manner. Within our transportation network, nodes correspond to street intersections and bus stops while arcs correspond to street segments between nodes. The theme of street network was created on the basis of digital map set (scale 1:10 000). The transportation system entities from the real world represent the themes in ArcView in form of points, lines or polygons. Two base themes represent the transportation system: the line theme representing the route network and the point theme representing bus stops were created in the view. The theme of bus stops correctly overlaps the nodes of the line theme (see Fig. 1).

* **Dana Sitányiová, Soňa Masarovičová**
University of Žilina, Faculty of Civil Engineering, Department of Geotechnics, Komenského 52, 010 26 Žilina, E-mail: dana.sitanyiova@fstav.utc.sk

Fig. 1 Street network with the theme of bus stops and route lines.

Focusing on the route-level is common in the case of a fixed-route bus system. In our system the routes have extensive overlaps and carry different route numbers. The bus routes could be considered being separate when specifying a transit route structure. However, these elemental routes should not be digitized independently on a separate GIS theme (layer), but should be defined by reference to the base street network. Provisions should be made so as to be able to combine elemental routes for the preparation route numbering. Partial arcs within the line theme were defined by a route number. It allows a user of the system to identify a route number by a simple click on a street segment.

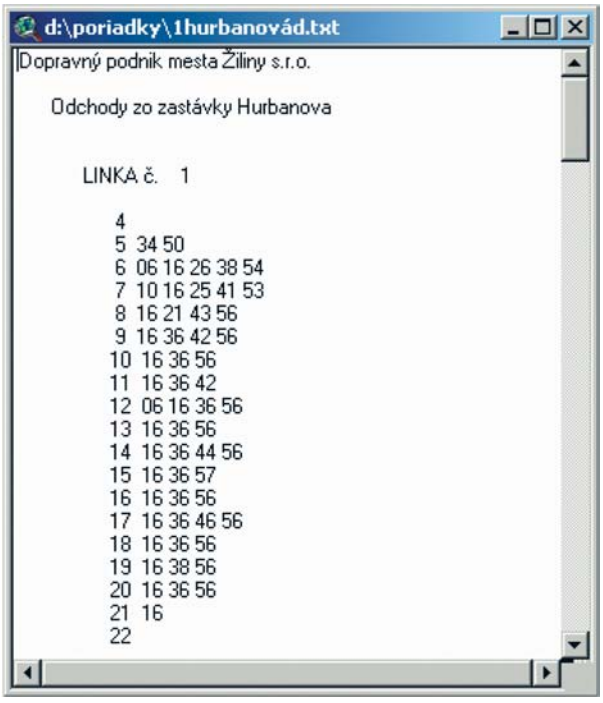

Fig. 2 Time schedule - Hurbanova bus stop (route No. 1).

Spatial entities in GIS ArcView system are connected with attribute data. Attribute data can contain comprehensive information on entity properties. We decided to store information especially about bus stops. The attribute table of bus stops theme includes information on:

- name,
- equipment (ticket machine, shelter construction, news stand, etc.),
- routes available, etc.

Therefore the user of our system is able to obtain information which bus or trolley bus route is available in the bus stop and/or if it is possible to buy a ticket there by clicking on the individual bus stop. The theme of bus stops is linked (ArcView hot link tool) with the external file containing the route timetable (see Fig. 2). Data symbolizing involves choosing the colours and a symbol that will represent a feature. The theme of bus stops can be symbolised by attribute information in several ways. There are bus stops equipped with ticket machines symbolised by yellow squares in Fig. 1. The bus stops without machines are symbolised by green circles. The result is the map showing visual information about the transportation network.

Service Coverage

Bus stops must be close to where the people who use them live, work or shop. If they take buses, they do not want to walk more than 500 metres to the nearest stop. And the company operating buses does not want its clients to walk very far to use its services.

The location of bus stops and a walking distance to those stops were the concern of the Transportation Company. The simple way how to generate a service coverage of bus stops is to do a circle with a radius 500 metres around it. But that is not sufficient. The circles very often overlap and there are buildings and other objects within their areas. We decided to use analysis tools available in GIS. The process is described step by step and illustrated by figures.

The co-ordinates of the bus stops were determined on the transformed map to the geographical co-ordinates. Distance mapping analysis was made to determine the area of distance. Distance mapping finds how far each cell is from the nearest source. Distance can be measured in term of how far objects are (Euclidean). Two principal groups of analyses utilize the Euclidean system for determining distance: proximity mapping and distance mapping. We decided to use the combination of both. The analysis is described as follows step by step. At first the analysis of distance was carried out. Since walking distance to the bus stop should be 500 metres, only the cells within 500 metres of the selected bus stops (four bus stops in the town centre) were symbolised by red colour (see Fig. 3).

Then the analysis of proximity was made with the aim to assign which bus stop serves to which cells (service area). Fig. 4 represents the combination of the analyses in the limited area.

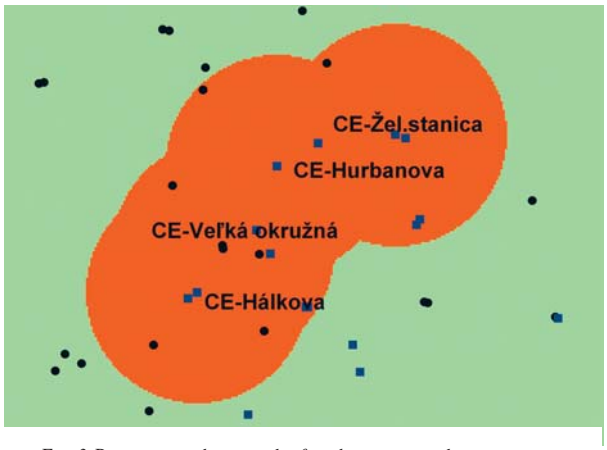

Fig. 3 Distance analysis on the four bus stops in the town centre.

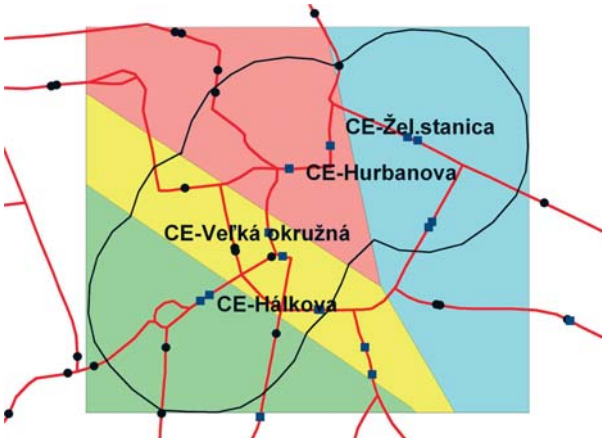

Fig. 4 Service coverage of the selected bus stops.

This combined analysis was made for all the bus stops in the town. It is also possible to include certain other parameters, which can be taken into account in the analysis. The importance of these parameters can be assigned based on the requirements of a public and/or transportation operator. As parameters we can consider:

- importance of locations such as hospitals or schools,
- density of population,
- time,
- availability of infrastructure and finance,
- traffic congestion,
- other modes of transport, etc.

Risk analysis for bus and trolley bus operating

Bus and especially trolley bus operating requires special conditions in term of infrastructure. The limited slope of the pavement is needed for smooth operation of vehicles. The slope below 12 % is required for bus operating and 15 % for trolley bus operating. Therefore, the Transportation Company required identifying those routes segments that have unsuitable slope of the pavement for the operating of the public transportation vehicles. Since the risk slope analysis is principally made up of surface, the analysis of surface elevation was made with the aim to solve this problem. A surface has steepness and direction, commonly referred to as slope and aspect. The Derive Slope choice on the surface menu in GIS ArcView can take a grid or TIN theme as input. The grid theme represents surface using a mesh of regularly spaced points. TIN (triangulated irregular network) represents surfaces using contiguous triangle facets. Since the lines (contours) were available as a source of information about elevation, we decided to use TIN to represent the surface (See Fig. 5).

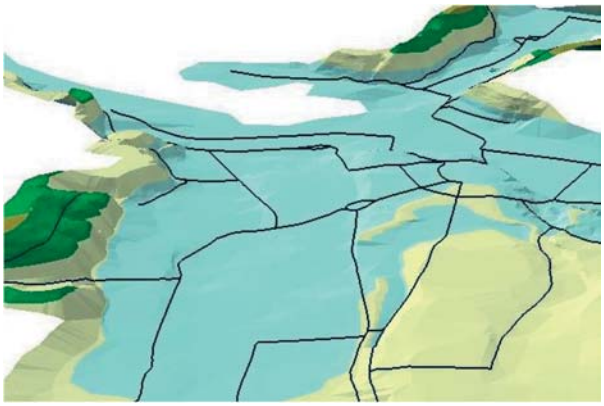

Fig. 5 3D scene with TIN representing the elevation with the bus routes [1].

The slope identifies the incline of a surface. The output slope theme can represent a slope in degrees or percentages. We have derived the slope map from TIN theme. There are two possibilities how to identify the areas with an unsuitable slope (15 % for trolley buses):

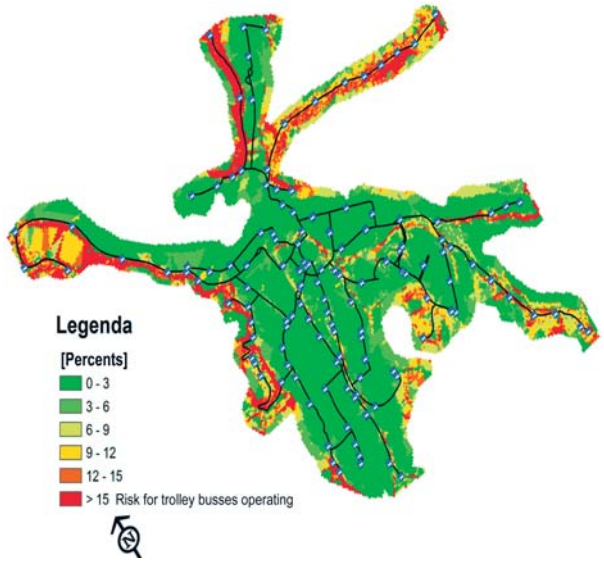

Fig. 6 The map of a risk slope – trolley buses [1].

1. to reclassify the slope map on three classes (< 15 %, > 15 %, no data), or
2. to query the slope map theme (find areas with adverse slope > 15 %).

We used the latter possibility. The output is represented by GRID – risk map, where the areas with the risk slope are represented by red colour (See Fig. 6). There are several parts of the routes within areas with an adverse slope (Hájik, Zástranie, Zilinská Lehota, etc.) In addition, the set of profile graphs for each route was created (See Fig. 7).

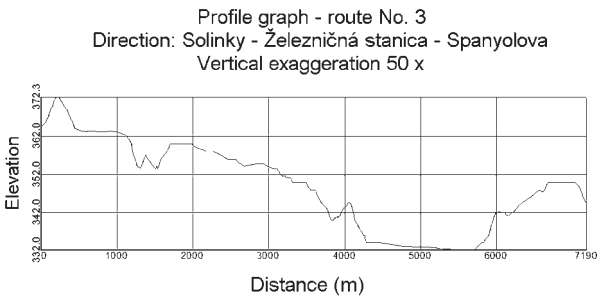

Fig. 7 Profile graph for the route No. 3 [1].

Conclusions

The study of public transportation system issues of Zilina was carried out by means of advanced methods of data analysis such as the use of GIS for the spatial analysis, which offers the following advantages:

- use of geospatial referenced data,
- graphical and attribute data input and editing,
- spatial and attribute query,
- advanced visualization, etc.

This way GIS can be used in all the ways to carefully analyse all the public transportation problems and to successfully give a good solution that is acceptable for everyone. GIS can also encourage a holistic approach to transportation analysis, supporting integrated analysis of transportation system components within its geospatial context.

References

[1] KONEČNÝ, A.: *Application of GIS for profile graph analysis of public transportation routes in Zilina* (in Slovak), Thesis, 2003.
[2] HARVEY, J. M., SHIH-LUNG, SH.: **Geographic Information Systems for Transportation**, Oxford University Press, 2001.

https://doi.org/10.26552/com.C.2004.3.51-54

Marián Drusa – Vladimír Gróf *

GEOTECHNICAL ASPECTS OF RAILWAY TUNNEL CONSTRUCTION NEAR RUDOLTICE

Construction of the tunnel in Třebovice v Čechách has been, from the geotechnical aspect, the most problematic issue ever, and, we would like to define some of the reasons and to sketch a potential solution.

1. Introduction

The article presents a project of railway tunnel from the point of view of potential short term or long term geotechnical risks; it means risks in the course realisation and operation time. There had been elaborated many variant projects for the new tunnel on main railroad between the cities Krasíkov and Česká Třebová in the Czech Republic in the leg Třebovice v Čechách – Rudoltice v Čechách. We would like to present some positive and negative aspects of one project variant presented by the company Metroprojekt, and, another one is "Study of Project Modification" presented by consortium Krasíkov.

2. Engineering-geological and Hydro-geological Conditions

Geological structure of the area where the railway line was traced is a typically complicated structure of lateral formation. There are quarternary fluvial and deluvial deposits of average thickness

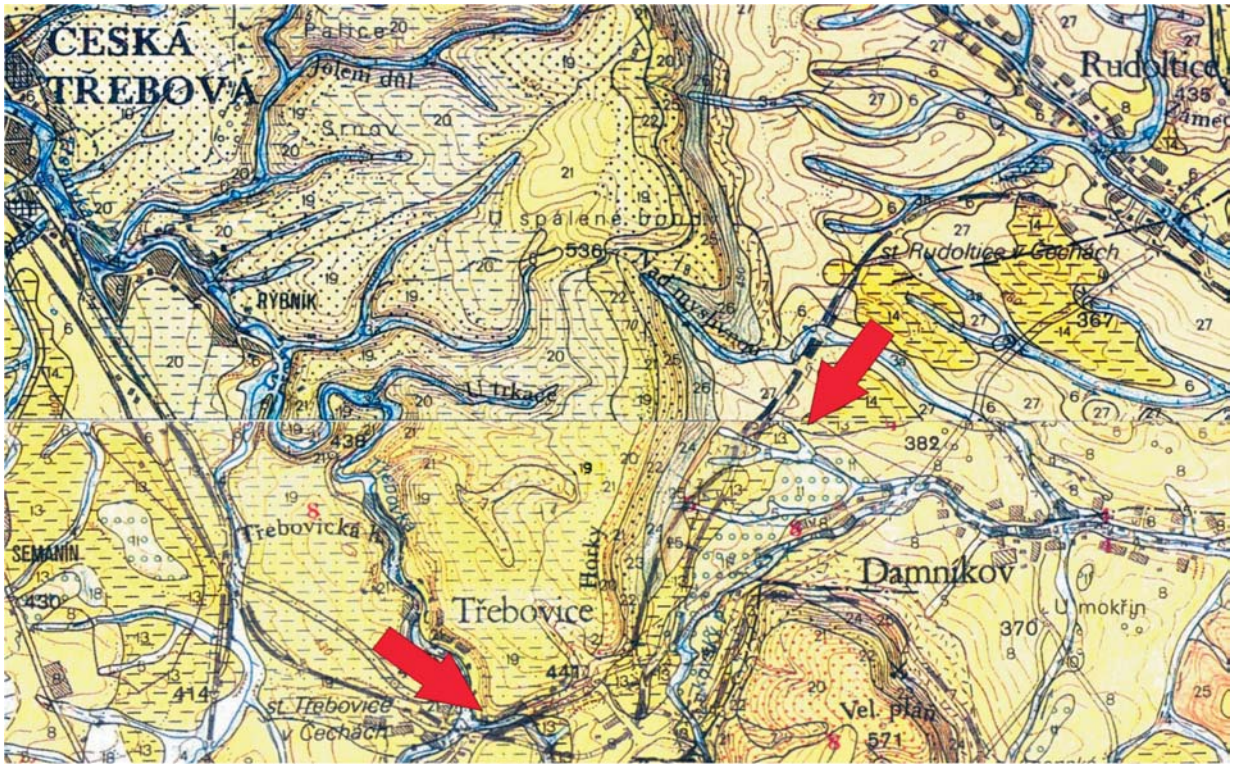

Fig. 1 General Geological Map of Area Near Rudoltice

* [1]Marián Drusa, [2]Vladimír Gróf
[1]Department of Geotechnics, Faculty of Civil Engineering, University of Žilina, Komenského 52, 010 26 Žilina, Slovak Republic. Tel: +421-41-7634818, Fax +421-41-7233502, E-mail: drusa@fstav.utc.sk
[2]GeoExperts Ltd. Žilina, Bytčická 82, 010 01 Žilina, Slovak Republic. Tel: +421-41-5006915, Fax: +421-41-5006915, E-mail: vladimir_grof@geoexperts.sk

of 6 up 8 m on Miocene's clays of significant thickness, which are occasionally calcareous, with thin closed layers of gravel and organic mixtures. General geological area map of the new tunnel projects is shown on Fig.1. Stronger rock environment of Mesozoic origin lies deeper. The described geological environment of Miocene's clays may be evaluated from the point of view its suitability for underground structures as an unacceptable for construction of new tunnel. Surroundings of the future tunnel excavation can be classified as very squeezed and unstable in changed conditions caused by tunnelling.

From the engineering-geological aspect the "Study of Project Modification" is more advantageous in comparison with the "Metroprojekt Tunnel Design", as there is only a little trenching of Miocene's unstable clayey layer.

Both presented variants of railway track leading of shaft sinking tunnel will infringe hydro-geological conditions in close geological environment. Deeper excavation into a rock mass on a considerably longer section should be great disadvantage of the first variant. A substantial part of the first variant new railway tunnel is situated in line of the old tunnel, which is draining surrounding rock environment, but, because of its smaller dimensions, it is less influential. In the presented geological environment, the water flows more through quarternary permeable soil layers than impermeable Miocene's clays. There should be taken into consideration the hydraulics impacts to the surrounding territory after being built-up a large scale barrier element, represented by the excavated tunnel.

3. Geotechnical Risks of Tunnel Construction

The scope of the second variant, presented by consortium "Krasíkov", is to reduce the tunnel length in order to minimize the impact to unsuitable layer of Miocene's clays. There are real fears from this geological formation, which have originated in construction difficulties of previous "Třebovice Tunnel" as well as from many foreign negative experiences with construction of tunnel in squeezing and swelling rock environment. It has been generally known that the tunnel construction in swell and squeezed rock materials is the most difficult task as an underground construction.

Based upon the existing state of tunnelling know-how the objective geological space might be classified into one of the groups:

- swell rock environment with a swelling based upon physical and chemical reaction with water and not upon a mechanical principle. There are very well known problems with osmotic swelling of clayey minerals group of smectites or clayey mixture-layered minerals. Further relevant swelling environments are anhydrite formations. These formations may produce high pressure on bottom tunnel vault;
- hardly squeezed rock formation occur mainly in faulty zones in the case of the tunnel excavation, where then acts all-round high rock stress on the tunnel lining;
- swell-squeeze rock environment, where swelling is of a mechanical character, i.e., in its deconsolidation, respectively, in plastic stress strain deformation of rock.

As it may be seen, the term "swelling" may be attributed to two various mechanisms of rock volume increase. As there has not been found any information concerning the presence of smectite minerals in the layer of Miocene's clay, it might be presumed that no chemical swelling mechanism in the course of construction "Třebovice tunnel" would occur. The authors Klepsatel, Kusý, (2003) state that possible reason of the swelling process in the old "Třebovice tunnel" had been haeving of organic matters, present in geological formation in substantial amount.

The precise composition of these substances is not known, thus, it is very important to understand the swelling mechanism for being able to forecast potential geotechnical risks, especially in a long-term horizon. If speaking about a short-term one - the construction will be in any case very demanding. From the long-term point of view, we are not able to evaluate exactly all geotechnical risks at the current state of information. When speaking only about mechanical swelling, with an adequate project of the tunnel, the first version would not bring any higher risk than the other one in the long-term horizon. It is presumed that on the basis of present knowledge of potential behaviour of Miocene's clay, it would be better to trace the railway tunnel line in accordance with the second version. Tracing the railway line above the layer of

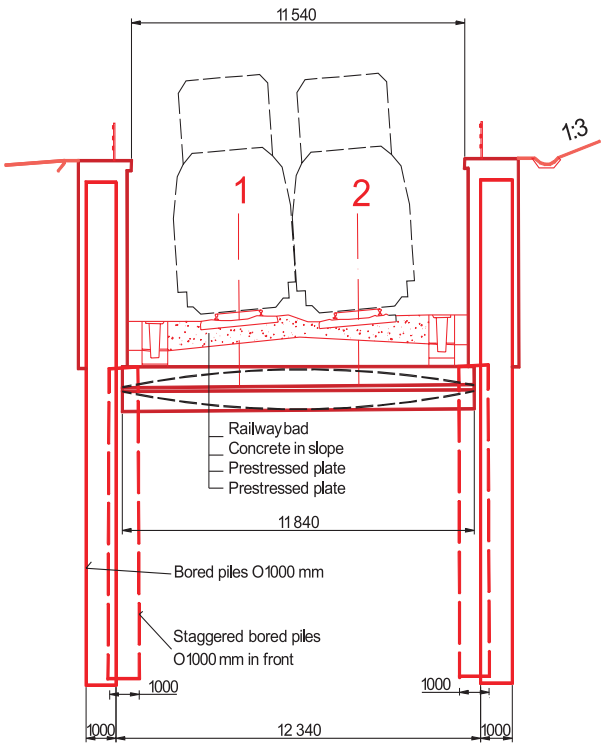

Fig. 2 Cross Section of Railroad

Miocene's clays and, also the designed geotechnical constructions, are technically correct.

The follow-up calculation of pile retaining wall and its external stability against sliding has been done; the calculation evaluated also the depth of fixation of double-row piled wall. Precise dimensioning and calculation of the other parts of construction should be solved in a final realization project. The basic idea of the projected second version presented by the consortium "Krasíkov" is shown in cross-section in Fig. 2.

4. Interference of New and Current Structures

The first version of the tunnel project will have to solve the crossing of the railway-line across a recultivated waste dump, analysis of the embankment stability and speeding-up consolidation will be next tasks. At this line section reinforcing and hardening of subsoil must be solved by appropriate geo-technology or the layer of anthropogenous artificial soils will be excavated to an adequate depth. The following technical task of project will be a stability analysis of the high embankment and evaluation of consolidation time of the embankment on soft soils. The project must involve also a calculation of consolidation velocity, according to a realization project, and, a designed distance of sand drains or geodrains (PSK, Alimac, Membradrain ...) or, there may be used trenching lime, cement or rock columns that would improve subsoil deformations properties, too. The second version should solve strengthening of rock environment around the tunnel excavation at the crossing of a new railway line over the old tunnel (inclined micropiles or use the appropriate manner) and the next back-filling of the old tunnel and build-up the drainage canal.

5. Geotechnical and Environmental Aspects

When considering the geotechnical point of view, the locality for construction of the tunnel must be taken as a very problematic, especially because of the existence of very thick Miocene's clays strata. Undoubtedly, a more convenient solution, when taking into consideration technical and economical aspects, would be the version of the consortium "Krasíkov" that avoids trenching of the Miocene's layer, as mentioned above, because of the stability problems of cuts and plastic bulging of embankments after construction of the tunnel.

When comparing the presented versions, the latter one has a substantially less negative impact on the hydro-geological conditions in the locality, as well as on the surrounding fauna and flora.

6. Comparison of Versions

Positives and negatives of the first version "Metroprojekt Tunnel Design" may be summarized in the following Table 1.

Tab. 1

Pros	Cons
+ very safe technology of tunnel construction in closed chambers with elimination of deformation zones of monolithic "Milan" walls	– presumption of unfavourable and unexpected geotechnical problems – depth of foundation of new structure and its impact on surroundings – hard excavation in layer of Miocene's clays – negative influence on underground water on long distance section of territory, where is railway traced – tracing of railway-line by high embankments on soft subsoil – expected three-dimensional deformations in tunnel surroundings – longer railway tunnel and retaining walls – more constable maintenance – construction time and its risks – demanding construction technology

Positives and negatives of "Study of Project Modification" presented by the consortium Krasíkov are shown in Table 2.

Tab. 2

Pros	Cons
+ reduction construction time + lover costs of geotechnical construction + shorter tunnel length and retaining walls length + less hydro-geological impact on tunnel environment + simple construction technology comparing with the first version + lower costs for ground excavation above the Miocene's clayey layer and safer technology + reduced length of the track line + future cost effective maintenance of tunnel and retaining walls	– higher inclination of the track line – higher deformation zones around piled walls – crossing new track line over the-existing tunnel

Having considered all the impacts and factors that could infringe the construction of the tunnel, we would like to recommend the tracing in the sense of the second version, submitted by the consortium "Krasíkov".

References

[1] KLEPSATEL, KUSÝ, MAŘÍK: *Construction of Tunnel in Rock Mass*, Jaga Bratislava, 2003
[2] MÍČA, L., HUBÍK, P., MYNÁŘ, J., MINÁŘ, L.: *Railway Corridors Construction Using Rigid Geogrid Reinforcement in the Czech Republic*, In. Proc. Second European Geosynthetics Conference, Bologna, Italy, pp. 403-409, 2000
[3] SLIVOVSKÝ, DRUSA, GRÓF, AMMAN, BUCHER: *Geotechnical Evaluation of Pliocene's Clays in subsoil of Railway-line Zlaté Moravce Lužianky*, Geotechnika Bratislava, 1997

https://doi.org/10.26552/com.C.2004.3.55-60

Tatiana Olejníková *

RELIABILITY OF ELECTRICAL SECURITY SYSTEMS IN EXTERNAL PROTECTION OF THE MILITARY OBJECTS

In this paper electrical security systems used in military objects and areas of the Slovak Republic Armed Forces are described. There is described a method of reliability calculation of the safety system elements as a probability that the system will operate without a failure during the defined time in the given conditions.

1. Introduction

To increase the security of military objects in current practice modern technical safety equipment is being used such as:
- electrical safety signalling,
- electrical fire signalling,
- access systems,
- industrial television.

Security systems using modern technical safety equipment consist of a set of scanning, transmitting and decoding devices which signal a dangerous situation in case of an object or area disturbance or in case of fire etc. An application of this equipment creates active inhibitions and barriers, which result in signalling the object disturbance or an unusual situation. Technical security of military objects supports classic security in the means of insurance and information delivery about its disturbance and attack and it increases the efficiency of physical security. The ammunition and armoury storage places and some regime workstations of the Slovak Republic Armed Forces are only areas where technical electrical safety equipment utilizing optical and sound signalling with outing in an operational centre (e.g. supervisory station) is used. Electrical cam sensors and switches installed at the entrances and points of access as well as signalling centres which signalise the opening or closing of these storage places are used. Another material storage (automobile, joint, equipment and another material) which does not require a level of security as ammunition and equipment storage is equipped with elementary cam mechanisms and seals, i.e. with a form of the classic security. In the last years featuring increase in criminality and loss of material, the significance of military objects security and overall interest in total security of property and persons grow continuously. With an increasing interest in a risk-free service of military objects it is necessary to realize a necessity of the professional systematic solution for security of objects using quality services and techniques, which ensure an effective and reliable exploitation of the equipment mounting and undisturbed usage of guarded areas. In choosing the security and regime systems, three basic principles of object security have to be taken into consideration:

1. The absolute security does not exist. Every security system can be overcome. It is only a question of time and appliances available to a disturber.
2. The only arrangement does not solve the safety of an object. There must be a complex solution.
3. The technical appliances are able to support but not to substitute a human.

2. Electrical safety systems

The technical security of objects is created by a set of scanning, transmitting and decoding devices which signalise the dangerous situation from the aspect of an attack, formation of fire etc. The application of these appliances creates a system of active barriers, which in case of overcoming attempts by a disturber result in alarm declaration or they signalise the disturbance of an object. The technical security supports the classic security and transforms efficiency of physical security. According to the space location the technical security can be classified as:
- external, where detectors decoding an attack of an object are situated outside a safety object and they detect the disturbance before the approach to the object,
- jacketed, where detectors decode the disturbance of a building jacket (entrance door, windows, skylights, ventilation and air-condition),
- space, where detectors decode the presence of entities in the safety space inside the building,
- anvil, where detectors decode the manipulation with safety entities.

3. Electrical safety used in the external military objects security

The external safety of objects is a significant component in monitoring large complexes of military buildings and areas, such as airports, industrial objects, military bases, etc. The mission of external safety is to detect the disturber with technical equipment

* **Tatiana Olejníková**
Technical University of Kosice, Faculty of Civil Engineering, Department of Descriptive Geometry, Vysokoškolská 4, 042 00 Košice,
E-mail: tolejnikova@post.sk

as soon as possible until he still does not make an actionable work in the safety area. By detecting a disturber on the periphery of the monitored object the intervener unit will have sufficient time to approach and execute an intervention in the place of disturbance. It mostly deals with an external guard, which is based on the following components:

- *Warning*
  The existence of a fence is the condition for application of an external safety system, because the disturbance can be defined only in this case. Without barrier or fence mechanical restrictions the disturber would enter the detected system or safety area. The action and right of recovery against a disturber would be problematic and at the same time then ineligible alarms would be raised. The fence construction, warning signals and boards should discourage a potential disturber.

- *Detection*
  The electrical detecting barrier detects impacts in the different physical values, which originate in the process of detecting the barrier disturbance attempts. The different systems are dissimilar in technology of detection by which the specific type of physical effect such as compression, vibrations, motion, thermal, etc are assured and analysed. Cameras are used to verify the presence of a disturber.

- *Detection - check*
  The check fence decelerates an action of a disturber before entering the safety area and it provides the intervention unit with necessary time between detection and access to the disturbed place for execution of the encroachment. The combination of all components and physical encroachments inhibits the disturber in achieving his goal.

- *Light*
  It affords an exterior illumination of an object. It must be intensive enough for searching of a disturber, but it is oriented outwards to assure that a driveway for a guard, or encroachment unit would be in relative darkness. Where cameras are used, a different type and density of exterior illumination is required.

- *Way for a watch walk*
  It affords a suitable and safety drive for walk execution and for an encroachment unit to access the disturbed place of an object periphery in the shortest time and in adequate weather conditions.

- *Communication system*
  It creates a line or radio connection between a detect security system installed on the object periphery and a main control place.

- *The main control system*
  It enables the control and monitoring of different emergency systems installed in a protected area. It ensures the command of watch service members and encroach units in "normal" or "warning" conditions via communication channels.

4. The reliability of an electrical safety system used in external security of military objects

Quantitavely the reliability can be defined as the probability that the system would carry out its function without a failure during the defined time in the given conditions. Reliability is a criterion of the effective operation probability of a system at the certain time. Estimation of reliability is initially administrated for components which will be used during the system lifetime phase. Reliability of components is directed by the reliable "bath curve".

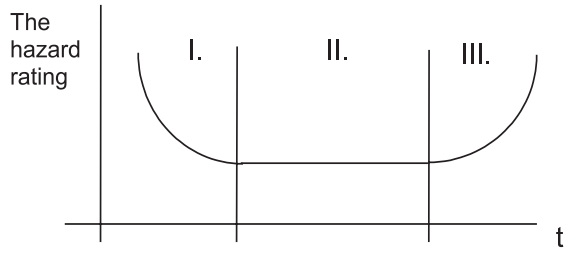

Fig. 1 Reliable bath curve

In the 1st phase the hazard rating is reduced by elimination of weak components.

In the 2nd phase (operation phase) the hazard rating is constant.

In the 3rd phase the components will be worn out and the hazard rating will increase

For a constant value of risk relation may express reliability of a system

$$R(t) = \lambda e^{-\lambda t}$$

- $R(t)$ is the reliability of a successful device operate of the time t
- λ is the grade of failures (constant)

If fault liability of a system can be tolerated and repair can be accomplished, then, the system functionality criterion is the system *availability* expressed by the relation

$$A = \frac{MTBF}{(MTBF + MTTR)},$$

where *MTBF* is the mean time between failures, which is an inverted value of accident intensity: $MTBF = 1/\lambda$, *MTTR* is the mean time of repair – it is the mean time between a system error and its operation.

Availability c*an be defined as an element of the total time in which* in which a system performs the desired function. Availability is marked as A and its complement unavailability as Q and after

$$A + Q = 1.$$

The system failure can be detected if there is a deposit requirement on its performance. Probability that the system will be in

failure status in the instant of time, can be represented by unavailability or proportionate dead time (*PDT*)

$$PDT = \lambda\left(\frac{\Phi}{2} + \tau\right)$$

- *PDT* – proportionate dead time
- Φ – an interval of a test
- τ – mean time for repair.

τ is much shorter than the test interval Φ and therefore *PDT* is often approximated by the relation

$$PDT = \frac{\lambda \cdot \Phi}{2}.$$

Probability of a system safety failure before the risk is the following

$$P_f = PDT \cdot D$$

- it is a product of the proportionate dead time *PDT* and required probability *D*.

Majority of methods for the reliability research is established on these relations.

4.1 Quantitative estimation of reliability and risk

Methods of reliability and risk detecting are included in the studies of different configurations of failure identification, which resulted in decreased system functions.

The study of a system malfunction includes a quantification of failures. The risk of failures can be reduced by money investments, but it is not possible to play for safety absolutely. In the function appraisal of a system it is necessary to define when the system is "functional enough".

The risk or "expected loss of a system malfunction" can be quantitatively defined as a product of the consequence rate of specific accidents and probability of these occurrences:

$$Risk = Effects \cdot Probability$$

The risk can be decreased by reduction of accident consequences or by reduction of probability of their occurrences. The methods for reduction of consecutive losses utilizing more elementary systems are included in different areas. If the risk is identified and evaluated, we can decide if it is acceptable or whether we should make an arrangements for the system upgrade of reliability. We must make decisions concerning realistic goals.

Quantitative evaluation of risk has four phases:
1. eventual menace identification of a system function
2. estimation consequences of each malfunction
3. estimation of probability of each malfunction occurrences
4. comparison of analysis effects with acceptable criteria.

Eventual menace identification of the system function may be defined using failure statistics from the production or from records about genesis of undesired incidents. Preliminary analysis of failure risk with an arrangement of critical effects in different inadequate conditions can be effectively used for identification of subsystems that can considerably endanger the global function of a system.

4.2 Reliability in the risk evaluation

The electrical security system manufacturers must consistently consider the reliability of a system during different phases of planning, so they can evaluate and be optimal for a failure-free operation of a system. It is often expensive to repair the defect in the later phase, especially directly in the object, where the electrical security system has been installed. The report that is based on the study of spectrum failure effects is the valuable project revise. In the project development, it is more appropriate to study the failure causes in more details and more systematically. The engineers still more and more assist the designers to crack the partial problems that relate to system reliability.

4.3 Quantification of element/system failure probability

Even very well designed systems once definitely fail. The basic task is to guarantee that even the system fails the frequency of its failures or probability to abide in the failure status in time will be acceptable. The acceptability can be evaluated by using either economic, activity, or safety criteria depending on a system type. The best adequate probability formulas for the description of element or system accomplishment are availability and reliability.

We consider a reparable element, which begins its life cycle in the operation status. It continues in this status for the specified time until it aborts and then its status changes from the operation status to the failure status. It stays in the failure status until repair is over and the element functions again. This alternation of failures and repair will continue throughout the element lifetime. Availability is an adequate power rate for these reparable elements. Availability can be considered in the following three meanings:

1. *Availability – probability that the system is functional when required.* This definition is adequate for electrical security systems, which operate when requested. Security systems monitor an occurrence of unacceptable accidents and they prohibit the expansion of a risky situation. If the security system is in the failure status in time when it should operate, it is unavailable. As the request for activity can come in a moment, the longer the system is in the function status, the bigger the chance is that it will operate in the given moment, i.e. its availability is bigger. The back up systems also must function on request. Requests for their operation will rise from the failure of a primary system. The character of these alternative systems is inactive in general, i.e. they do not need to carry out an action in normal condi-

tions. The elements, which fail as inactive, fail, unrecognised. The time of their repair depends on the following factors:
- the time it took to detect that a system failed
- availability of a maintenance team
- character of a failure (reparable or irreparable, in the second case the time of exchange depends on the existence of storage or it needs to be ordered from the contractor)
- the time for a system check before its activation

By decreasing the time of a factor activity the dead time is abbreviated and system availability increases.

2. *Availability in the time t - probability that the system functions in the special time t* is a definition of the availability adequate for constantly operated systems of which a failure is immediately detectable and a repair process can start immediately after the failure.

3. *Availability - fraction of the total time when the system functions.* This definition is important for calculation of the productivity of manufacturing process. In this aspect we can use the fraction of the total time when a system functions, to estimate the aggregate output and also the expected advantages in the given time. Probability that system is non-functional in the time t is unavailability where

$$Unavailability = 1 - Availability.$$

In some systems the failure cannot be tolerated. Especially when the failure represents a catastrophic case which damages the device. In this case the zero presence of failure will be a fundamental indicator of accomplishment during the whole-expected system lifetime. We must consider the system *reliability*. Probability that system fails in the specific conditions is known as its *faithlessness* where

$$Faithlessness = 1 - Reliability.$$

In the situation where the system is irrecoverable, then, if the system functions in the time t, it must have acted also during the period (t_0, t), where t_0 is the beginning of the operation status. For irrecoverable systems the unavailability equals faithlessness.

In the simplest models for derivation of probability that system fails, it is assumed that the system can exist only in two forms of status: in the operation status and in the failure status. It is assumed that a system begins its life in the operation status. After definite time the system fails and it changes its status into the failure status. If the system is unrecoverable this status is definite. The reparable element of the system stays in the failure status until the repair is finished and the element is again in the operation status. Two assumptions were defined for this model:
1. only one alternation can arise in the short moment dt
2. alternation between two discrete forms of status is too short.

The alternation from the operation status to the non-functional status is called the *failure*. The regress process is the *repair*. It is also assumed that after the repair the element functions as well as it was new. The life cycle of an element consists of alternation series between these two stages.

4.4 The process of a failure

The time of the failure cannot be predicted accurately for an element. The elements of the same type will fail in different time. The time until the element fails can be applied for probability separation, which states the probability that the element will fail before the defined time t. Different elements will have different separation time until they fail. The separations can be estimated by the element testing in the control conditions or by collecting and analysing data about elements in the operation.

The faithlessness of the element $F(t)$ in the failure status represents the probability that the element will fail some time before the time t

$$F(t) = P[\textit{The element will fail in the time interval } (0,t)].$$

The function of probability density $f(t)$ is

$$f(t) = \frac{dF(t)}{dt}$$

that $f(t)dt = P[\textit{The element will fail in the time interval } (t, t + dt)]$,

$$F(t) = \int_0^t f(t)dt.$$

The change into the failure status can be characterised by the conditional failure rate $h(t)$. Sometimes it is described as a risk rate (risk function). It is a criterion of the failure origination rate with regard to the number of elements with the potential to fail, i.e. elements which operate in the time t has the form:

$$h(t)dt = P[\textit{The element will fail in the time interval } (t, t + dt) \,|\, \textit{does not fail in the time interval } (0,t)],$$

that $h(t)dt$ is conditional probability.

From the conditional probability formula

$$P[A \,|\, B] = \frac{P[A \cap B]}{P[B]}$$

where cases A,B can be characterized as follows:

A – the element will fail between t and $t + dt$

B – the element does not fail in the time interval $(0,t)$, follow

$$h(t)dt = \frac{P[A]}{P[B]} = \frac{f(t)dt}{1 - F(t)},$$

because $P[A \cap B] = P[A]$, if an element fails in the time $(t, t + dt)$, it means that it could not fail before the time t. It means that

$$\int_0^t h(t')dt' = \int_0^t \frac{f(t')}{1 - F(t')} = \ln |\, 1 - F(t) \,|,$$

therefore

$$F(t) = 1 - \exp\left(-\int_0^t h(t')dt'\right),$$

where $h(t)$ is the rate of the failure.

If we draw this function depending on time, we will get the graph in the shape of the known "bath curve". This curve is characterised by a declining failure rate in the 1st phase, in the middle it is nearly constant and by a rising failure rate in the 3rd phase. There are these arguments for it:

1st phase is the phase of the element launch where some manufacturing errors can occur
2nd phase is the phase where the failure is accidental
3rd phase is the phase of abrasion where the failure rate rises.

If we consider only the 2nd phase of the element service, the failure rate can be considered as constant.

$$h(t) = \lambda,$$

then

$$F(t) = 1 - e^{-\lambda t}.$$

Then the reliability $R(t) = \lambda e^{-\lambda t}$ is the probability that the element operates continuously in the time $(0, t)$ and it is given by the exponential function. As the failure rate is constant, this function is named "random failure distribution". The function of probability for $F(t)$ is $f(t) = \lambda e^{-\lambda t}$. The mean value of the distribution presents a mean time of a failure:

$$\mu = \int_0^\infty t\, f(t)dt = \int_0^\infty t\, \lambda\, e^{-\lambda t}\, dt = \frac{1}{\lambda}.$$

If we have the constant failure rate then the mean time to a failure is the reciprocal value.

4.5 The process of repair

The parameters, which represent the process of repair, can be given by the following procedures:

Let $G(t) = P[$*The given failure element will be repaired in the time interval* $(0, t)]$ if $g(t)$ is a function of the density, then for the intensity of the conditional repair $m(t)$ is:

$$m(t) = \frac{g(t)}{1 - G(t)}.$$

From this, after the integration, we will get

$$G(t) = 1 - \exp\left(-\int_0^t m(t')dt'\right).$$

If we assume that the repair rate is constant

$$m(t) = v,$$

then

$$G(t) = 1 - e^{-vt}.$$

If the repair rate is constant then the mean time to the repair τ is a reciprocal value of the repair rate:

$$\tau = \frac{1}{v}.$$

If we want to determine the unavailability of the element, we must simulate the all life cycle of the element and we must consider the process of a failure and the process of repair concurrently.

5. Conclusion

The next parameters affect capacity of the element:

The availability $A(t)$ – the probability that a system is in operation in the time t
The unavailability $Q(t)$ – the probability that a system failures in the time t
The intensity of an unconditional failure $w(t)$ – the probability that the element fails in the unit time in the time t, and it operated in $t = 0$. It is the probability that the element fails in $(t, t + dt)$, and it operates in $t = 0$.
The expected number of the failures $W(t_0, t_1)$

$W(t , t + dt) =$ *the expected number of the failures in the time interval* $(t, t+dt) = \sum_{i=1}^{\infty} P[i$ *failures during the* $(t, t + dt)]$.

As during the short time interval dt there is one failure

$W(t, t + dt) = P[$*one failure during the* $(t, t + dt)] = w(t)\, dt.$

Then

$$W(t_0, t_1) = \int_{t_0}^{t_1} w(t')dt'.$$

If the element is not repairable then

$$W(0, t) = F(t).$$

The intensity of the unconditional repair $v(t)$ – the probability that the failed element will be repaired in the unit time in the time t, if it operated in $t = 0$.

The expected number of the repairs $V(t_0, t_1)$ – the expected number of the repairs of a failure element in the time (t_0, t_1)

$$V(t, t + dt) = v(t)dt.$$

After the integration

$$\mathrm{V}(t_0, t_1) = \int_{t_0}^{t_1} v(t)dt.$$

The intensity of the conditional failure $\lambda(t)$ – the probability that the element fails in the unit time in the time t, and it operated in the time $t = 0$. The difference between conditional and unconditional intensity of the failure w is that λ is the failure rate which is established on the elements which operate in the time t and $t = 0$.

$\lambda(t)dt$ is the probability that the element fails during the $(t, t + dt)$ and it operated in the time t and $t = 0$.

$w(t)dt$ is the probability that the element fails during the $(t, t + dt)$ and it operates continuously from $t = 0$ to t. The relation between the intensity of the conditional failure $\lambda(t)$ and the intensity of the unconditional failure $w(t)$ can be derived by the conditional probabilities:

$$\lambda(t)dt = P[\textit{the element fails in the time interval } (t, t + dt),$$

$$\textit{and it operated in time } t = 0] =$$

$$= \frac{P[\textit{the element fails in time interval } (t + dt)]}{P[\textit{the element operated in time } t]} =$$

$$= \frac{w(t)dt}{A(t)} = \frac{w(t)dt}{1 - Q(t)}$$

then

$$w(t) = \lambda(t)[1 - Q(t)].$$

The intensity of the conditional repair $\mu(t)$ – the probability that the element will be repaired in the unit time and in the time t it did not operate and in the time $t = 0$ it operated.

References

[1] KOSTKA, V.: *Information Safety in the Security System* (in Czech), The lecture on the Exposition PRAGOALARM 1996.
[2] FALISOVÁ, B.: *Equipment of Technical Security of Objects* (in Slovak), Academy PZ SR, Bratislava, 1997.
[3] MESÁROŠ, M., LOŠONCZI, P.: *Active Security of Protected Objects as a Component of Security Management* (in Slovak), Acta Avionica, Scientific Magazine of VLA in Košice, vol. IV, num. 5, ISSN 1335-9479, pp. 38–41.
[4] OLEJNÍKOVÁ, T.: *The Disturb Warning Devices of the safety Actives* (in Slovak), Acta Avionica, Scientific Magazine of VLA MRŠ in Košice, 2003, vol. V, num. 7, ISSN 1335-9479, pp. 49–53.
[5] OLEJNÍKOVÁ, T.: *The Integrated System of the Object Security* (in Slovak), Crisis Management, Scientific-Technical Magazine of Faculty of Special Engineering at University of Žilina in Žilina, 2003, vol. 2 , num. 2, ISSN 1336-0019, pp. 43-47.
[6] KOLESÁR, J.: *Simulation of the system Optimization of Safety and Security of a Military Airport* (in Slovak), Dissertation, Košice 2002.
[7] SIVÁK, J.: *The Pilot Project of Integrated Security Systems in the Implementation of the Slovak Republic Armed Forces* (in Slovak), KelcomInfo, Technical Magazine of the Association KELCOM International Liptovský Mikuláš s.r.o., vol. IV, num. 1, Liptovský Mikuláš 2002, pp. 4–7.
[8] PIVKO, D.: *The Equipment of the Jacketed Security* (in Slovak), KelcomInfo, Technical Magazine of the Association KELKOM International Liptovský Mikuláš s.r.o., vol. IV, num. 1, Liptovský Mikuláš 2002, pp. 13–18.

Title of thesis:	**The methodology of the public phone service level using mathematic-statistical methods**
Author:	**Ing. Miriam Jankalová**
Field of science:	**62-03-9 Branch and Cross-Section Economics**
Department:	**Department of Communications**
Faculty:	**Faculty of Operation and Economics of Transport and Communications**
Name of university:	**University of Žilina**
Tutor:	**prof. Ing. Jana Štofková, PhD.**

ŽILINSKÁ UNIVERZITA V ŽILINE
Fakulta prevádzky a ekonomiky dopravy a spojov
Katedra spojov

Doktorandská dizertačná práca

METODIKA HODNOTENIA ÚROVNE POSKYTOVANIA VEREJNEJ TELEFÓNNEJ SLUŽBY S VYUŽITÍM MATEMATICKO-ŠTATISTICKÝCH METÓD

Vedný obor:
62-03-9 Odvetvové a prierezové ekonomiky

Autor: Ing. Miriam Jankalová - Suchaničová
Školiteľ: prof. Ing. Jana Štofková, PhD.

Žilina 2003

Abstract:

At the beginning of the 21st century, for the successful integration into the information society, for each country including the Slovak republic, it is necessary to provide access to suitable communication services.

Therefore the goal of the European Union new policy, new regulations in the area of electronic communication, is to create conditions for the development of high quality, widely available and price acceptable services. This relates to the support and maintenance of sufficient level of competition in the markets with electronic communications, to the process of state regulation, to the assurance of end-user protection and mostly to the creation of one single European market.

Regarding the successful participation of the Slovak republic in the single European market, it is necessary to equalize the level of communication services concerning all European context. The present situation in the market of public phone services, despite the official starting date of liberalization (1. January 2003), does not respond to these conditions. Mostly in the possibility of provider selection, the liberalization process contributions have not arrived yet. In spite of this statement, already now it is necessary to think about the possibility of permanent change of the telecommunication provider and/or about the possibility of using selected types of calls by any other telecommunication provider.

With regard to the mentioned facts, this thesis focuses on the methodology of creation of a system of fixed determined criteria and indicators of public phone services, which will allow to evaluate the level of provided public phone services. One of the possibilities offers the suggested index "provider selection" and index "carrier selection " whose practical application falls into the area of regulation, support of effective economic competition, development of domestic market and these indexes also contribute to the support and allowance of interest of citizens of the Slovak Republic. The statements listed in Chapter V. proof these facts.

From the theoretical point of view, the proposed indexes represent the methodology for quantitative evaluation of the provided service level; a new model of the multiple discrimination analyses; the base for creation of the economic-statistical model for quantitative evaluation of information. As a synergic effect is considered the interconnection of .four sciences: economic statistic, marketing, management and economic analyses with praxis, which necessitated the extended use of economic statistics and exact mathematical methods in the area of business management and customer relationships.

By working on this thesis, the researcher draw the conclusion that the base for decision making should be an objective evaluation of the situation using exact methods, because the right decision, the choice of optimal solution requires an accurate and actual information about the customer needs and possibilities of their satisfaction. It is only up to the provider which method he will select; which priorities in the area of evaluation of the reached level of public phone services he will choose.

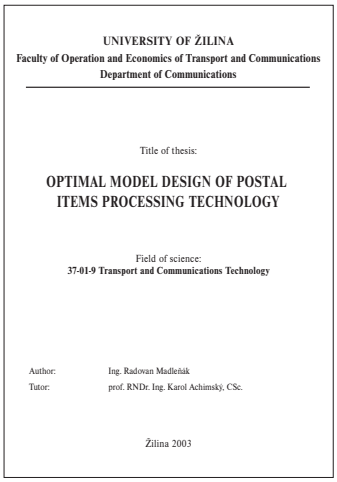
UNIVERSITY OF ŽILINA
Faculty of Operation and Economics of Transport and Communications
Department of Communications

Title of thesis:

OPTIMAL MODEL DESIGN OF POSTAL ITEMS PROCESSING TECHNOLOGY

Field of science:
37-01-9 Transport and Communications Technology

Author: Ing. Radovan Madleňák
Tutor: prof. RNDr. Ing. Karol Achimský, CSc.

Žilina 2003

Title of thesis:	**Optimal model design of postal items processing technology**
Author:	**Ing. Radovan Madleňák**
Field of science:	**Transport and Communications Technology**
Training institute:	**Department of Communications**
Department:	**Department of Communications**
Faculty:	**Faculty of Operation and Economics of Transport and Communications**
Name of university:	**University of Žilina**
Tutor:	**prof. RNDr. Ing. Karol Achimský, CSc.**
Viva voce:	**10th December 2003**

The determination of a suitable system of postal technology is the most important issue for fullfilling the elementary functions of the postal enterprise. A correct technology decision depends on the chosen postal infrastructure model and specific technological method and process. Therefore the main objective of this dissertation thesis is to suggest a new or to re-evaluate the existing model of the postal infrastructure. This designed model takes into consideration the demands of the outer postal environment and the requirements of the high level automatization equipment in the conditions of postal enterprises.

On the basis of essential postal technology terms main areas influencing the whole technological process of the postal items processing were analyzed. The analysis determined the critical part of the whole optimization process – the choice of a suitable construction variant of the postal transportation network.

The most suitable construction variant of the postal transportation network was selected from experiences of the postal enterprises in two European countries which are comparable to Slovakia in geomorphological character and demographical structure. The construction variant of the transportation network, which seems to be the optimum for these countries conditions, was chosen.

After choosing the construction model of the transportation network, is necessary to determine the number and placement of the each node at all levels of the postal network. For reasons to reach the real results, the postal optimization process was done in conditions of the Slovak postal enterprise - Slovak Post.

The existence of transportation network of Slovak Post determined the optimization process. Therefore the two phase optimization method was created, which at first re-evaluates the existence of middle level nodes and then suggests number and placement of the highest level nodes of the postal transportation network.

In the first optimization phase were used mathemathic-statistics methods to reduce the number of middle level nodes and to re-evaluate the position of the zone centers. The part-optimized model of the transportation network is depicted in the form of graph, which served as the basis for the second phase of the optimization.

In the second part of optimization the suitable optimization method was chosen to find the optimum number and placement of the highest level nodes of the postal transportation network. Two optimization methods suitable for the second part realization were identified. The variant approach was used to find a position and number of mentioned nodes.

The result of the whole optimization process was the creation of the flowchart diagram which describes the optimum model construction of the postal transportation network. It shows the sequence of steps possible to be used not only in condition of the Slovak postal enterprise, but in conditions of any comparable postal operator.

Taking into consideration all these facts, it is possible to say that this dissertation thesis includes general knowledge and all methods suitable for optimization of the national postal operator's transportation network.

By creating the optimal model of postal item's processing technology, the space for the implementation of this model for specific postal operator's requirements is opened. That accomplishes the main, but also partial objectives of this dissertation thesis, determined at the beginning.

COMMUNICATIONS – Scientific Letters of the University of Žilina
Writer's Guidelines

1. Submissions for publication must be unpublished and not be a multiple submission.
2. Manuscripts written **in English language** must include abstract also written in English. The submission should not exceed 7 pages (format A4, Times Roman size 12). The **abstract** should not exceed 10 lines.
3. Submissions should be sent: **by e-mail** (as attachment in system Microsoft WORD) to one of the following addresses: *holesa@nic.utc.sk* or *vrablova@nic.utc.sk* or *polednak@fsi.utc.sk* **with a hard copy** (to be assessed by the editorial board) **or on a 3.5″ diskette** with a hard copy to the following address: Zilinska univerzita, OVaV, Moyzesova 20, SK-10 26 Zilina, Slovakia.
4. Abbreviations, which are not common, must be used in full when mentioned for the first time.
5. Figures, graphs and diagrams, if not processed by Microsoft WORD, must be sent in electronic form (as GIF, JPG, TIFF, BMP files) or drawn in contrast on white paper, one copy enclosed. Photographs for publication must be either contrastive or on a slide.
6. References are to be marked either in the text or as footnotes numbered respectively. Numbers must be in square brackets. The list of references should follow the paper (according to **ISO 690**).
7. The author's exact **mailing address of the organisation where the author works, full names, e-mail address or fax or telephone number,** must be enclosed.
8. The editorial board will assess the submission in its following session. In the case that the article is accepted for future volumes, the board submits the manuscript to the editors for review and language correction. After reviewing and incorporating the editor's remarks, the final draft (before printing) will be sent to authors for final review and adjustment.
9. The deadlines for submissions are as follows: September 30, December 31, March 31 and June 30.

POKYNY PRE AUTOROV PRÍSPEVKOV DO ČASOPISU KOMUNIKÁCIE – vedecké listy Žilinskej univerzity

1. Redakcia prijíma iba príspevky doteraz nepublikované alebo inde nezaslané na uverejnenie.
2. Rukopis musí byť **v jazyku anglickom**. Príspevok by nemal prekročiť 7 strán (formát A4, písmo Times Roman 12 bodové). K článku dodá autor **resumé** v rozsahu maximálne 10 riadkov (v anglickom jazyku).
3. Príspevok prosíme poslať: **e-mailom**, ako prílohu spracovanú v aplikácii Microsoft WORD, na adresu: *holesa@nic.utc.sk* alebo *polednak@fsi.utc.sk* príp. *vrablova@nic.utc.sk* (alebo doručiť na diskete 3,5″) **a jeden výtlačok** článku na adresu Žilinská univerzita, OVaV, Moyzesova 20, 010 26 Žilina.
4. Skratky, ktoré nie sú bežné, je nutné pri ich prvom použití rozpísať v plnom znení.
5. Obrázky, grafy a schémy, pokiaľ nie sú spracované v Microsoft WORD, je potrebné doručiť buď v digitálnej forme (ako GIF, JPG, TIFF, BMP súbory), prípadne nakresliť kontrastne na bielom papieri a predložiť v jednom exemplári. Pri požiadavke na uverejnenie fotografie priložiť ako podklad kontrastnú fotografiu alebo diapozitív.
6. Odvolania na literatúru sa označujú v texte alebo v poznámkach pod čiarou príslušným poradovým číslom v hranatej zátvorke. **Zoznam použitej literatúry** je uvedený za príspevkom. Citovanie literatúry musí byť **podľa STN 01 0197 (ISO 690)** „Bibliografické odkazy".
7. K rukopisu treba pripojiť **plné meno a priezvisko autora a adresu inštitúcie v ktorej pracuje, e-mail adresu** alebo číslo telefónu event. faxu.
8. Príspevok posúdi redakčná rada na svojom najbližšom zasadnutí a v prípade jeho zaradenia do niektorého z budúcich čísiel podrobí rukopis recenziám a jazykovej korektúre. Pred tlačou bude poslaný autorovi na definitívnu kontrolu.
9. Termíny na dodanie príspevkov do čísiel v roku sú: 30. september, 31. december, 31. marec a 30. jún.

komunikácie
COMMUNICATIONS

VEDECKÉ LISTY ŽILINSKEJ UNIVERZITY
SCIENTIFIC LETTERS OF THE UNIVERSITY OF ŽILINA
6. ROČNÍK – VOLUME 6

Adresa redakcie:
Address of the editorial office:
Žilinská univerzita
Oddelenie pre vedu a výskum
Office for Science and Research
Moyzesova 20, Slovakia
SK 010 26 Žilina
Tel.: +421/41/5620 392
Fax: +421/41/7247 702
E-mail: polednak@fsi.utc.sk, holesa@nic.utc.sk

Každý článok bol oponovaný dvoma oponentmi.
Each paper was reviewed by two reviewers.

Časopis je excerpovaný v Compendexe
Journal is excerpted in Compendex

Vydáva Žilinská univerzita
v EDIS – vydavateľstve ŽU
J. M. Hurbana 15, 010 26 Žilina
pod registračným číslom 1989/98
ISSN 1335-4205

It is published by the University of Žilina in
EDIS - Publishing Institution of Žilina University
Registered No: 1989/98
ISSN 1335-4205

Objednávky na predplatné prijíma redakcia
Vychádza štvrťročne
Ročné predplatné na rok 2005 je 500,– Sk

Order forms should be returned to the editorial office
Published quarterly
The subscription rate for year 2005 is 500 SKK

Jednotlivé čísla časopisu sú uverejnené tiež na:
http://www.utc.sk/komunikacie
Single issues of the journal can be found on:
http://www.utc.sk/komunikacie